

Candidate Isolated Neutron Stars  
and Other Stellar X-ray Sources from  
the *ROSAT* All-Sky and Sloan Digital Sky Surveys

Marcel A. Agüeros

A dissertation submitted in partial fulfillment  
of the requirements for the degree of

Doctor of Philosophy

University of Washington

2006

Program Authorized to Offer Degree: Astronomy

UMI Number: 3230726

## INFORMATION TO USERS

The quality of this reproduction is dependent upon the quality of the copy submitted. Broken or indistinct print, colored or poor quality illustrations and photographs, print bleed-through, substandard margins, and improper alignment can adversely affect reproduction.

In the unlikely event that the author did not send a complete manuscript and there are missing pages, these will be noted. Also, if unauthorized copyright material had to be removed, a note will indicate the deletion.



---

UMI Microform 3230726

Copyright 2006 by ProQuest Information and Learning Company.

All rights reserved. This microform edition is protected against unauthorized copying under Title 17, United States Code.

ProQuest Information and Learning Company  
300 North Zeeb Road  
P.O. Box 1346  
Ann Arbor, MI 48106-1346

University of Washington  
Graduate School

This is to certify that I have examined this copy of a doctoral dissertation by

Marcel A. Agüeros

and have found that it is complete and satisfactory in all respects,  
and that any and all revisions required by the final  
examining committee have been made.

Chair of the Supervisory Committee:

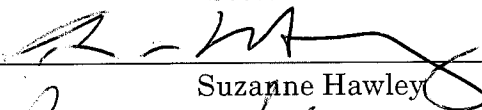


Scott Anderson

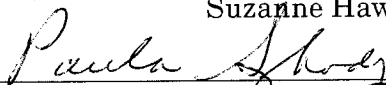
Reading Committee:



Scott Anderson

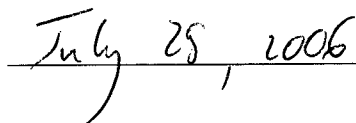


Suzanne Hawley



Paula Szkody

Date:



In presenting this dissertation in partial fulfillment of the requirements for the doctoral degree at the University of Washington, I agree that the Library shall make its copies freely available for inspection. I further agree that extensive copying of this dissertation is allowable only for scholarly purposes, consistent with "fair use" as prescribed in the U.S. Copyright Law. Requests for copying or reproduction of this dissertation may be referred to Proquest Information and Learning, 300 North Zeeb Road, Ann Arbor, MI 48106-1346, 1-800-521-0600, to whom the author has granted "the right to reproduce and sell (a) copies of the manuscript in microform and/or (b) printed copies of the manuscript made from microform."

Signature Rafael Agüeros

Date July 29, 2006



University of Washington

Abstract

Candidate Isolated Neutron Stars  
and Other Stellar X-ray Sources from  
the *ROSAT* All-Sky and Sloan Digital Sky Surveys

Marcel A. Agüeros

Chair of the Supervisory Committee:  
Professor Scott Anderson  
Astronomy

Although extrasolar X-ray sources were first observed almost fifty years ago, the first all-sky imaging X-ray survey was only recently completed. The *ROSAT* All-Sky Survey (RASS) Bright and Faint Source Catalogs include approximately 124,000 X-ray sources detected in the 0.1 – 2.4 keV range. However, while X-ray source counterparts are known to range from distant quasars to nearby M dwarfs, the RASS data alone are often insufficient to determine whether an X-ray source is Galactic or extragalactic. As a result, no more than 10% of RASS sources have had their counterparts identified and fully characterized. A major obstacle to identifying more RASS sources was the absence of a large-area optical survey of equivalent sensitivity with which to correlate the RASS catalogs. In the Sloan Digital Sky Survey (SDSS) we now have the needed optical survey; SDSS provides a uniform optical photometric and spectroscopic dataset with which to identify RASS sources. In this thesis, I present results from a campaign to identify and characterize stellar counterparts to RASS sources falling within the SDSS footprint.

Of order one-third of the RASS source counterparts are likely to be stars. Most of these are bright stars with coronal X-ray emission, and are not suitable for optical identification based on routine SDSS multi-fiber spectroscopy, which is not designed for  $m < 15$  objects. Instead, I used SDSS imaging photometry, correlations with the

Two Micron All Sky Survey and other catalogs, and spectroscopy from the Apache Point Observatory 3.5-m telescope to identify these stellar X-ray counterparts in the SDSS Data Release 1 region. In addition, I describe efforts to identify and characterize other, rarer stellar X-ray sources in the entire SDSS area: cataclysmic variables, white dwarfs, and especially elusive isolated neutron stars, of which only a handful are currently known.

## TABLE OF CONTENTS

List of Figures . . . . .	iii
List of Tables . . . . .	vii
Chapter 1: Introduction . . . . .	1
1.1 Stellar X rays, the <i>ROSAT</i> All-Sky Survey, and SDSS . . . . .	1
1.2 Identifying Stellar X-ray Sources... . . . .	4
1.3 The RASS and SDSS, and a Thesis Preview . . . . .	12
Chapter 2: A Catalog of X-ray-Emitting Stars from the <i>ROSAT</i> All-Sky Survey and the Sloan Digital Sky Survey Data Release 1 . . . . .	15
2.1 Introduction . . . . .	15
2.2 Mechanisms for Stellar X-ray Emission . . . . .	16
2.3 Selection of X-ray Emitting Stars from the RASS and SDSS DR1 . . . . .	23
2.4 The RASS/SDSS DR1 Catalogs of Stellar X-ray Sources . . . . .	27
2.5 Appendix: The Catalogs . . . . .	50
Chapter 3: A Catalog of X-ray-Emitting Cataclysmic Variables from the <i>ROSAT</i> All-Sky and Sloan Digital Sky Surveys . . . . .	58
3.1 Introduction . . . . .	58
3.2 X-ray Emission in Cataclysmic Variables . . . . .	60
3.3 Published X-ray-Emitting SDSS Cataclysmic Variables . . . . .	63
3.4 New Candidate X-ray-Emitting SDSS Cataclysmic Variables . . . . .	80
Chapter 4: A Catalog of X-ray-Emitting White Dwarfs from the <i>ROSAT</i> All-Sky and Sloan Digital Sky Surveys . . . . .	85
4.1 Introduction . . . . .	85
4.2 X-ray-Emitting SDSS White Dwarfs . . . . .	88
4.3 Composite DA White Dwarf Spectra . . . . .	105

Chapter 5:	Candidate Isolated Neutron Stars and Other Optically Blank X-ray Fields Identified from the <i>ROSAT</i> All-Sky and Sloan Digital Sky Surveys . . . . .	109
5.1	Introduction . . . . .	109
5.2	RASS and SDSS: A Match Made in the Heavens . . . . .	112
5.3	Using SDSS to Identify Optically Blank RASS Fields . . . . .	113
5.4	Properties of the Candidate Isolated Neutron Star Fields . . . . .	120
5.5	Discussion . . . . .	121
5.6	Conclusion . . . . .	126
5.7	Appendix: Additional Interesting Fields . . . . .	127
Chapter 6:	Conclusion . . . . .	134
Bibliography	. . . . .	139

## LIST OF FIGURES

Figure Number	Page
<p>2.1 The SDSS DR1 imaging area, in Galactic coordinates. The DR1 spectroscopic area is smaller; spectroscopic targets are selected largely based on their photometric properties, and the spectroscopic survey trails the imaging one. . . . .</p>	25
<p>2.2 <i>Left panel:</i> Distribution of positional offsets between the RASS sources and the candidate bright SIMBAD stellar counterparts. <i>Right panel:</i> The same distribution, expressed in terms of the cataloged X-ray positional uncertainty. In both panels the colored histograms show the distribution by spectral type. Our discussion focuses on those stars to the left of the dashed line in the right panel. . . . .</p>	27
<p>2.3 Cataloged X-ray count rate versus optical magnitude for the stars for which <math>\sigma \leq 2</math>; <math>V</math> was used for all the stars for which they were available. The brightest X-ray source is Hercules X-1. . . . .</p>	28
<p>2.4 <i>Left panel:</i> 2MASS <math>K_S</math> versus SDSS <math>u</math> for the SIMBAD bright stars within <math>2\sigma</math> of a RASS source in DR1. The clump of stars with <math>u \approx 14</math> and <math>4 &lt; K_S &lt; 8</math> is probably due to bad photometry, as those stars are not well characterized by the dashed lines, which correspond to the predicted <math>u</math> given the <math>K_S</math> magnitude. <i>Right panel:</i> The 2MASS <math>K_S</math> versus SIMBAD <math>V</math> plot is much cleaner, suggesting that the SDSS photometry is indeed suspect for many of these bright stars. . . . .</p>	30
<p>2.5 Log <math>(f_X/f_V)</math> histograms for the SIMBAD F, G, K, and M stars. The dashed blue histograms are the Krautter et al. (1999) observed distributions. In the first three panels, the red vertical line corresponds to the mean flux ratio, and the green vertical lines bracket the <math>2\sigma</math> range, for SIMBAD stars of that spectral class. The horizontal lines are ratio ranges from the literature: the solid lines are from the Maccacaro et al. (1988) <i>Einstein</i> survey, while the dotted extensions are from Krautter et al. (1999). In each panel, we indicate the number of stars with a cataloged <math>V</math>. . . . .</p>	31

2.6	Log ( $f_X/f_K$ ) ratios for the SIMBAD F, G, K, and M stars. As in Figure 2.5, the red vertical lines are the mean flux ratios, and the green vertical lines bracket the $2\sigma$ ranges. The number of stars from Figure 2.5 used to calculate these $2\sigma$ ranges is indicated in the first three panels; 20 M stars have a $K_S$ magnitude. . . . .	32
2.7	SDSS images of three RASS fields (left column) and of the proposed stellar counterpart for which an APO spectrum was obtained (right column). . . . .	38
2.8	APO spectra of the three stars in Figure 2.7. The green lines delimit the overlap between the DIS blue and red spectrum for each object. The prominent features visible in this area in the top and bottom panels are due to the dichroic. The red dashed lines in the middle panel indicate the positions of two telluric features, the Fraunhofer A (7600 Å) and B (6800 Å) bands. The fringing to the red of the Fraunhofer A band is due to the red DIS CCD, which is a thinned chip. For each spectrum, the name of the corresponding RASS source is included. . . . .	39
2.9	<i>Left panel:</i> Distribution of positional offsets between the RASS sources and 800 candidate SDSS stellar counterparts with APO spectra. <i>Right panel:</i> The same distribution, expressed in terms of the cataloged X-ray positional uncertainty. In both panels the colored histograms show the distribution by spectral type. . . . .	41
2.10	Log ( $f_X/f_K$ ) ratios for the proposed SDSS counterparts with APO spectroscopy (black), along with the distributions for the RASS/SIMBAD F, G, K, and M stars (dashed blue), within $2\sigma$ of a RASS source. In the first three panels, the red vertical lines are the mean flux ratios, and the green vertical lines bracket the $2\sigma$ ranges, derived from the RASS/SIMBAD sample. The mean and $2\sigma$ range are derived directly from the APO sample for the M stars. The number of stars with an APO spectrum is indicated in each panel. . . . .	43
2.11	Cataloged X-ray count rate versus optical magnitude for the F, G, K, and M stars X-ray emitters. <i>Left:</i> RASS/SIMBAD stars. <i>Right:</i> RASS/SDSS stars. . . . .	44
2.12	APO spectra of the proposed stellar counterpart to 1RXS J0808+4347. <i>Top:</i> The spectra are artificially offset from each other in flux; two spectra were obtained on 2005 Apr 21 and Dec 20. The dotted lines indicate the positions of the Balmer lines. <i>Bottom:</i> The blue continuum and strong Balmer emission visible in the 2004 Dec 03 spectrum are even more apparent when all of the spectra are normalized to their flux value at 4600 Å. The dot-dashed lines indicate the positions of the Ca H & K lines (at this resolution, Ca H is blended with H $\epsilon$ ), while the dashed line is HeI at 4471 Å. . . . .	52

2.13	APO spectra of the proposed stellar counterpart to 1RXS J1714+5851. The spectra are presented as in Figure 2.12. Two spectra were obtained on 2006 Apr 16. . . . .	53
3.1	<i>Left panel:</i> Distribution of $\log(f_X/f_g)$ for all of the published SDSS/RASS CVs. <i>Right panel:</i> The same distribution for the known dwarf novae and polars. . . . .	65
3.2	$\log(f_X/f_g)$ versus equivalent width of the $H\beta$ line for the 40 published SDSS/RASS CVs. The predicted $f_X/f_g$ is from Patterson & Raymond (1985a). . . . .	66
3.3	SDSS spectra for the X-ray-emitting CVs in Table 3.2. The y axis is flux density ( $10^{-17}$ ergs $\text{cm}^{-2}$ $\text{s}^{-1}$ $\text{\AA}^{-1}$ ); the x axis is wavelength ( $\text{\AA}$ ). . . . .	71
3.4	APO spectra showing the outburst and quiescence of SDSS J1730. The fluxes have units of $10^{-16}$ ergs $\text{cm}^{-2}$ $\text{s}^{-1}$ $\text{\AA}^{-1}$ . . . . .	77
3.5	APO spectra showing the variation of the $H\beta$ line profile of SDSS J1730 throughout an orbital period during outburst. . . . .	78
3.6	Best fit to the radial velocity curve of SDSS J1730 at outburst using the $H\alpha$ emission line. The open circles produced large deviations to a sine fit and were therefore left out of the best solution, which is shown as the solid line. . . . .	80
3.7	$\log(f_X/f_g)$ versus equivalent width of the $H\beta$ line. The two recently recovered CVs and four new CV candidates have been added. . . . .	82
3.8	SDSS spectra of the unpublished candidate X-ray emitting CVs. The axes are as in Figure 3.2. . . . .	84
4.1	$\log(f_X/f_g)$ distributions for X-ray-emitting DA WDs. The black histogram is for the 36 Fleming et al. (1996) DAs in the SDSS footprint; the dashed blue one is for the sample identified here (eight recovered Fleming et al. (1996) DAs are not included in the latter histogram). The red vertical line is the mean flux ratio, and the green vertical lines bracket the $2\sigma$ ranges, for the Fleming et al. (1996) sample. . . . .	103
4.2	Temperature distributions for X-ray-emitting and “ordinary” DA WDs. The black histogram is the Fleming et al. (1996) sample of X-ray emitters; the blue dashed one is the sample identified here. The green histogram is the normalized distribution for 7578 Eisenstein et al. (2006) DAs. . . . .	104
4.3	SDSS spectra for our candidate cool DA X-ray emitters. The x axis is wavelength in $\text{\AA}$ ; the fluxes have been smoothed and normalized and are offset for plotting purposes. The $g$ band signal-to-noise ratio for these spectra range from $\sim 3$ for SDSS J1013+0615 to $\sim 6$ for SDSS J1204+5819 (Eisenstein et al., 2006). . . . .	105

4.4	Composite DA WD spectra. The x axis is wavelength in Å; the fluxes have been normalized and offset for plotting purposes. About 1100 DR1 WDs were used to make these composites. . . . .	106
4.5	Composite spectra for both the X-ray and the “ordinary” (in green) DA WDs. The spectra are plotted as in Figure 4.4. . . . .	108
5.1	SDSS composite $g, r, i$ images of our best INS candidate fields, with the stretch being the same for all. North is up and east is to the left; the images are roughly 3.5' on a side. The 4 <i>p.e.</i> RASS error circle is shown in each image. The brightest SDSS object within any of the error circles is $g = 21.04$ mag. Rutledge et al. (2003) rejected 1RXS J130547.2+641252 as an INS; 1RXS J160518.8+324907 is a known INS. . . . .	118
5.2	SDSS composite $g, r, i$ images of candidate fields that did not survive the cluster-detecting stage of our algorithm. The orientation and scale are the same as in Fig. 5.1. The brightest object in any of the 4 <i>p.e.</i> error circles is $g = 19.35$ mag; for most fields the brightest object is $g > 21.0$ . Rutledge et al. (2003) identified 1RXS J145234.9+323536 as a candidate INS, but no X-ray source was detected by their follow-up <i>Chandra</i> observations. . . . .	128
5.3	SDSS composite $g, r, i$ images of six fields that did not survive our final version of the algorithm but may host interesting X-ray emitters. The orientation and scale are the same as in the previous figures. The brightest object in any of the 4 <i>p.e.</i> error circles is $g = 22.08$ mag. . . . .	131



## LIST OF TABLES

Table Number	Page
1.1 Observed X-ray-to-optical flux ratios, from Maccacaro et al. (1988). . .	5
2.1 $\log (f_X/f_K)$ ratios derived from the RASS/SIMBAD stars. . . . .	33
2.2 RASS/SIMBAD stars. The full $f_X/f_V$ ranges are given. . . . .	35
2.3 The white dwarfs (first six objects) and cataclysmic variables among the RASS/SIMBAD matches. For the white dwarfs $V$ is given, except for WD 1125–025. For this object and the four cataclysmic variables $B$ is listed.	36
2.4 X-ray, optical, and infrared data for RASS fields with multiple candidate stellar counterparts. 2MASS magnitudes with an asterisk indicate problematic PSF fitting. “CC” is short for close companion. . . . .	45
2.5 X-ray and optical data for the first 18 RASS/APO stars. . . . .	54
2.6 X-ray and optical data for the first 18 RASS/SIMBAD stars. . . . .	56
3.1 Cataclysmic variable nomenclature. . . . .	59
3.2 Optical and X-ray properties of the published SDSS CVs; these data originally appeared in Szkody et al. (2002, 2003, 2004a, 2005, 2006). Fluxes are calculated for a 2 keV bremsstrahlung spectrum. . . . .	68
3.3 Follow-up data from APO and MRO for SDSS J1730. . . . .	76
3.4 Radial velocity solution for SDSS J1730. . . . .	79
3.5 Optical and X-ray properties of the unpublished SDSS candidate CVs. Fluxes are calculated as in Table 3.2. SDSS J215101.33+123737.9 is saturated; we give its $\log (f_X/f_V)$ based on its SIMBAD $V = 8.65$ . The $H\beta$ EW is measured in Å. . . . .	83
4.1 Optical and X-ray properties of the previously known DAs. . . . .	89
4.2 Optical and X-ray properties of the new SDSS DAs. . . . .	92
4.3 Optical and X-ray properties of the other new SDSS WDs. The first two objects are DB WDs; the third is a PG 1159 star; the final three are DA/M dwarf binaries. The $T_{eff}$ and $\log g$ values for the latter four objects are suspect. . . . .	94
4.4 Optical and X-ray properties of the post-DR4 SDSS WD/RASS associations. The last two are the known DAs WD 1325+512 and WD 1415+132 (McCook & Sion, 1999). . . . .	99

4.5	Optical and X-ray properties of the less likely post-DR4 SDSS WD/RASS associations. . . . .	100
4.6	Number of DAs used to create the composite spectra in Figure 4.4. . . .	107
5.1	X-ray and optical data for the 11 candidate isolated neutron star fields. Note that 1RXS J003413.7-010134 and 013630.4+004226 are outside of the optical cluster catalog footprint; 1RXS J130547.2+641252 was rejected as an INS (Rutledge et al., 2003); and 1RXS J160518.8+324907 is a known INS. . . . .	117
5.2	X-ray and optical data for seven cluster candidates. Six other interesting fields are listed below the horizontal line. 1RXS J145234.9+323536 was previously identified as a candidate INS, but no source was detected by <i>Chandra</i> (Rutledge et al., 2003); 1RXS J162526.9+455750, 162526.9+455750, and 205334.0-063617 have cataloged X-ray positional errors that appear to be underestimated; and 1RXS J205334.0-063617 is outside of the optical cluster catalog footprint. . . . .	130

## ACKNOWLEDGMENTS

Besides being perhaps the gentlest man on Earth, Scott Anderson is a wonderful teacher and mentor. It has been a pleasure learning from and working with him. When in Seattle, I headed over to Scott's office at least once a day, and I will miss our chats.

I am very grateful to the other members of my reading committee, Suzanne Hawley and Paula Szkody, for their investment in my research, and particularly for helping me improve this thesis. Over the last three years, Julianne Dalcanton, my fourth committee member, has for my benefit convincingly feigned an interest in Galactic stars, for which I thank her. While not officially duty-bound to look after me, David Helfand, Željko Ivezić, Bruce Margon, and Keivan Stassun did so anyway, helping me grow professionally and personally. Thank you.

I am thrilled to have talked Stu Scheingold into being my GSR—and not only because I could not otherwise schedule a July defense. Stu and his wife Lee adopted me as an honorary grandson when I arrived in Seattle, an appointment whose perks I have greatly enjoyed. Consider the pension debt forgiven.

I would not have gotten through my first year, let alone graduated, without the assistance of Kevin Covey and Anil Seth (and no, I did not plagiarize Anil's acknowledgments). Looking over the table in the conference room in September 2000, I had no idea I was about to make lifelong friends. I also have no idea why I will now have to go to Boston to enjoy their company, but they can count on me to bring the noir. Kristine Washburn and Ricardo Covarrubias pulled me through the qual, and I am still figuring out how to repay them for that. I shared an office with Dan Zucker and Nino Miceli and we nevertheless remain on excellent terms. Daryl Haggard is a model of generosity and warmth, and I am fortunate to count her as a friend. John Bochanski provides me with beats and laughs at my jokes, sometimes—what more can I ask for?

Among my non-astronomer Seattle friends I would especially like to thank Chris Himes and Mike Keim for the highly enjoyable lunch dates we struggled to schedule. Seth Bridges, Justin Goshi, Jon Ko, and Wil Li were reliable companions in basketball ignominy. I will never forget all that losing we did, whether as Chowder Dawgs or as Fighting Llamas (maybe it was the names), and I already ache for our Friday morning get-togethers. Away from Seattle, I am indebted to Manu Platt for filling the role of my token friend from Delaware with panache, and to Joe Ayala, Jessica Delbaum, Eddie Griffin, and Kunal Jajoo for sticking by me for over ten years now. I think there is something in it for them, but I am not always sure. To my friends in Europe, particularly from the Bagno Riviera, the Lycée Français Jean Monnet, Emma, and L'OP XV, I say: Bises et à bientôt!

My family's support and patience while I went off to do whatever I was doing over the last decade have been absolute, and for that I am very thankful. Mom, Papi, Nathalie, Kado (or whatever it is these days), Alan, love you. By the way, I have the most beautiful niece in the world. See you soon, Mari.

Over the last few months, Melissa Phillips has metamorphosed into a housewife so that I could focus on producing this thesis, an effort that came close to killing her. I think this means we can go back to the way things used to be... Thank you for giving up Seattle for me. New York won't be so bad, I promise. And if we can make it there, we can etc.

Finally, I am grateful to the Hispanic Scholarship Fund, the NASA Harriett G. Jenkins Predoctoral Fellowship Program, and the NSF Graduate Teaching in K-12 Education Program for together providing me with four years of financial independence, and for taking me places I probably would not have gone otherwise (and not just San Jose, either). In particular, I spent three great years in Sharon Acena's 4/5<sup>th</sup> grade Bilingual Orientation Classroom at Thurgood Marshall Elementary. I cannot imagine a more rewarding teaching experience.

## **DEDICATION**

In loving memory of my grandmothers, Madeleine (Badi) Ledivelec–Gloeckner and Carmen Díaz Agüeros.

## Chapter 1

### INTRODUCTION

...la tête dans les étoiles

mes écouteurs

crachaient le son de Marley Marl...

—IAM, Quand Ils Rentraient Chez Eux

#### **1.1 *Stellar X rays, the ROSAT All-Sky Survey, and SDSS***

Historically, the study of stellar X rays is first and foremost the study of X rays from the Sun. The presence of a hot, tenuous, X-ray-emitting gas around the Sun—the X-ray corona—was inferred and confirmed roughly 60 years ago (Edlén, 1943; Friedman et al., 1951)<sup>1</sup>. The Sun is quite naturally the best studied X-ray source in the sky, which is not to say that the mechanisms producing its X-ray emission are fully understood. The existence of similar coronae around other stars, however, was a matter of speculation until the detection during a rocket flight just over 30 years ago of Capella (Catura et al., 1975). Capella has been observed by almost all subsequent X-ray missions, and is a far stronger persistent source of coronal X rays than the (quiet) Sun, with an X-ray luminosity several orders of magnitude greater and a coronal temperature of  $\sim 10^7$  K, several times that of the Sun's corona (e.g., Linsky et al., 1998; Ishibashi et al., 2006).

Despite Capella's detection, however, the consensus until fairly recently was that stellar X-ray astronomy would not be a particularly rich field of study, largely because of our heliocentric view. For example, if one takes the Sun's X-ray luminosity of  $2 \times$

---

<sup>1</sup>See also the historical review in Haisch & Schmitt (1996), Favata & Micela (2003), and Güdel (2004).

$10^{27} \text{ erg s}^{-1}$  and compares it to the *ROSAT* (*Röntgensatellit*) All-Sky Survey (RASS; Voges et al., 1999) typical flux limit of  $\sim 2 \times 10^{-13} \text{ erg cm}^{-2} \text{ s}^{-1}$  in the 0.1 – 2.4 keV energy band, one would expect the RASS to be sensitive only to stars within roughly 9 pc of the Sun—a sample of only a few hundred stars (Schmitt et al., 1995)<sup>2</sup>. The discovery instead in *Einstein Observatory* data and the RASS of many X-ray-emitting stars can therefore be safely described as a major surprise (Haisch & Schmitt, 1996).

Today, X-ray source counterparts are known to be a heterogeneous mix of objects, ranging from distant quasars to nearby active M dwarfs (e.g., Stocke et al., 1983, 1991; Schmitt et al., 1995; Anderson et al., 2003; Zickgraf et al., 2003; Green et al., 2004), and stars are recognized as one of the most prominent classes of X-ray emitters (Güdel, 2004). While our detection of X rays from numerous stars might seem to signal an end to the historically heliocentric view of stellar X rays, the Sun continues to play an essential role in this field. In particular, the X-ray activity of a late-type star such as the Sun is thought to depend heavily on the behavior of the magnetic dynamo produced in the stellar interior<sup>3</sup>. While there is still no entirely satisfactory model for how this dynamo forms or functions, the consensus, based on studies of the Sun, is that its existence and properties are related to the complex interplay of convection and rotation (Favata & Micela, 2003). If this mechanism is in fact universal for late-type stars, observations of other stars can test our models, since in a sense they allow us to vary the solar parameters (Haisch & Schmitt, 1996). What would happen to the solar corona if we sped up the Sun’s rotation? If we slowed it down? If we made the Sun more massive? Younger? Older? Fully convective?

In addition, surveys have discovered that many unusual types of stars are also X-ray emitters, including accreting binaries such as cataclysmic variables (e.g., Verbunt et al., 1997) and compact remnants such as white dwarfs (e.g., Fleming et al., 1996) and neutron stars (e.g., Walter et al., 1996; Haberl et al., 1997). The physics of these

---

<sup>2</sup>Because of the scanning protocol, the RASS exposure times and thus sensitivity limits vary markedly from ecliptic pole to equator.

<sup>3</sup>Throughout this thesis I use late-type to describe stars of spectral types F and later.

systems have their own particularities<sup>4</sup>, and the X-ray data provide us with insights unavailable at other wavelengths. Collecting larger samples of X-ray-emitting stars is therefore essential for exploring the full range of possible connections between the physics of stellar interiors, atmospheres, coronae, and accretion.

Frequently, however, the X-ray data alone are insufficient to determine unambiguously whether an X-ray source is Galactic or extragalactic, much less to make finer distinctions about its nature. This is the case, in particular, with RASS data, collected as part of the first *imaging* X-ray survey of the entire sky. Voges et al. (1999) included 18,811 sources with count rates  $> 0.05 \text{ cts s}^{-1}$  in the RASS Bright Source Catalog (BSC); another 105,924 with count rates  $< 0.05 \text{ cts s}^{-1}$  are listed in the Faint Source Catalog (FSC; Voges et al., 2000). The fraction of identified and fully characterized RASS BSC/FSC sources is only  $\sim 10\%$  (Mickaelian et al., 2006), with the majority of the identifications being of the BSC sources (e.g., Bade et al., 1998; Zickgraf et al., 2003). Large-scale programs to find the optical counterparts to RASS sources are therefore still very much needed.

The work presented in this thesis is part of one such program, which aims to produce a complete sample of RASS X-ray source identifications from correlations with the Sloan Digital Sky Survey (SDSS; York et al., 2000). SDSS provides a uniform optical photometric and spectroscopic dataset with which to correlate the RASS catalogs. The survey uses a dedicated 2.5-m telescope at the Apache Point Observatory, NM, to produce five color  $u, g, r, i, z$  CCD images to a depth of  $r \sim 22.5$  (Fukugita et al., 1996; Gunn et al., 1998; Hogg et al., 2001; Smith et al., 2002; Gunn et al., 2006); the associated photometric accuracy is  $\sim 0.02$  magnitudes (Ivezić et al., 2004). The survey will eventually cover  $\sim 10^4 \text{ deg}^2$  around the north Galactic cap and  $\sim 200 \text{ deg}^2$  in the southern Galactic hemisphere, resulting in photometry for over  $10^8$  stars and a similar number of galaxies. Crucially for our purposes, SDSS is also a spectroscopic survey, and will obtain spectra for  $10^6$  galaxies,  $10^5$  quasars, and  $10^5$  stars.

In the following Section, I review past efforts to identify optical counterparts to

---

<sup>4</sup>and aficionados!



sources detected by some of the principal X-ray satellite missions of the past several decades, namely *Einstein*, *ROSAT*, the *Chandra X-ray Observatory*, and the *XMM-Newton X-ray Observatory*. In Section 1.3, I touch on the complementarity of RASS and SDSS data before outlining this thesis, which focuses on identifying stellar X-ray emitters (both common and rare) in the RASS/SDSS overlap region.

## 1.2 Identifying Stellar X-ray Sources...

*from the Einstein surveys*

Although not designed to perform very large-area surveys, the two imaging instruments flown on the *Einstein Observatory* provided the first large samples of X-ray-detected sources. To create the Medium Sensitivity Survey (MSS), Gioia et al. (1984) collected 112 sources serendipitously detected in pre-existing targeted *Einstein* observations; this survey was followed by the Extended Medium-Sensitivity Survey (EMSS; Gioia et al., 1990). Both surveys included sources with X-ray fluxes between roughly  $5 \times 10^{-14}$  and  $3 \times 10^{-12}$  ergs cm $^{-2}$  s $^{-1}$  in the 0.3 – 3.5 keV energy band, but the EMSS cataloged a total of 835 sources in a significantly larger area of sky:  $\sim 800$  deg $^2$  versus  $\sim 40$  deg $^2$  for the MSS. For both surveys, painstaking programs to identify the optical counterparts to the X-ray sources were undertaken. For example, to find the counterparts to 63 MSS sources, Stocke et al. (1983) obtained spectra for *all* of the optical objects inside or just outside the X-ray 90% confidence positional error circles—typically an area of radius  $\sim 30''$  to  $70''$  for each source. Once they found a plausible counterpart by comparing its  $f_X/f_V$  ratio<sup>5</sup> to that of similar objects detected in pointed *Einstein* observations, they *continued* to collect spectra for the optical objects until they reached objects at least four times fainter than the proposed counterpart or the limit of the Palomar Observatory Sky Survey (roughly 20.5 mag; Stocke et al., 1983)<sup>6</sup>. They found that  $\sim 25\%$  of these MSS sources were “ordinary” stars, primarily late-type dwarfs;

---

<sup>5</sup>As defined by Maccacaro et al. (1988):  $\log(f_X/f_V) = \log f_X + \frac{V}{2.5} + 5.37$ .

<sup>6</sup>Very Large Array observations were also used to search for radio sources near the MSS positions; these are very useful for identifying extragalactic X-ray sources (Stocke et al., 1983).

they also found one cataclysmic variable (see Chapter 3).

Stocke et al. (1991) used much the same strategy to identify counterparts to the 835 EMSS sources, but did not obtain spectra for every optical object near the new X-ray positions. Instead, they began by identifying plausible counterparts based on their optical properties as described by the Palomar data. Their work with the MSS confirmed that a given class of X-ray emitters has a fairly narrow range of possible X-ray-to-optical flux ratios (e.g., for active galactic nuclei,  $-1.0 \leq \log (f_X/f_V) \leq +1.2$ ), and, perhaps more importantly, that the overlap between broad classes (e.g., Galactic and extragalactic sources) is fairly small; see Table 1.1. Furthermore, in ambiguous cases, one could discern whether a given potential counterpart was in fact likely to belong to the class suggested by its  $f_X/f_V$  ratio by examining its morphology and/or color on the Palomar plates. For example, extragalactic X-ray sources with very low  $f_X/f_V$  ratios are often resolved galaxies or very blue point sources on the Palomar plates, while Galactic sources with high  $f_X/f_V$  ratios are generally very red late-type stars (Stocke et al., 1991).

Table 1.1: Observed X-ray-to-optical flux ratios, from Maccacaro et al. (1988).

Object class	$\log (f_X/f_V)$ range
Active Galactic Nuclei	-1.0 to +1.2
BL Lac objects	+0.3 to +1.7
Clusters of galaxies	-0.5 to +1.5
Normal galaxies	-1.8 to -0.2
M stars	-3.1 to -0.5
K stars	-4.0 to -1.5
G stars	-4.3 to -2.4
B-F stars	-4.6 to -3.0

Even with a more efficient algorithm for identifying plausible optical counterparts,

however, Stocke et al. (1991) were forced to obtain two to five spectra in each X-ray field, a very time-intensive exercise<sup>7</sup>. They confirmed that roughly one-quarter of the X-ray sources detected by *Einstein* are Galactic stars; in addition, using further (échelle) observations, they determined  $v \sin i$  for a subsample of these stars to examine the relationship between rotation and activity discussed in §2.2 (Stocke et al., 1991).

*from the ROSAT surveys*

While admirably thorough and essential in producing an unbiased sample of X-ray source counterparts, the approach described above is simply too time-consuming to be applied when searching for counterparts to the sources detected at soft X-ray energies (0.1 – 2.4 keV) by the *ROSAT* All-Sky Survey (RASS; Voges et al., 1999). More than 124,000 sources are included in the combined Bright and Faint Source Catalogs (BSC, FSC; Voges et al., 1999, 2000). Only a relatively small fraction of these sources, however, can be identified from correlations to existing databases. For example, Bade et al. (1998) found that 35% of the 80,000 RASS sources they considered had counterparts in SIMBAD and the NASA/IPAC Extragalactic Database, with the rest being previously unknown. While the typical positional uncertainty for these RASS sources ( $\sim 20''$ ) is smaller than that of the *Einstein* sources, using the Stocke et al. approach in this case would still imply taking spectra for one or more objects in more than 50,000 X-ray fields!

Instead, Bade et al. (1998) used objective prism spectra previously obtained with the Hamburg Schmidt telescope located in Calar Alto, Spain, as part of a large-scale search for quasars, the Hamburg Quasar Survey (HQS; Hagen et al., 1995). The HQS aimed to build a complete sample of fairly bright quasars in 14,000 deg<sup>2</sup> of northern sky through the extraction and classification of spectra from objective prism plates. Each such plate included spectra for objects brighter than  $B \approx 18.5$  mag within the  $5.5 \times 5.5$  deg<sup>2</sup> field of view, and was complemented by a direct (imaging) plate of the same area of the sky, which recorded objects brighter than  $B \approx 20$  (Hagen et al., 1995; Bade et al.,

---

<sup>7</sup>For example, six to eight nights a year over seven years were needed at the Multiple Mirror Telescope Observatory, Mt. Hopkins, AZ, to identify 665 of these sources (Stocke et al., 1991).

1998). The exposure times to reach these magnitude limits and appropriate signal-to-noise ratios were 60 and 45 min, respectively, for the objective prism and direct plates, making it possible to cover the northern sky in a reasonable amount of time<sup>8</sup>.

Bade et al. (1998) began by identifying the RASS BSC sources that fell within a given HQS field. For each such source, they proceeded to search the HQS data for all optical objects within the greater of  $40''$  and  $20'' + 2\sigma$ , where  $\sigma$  is the quoted RASS positional uncertainty. All of the spectra thus flagged were then classified interactively and their  $f_X/f_B$  ratios were calculated. A given object was suggested as the likely optical counterpart if it was reasonably close to the X-ray position, had the spectrum of a known type of X-ray emitter, and had an X-ray-to-optical flux ratio consistent with other similar X-ray emitters (Bade et al., 1998). The source's X-ray properties, such as its hardness ratios (relatively crude measurements of the spectral energy distribution<sup>9</sup>) and extent, were also invoked to strengthen the identification (e.g., clusters of galaxies appear as extended sources in the RASS). In this manner they found candidate counterparts for 81.2% of the 3847 RASS BSC sources within the HQS<sup>10</sup>. Of these, 155 (4%) were identified as M stars, 136 (3.5%) as K stars, 4 (0.1%) as F or G stars; a further 956 (24.9%) were saturated bright stars ( $B \leq 14$  mag), for which no spectral class is available. There was also a smattering of white dwarfs (31, or 0.8%) and cataclysmic variables (16, or 0.4%) (Bade et al., 1998). While there are uncertainties associated with these identifications—due to the very low resolution of the spectra ( $R \approx 100$  at  $H\gamma$ ), for example, or to the presence of multiple plausible counterparts within a field—the RASS/HQS program suggests that roughly one-third of the X-ray sources detected by *ROSAT* are Galactic stars.

This work was continued by Zickgraf et al. (2003), who applied the same technique to produce a catalog of optical counterparts for all 5341 RASS BSC sources with  $\delta \geq 0^\circ$

---

<sup>8</sup>In fact, the truly time-consuming part of the HQS was the digitization of the plates, which took three hours for each of the objective prism plates and nine hours for the direct plates (Hagen et al., 1995).

<sup>9</sup> $HR1 = \frac{(0.5-2.0)-(0.1-0.4)}{(0.1-0.4)+(0.5-2.0)}$  and  $HR2 = \frac{(1.0-2.0)-(0.4-1.0)}{(1.0-2.0)}$ , where, for example, (0.5 – 2.0) indicates the number of counts in the 0.5 – 2.0 keV energy range (Motch et al., 1998).

<sup>10</sup>Bade et al. (1998) suggest that the unidentified sources are likely to be faint active galactic nuclei and clusters.

and Galactic latitudes  $|b| \geq 30^\circ$ . The search radius was expanded to  $60''$ , and imaging data from the Digitized Sky Survey was used when there was no HQS direct Schmidt plate for a given field; the total area thus covered was  $10,313 \text{ deg}^2$  (Zickgraf et al., 2003). Candidate counterparts for 82.2% of the RASS sources were found; the “missing” counterparts are, for the most part, faint optical objects whose poor-quality prism spectra preclude classification. The fraction of the 5341 BSC sources due to coronal emission from stars increased from one-third to roughly 38% when one estimated the number of likely stellar sources among the “missing” counterparts (Zickgraf et al., 2003). Interestingly, this is a higher fraction than that of stellar sources in the EMSS, a difference that may be due to the slightly different energy sensitivities of *ROSAT* and *Einstein* (Gioia et al., 1990; Zickgraf et al., 2003). The final RASS/HQS sample includes 197 M stars, 141 K stars, 45 F/G stars, and 1219 saturated stars without spectral classifications, along with 45 white dwarfs and 26 cataclysmic variables.

A number of other programs have used variants on this technique either to identify large numbers of counterparts to RASS sources or to identify all of the counterparts to RASS sources in a small area of sky (e.g., 442 sources in  $80.6 \text{ deg}^2$  around the north ecliptic pole; Henry et al., 2006). However, the Zickgraf et al. (2003) catalog remains the single largest sample of RASS sources for which counterparts have been proposed in this manner; in fact, close to 90% of the X-ray sources detected by *ROSAT* have yet to have likely counterparts identified through some such combination of photometry and spectroscopy (Mickaelian et al., 2006).

Parallel efforts have been made to produce large-scale catalogs of RASS counterparts *without spectroscopy*. As part of the BSC data release, Voges et al. (1999) correlated its 18,811 X-ray sources with a number of existing catalogs, including, for example, of bright stars (Tycho) or of radio and ultraviolet sources (FIRST, NVSS, and EUVE). They found at least one cataloged counterpart within  $90''$  for 90% of the BSC sources. 7,117 X-ray sources had a single cataloged counterpart, which Voges et al. (1999) used to establish the overall statistical properties of the BSC sources: 58% of these counterparts were Galactic in origin. This matching was entirely based on positional coincidence (i.e., only the closest match was considered) and relied on the

relatively low surface densities of the BSC sources and the various cataloged counterparts, along with the X-ray properties of the counterparts (especially their  $f_X/f_{opt}$  ratio, hardness ratios, and extent), to claim an association between a BSC source and a counterpart (Voges et al., 1999).

Rutledge et al. (2000) adapted this method to match statistically the BSC to the USNO A-2 catalog. Factoring in both the proximity and the  $B$  magnitude of the USNO objects found within  $75''$  of the RASS sources, and carefully estimating the contamination rate by comparisons to background fields, they sifted through the more than 320,000 possible optical counterparts to identify those with the highest probability of being the X-ray sources. Their final catalog included 11,301 BSC sources—three-fifths of the total number—for which they identified a USNO object with a  $\geq 50\%$  probability of being the counterpart (2705 had a probability  $\geq 98\%$ ; Rutledge et al., 2000).

In an even more ambitious effort, Flesch & Hardcastle (2004) matched X-ray data from *all* of the major *ROSAT* catalogs to multiple radio and optical surveys, thereby creating an all-sky catalog of radio/optical counterparts to some 500,000 X-ray sources<sup>11</sup>. Nearly 120,000 of these sources were previously identified in the literature, while an additional 86,000 are estimated to be 40% to 99% likely to be previously unknown quasars. The likelihood of a given association was calculated first by examining the proximity of a proposed counterpart, its  $B - R$  color, and its optical classification, and then by comparing the density of all candidate counterparts with these properties to their all-sky density (Flesch & Hardcastle, 2004)<sup>12</sup>.

These catalogs are clearly very useful for developing a statistical overview of a given category of X-ray emitters; typically, their production is driven by the desire to obtain a large sample of quasars (e.g. Bauer et al., 2000; Flesch & Hardcastle, 2004)<sup>13</sup>.

---

<sup>11</sup>Matching to the radio sources is done first; the assumption is that the surface densities of radio sources and X-ray sources are both sufficiently low that matches can be safely associated. The radio positions can then be substituted to the far less certain X-ray positions and used to match to the optical catalogs (Bauer et al., 2000).

<sup>12</sup>For example, if the density of stars with  $(B - R) = 0$  within  $5''$  of the X-ray sources is 10 times greater than elsewhere on the sky, the likelihood that these are the X-ray counterparts is 90%: for 10 such objects, 9 are X-ray sources, and 1 is not (Flesch & Hardcastle, 2004).

<sup>13</sup>As a consequence, there is usually almost no discussion of the stellar emitters found in these catalogs.

However, because they rely in large part on the properties of known counterparts to identify new counterparts, the catalogs cannot tell us anything more about the overall properties of X-ray sources than the smaller catalogs on which they are based (Flesch & Hardcastle, 2004). In that sense, these catalog-based approaches cannot fully replace the combined photometric and spectroscopic method first developed for identifying *Einstein* sources.

*from Chandra and XMM surveys*

While *Chandra* and *XMM* are both equipped with more sensitive X-ray detectors than *ROSAT* (albeit in different energy bands), they were designed primarily to conduct pointed observations and not wide-field surveys<sup>14</sup>. However, growing data archives have allowed the creation of a number of fairly deep, relatively small-area surveys, with the lists of X-ray sources being assembled in much the same way as for the *Einstein* MSS and EMSS surveys—and with the X-ray counterparts being identified using variations on the classic *Einstein* method. Generally, these counterparts are far fainter than for the *Einstein* sources; Dietrich et al. (2006) find that only 15% of the counterparts to their *XMM* sources are brighter than the Digital Sky Survey limit of 20.5 mag. Programs to find these counterparts therefore tend to rely on dedicated deep optical imaging, as opposed to pre-existing survey data, to select targets for follow-up spectroscopy. This selection is often easier than for the earlier generation of X-ray surveys because the X-ray and optical positional uncertainties are comparable and very small (typically less than 1'' for *Chandra*). However, the proposed counterparts are sometimes simply too faint and the corresponding spectra cannot be classified, limiting the number of X-ray sources for which a counterpart can be confirmed.

The *Chandra* Multiwavelength Project (ChAMP; Kim et al., 2004) collected X-ray sources from 137 targeted observations of objects away from the Galactic plane. The total ChAMP area is roughly 14 deg<sup>2</sup> and includes 486 X-ray sources with fluxes between  $3 \times 10^{-16}$  and  $2 \times 10^{-13}$  ergs cm<sup>-2</sup> s<sup>-1</sup> in the 0.3 – 8 keV energy band in which *Chandra*

---

<sup>14</sup>A notable exception is the recent *XMM-Newton* Slew Survey, which collected exposures of  $\leq 15$  s taken as the satellite slewed to produce a list of  $\sim 4000$  sources in 6300 deg<sup>2</sup> (Freyberg et al., 2005).

operates (Green et al., 2004). An initial catalog of ChaMP counterparts was produced from matching the X-ray source positions to those of optical objects found in follow-up imaging of the fields. Spectroscopy was then used to characterize these optical counterparts. Of the 356 ChaMP sources with high-confidence spectroscopic identifications, only 64 are stars (P. J. Green 2006, private communication). This represents a relatively small fraction (18%) of the ChaMP sources, but is entirely consistent with the survey’s extragalactic focus<sup>15</sup>.

The *Chandra* Multiwavelength Plane (ChaMPlane; Grindlay et al., 2005) survey is very similar in design to ChaMP, but uses archival observations of 105 distinct fields covering roughly  $23 \text{ deg}^2$  of the Galactic plane; the typical limiting X-ray flux for these observations is  $\sim 1 - 6 \times 10^{-15} \text{ ergs cm}^{-2} \text{ s}^{-1}$ . ChaMPlane aims to add to the population of known low-luminosity X-ray binaries ( $L_X \leq 10^{34} \text{ erg s}^{-1}$ ), and one would of course expect it also to catalog many coronal emitters. Grindlay et al. (2005) predict that it will eventually expand the *ROSAT* sample of such sources by one to two orders of magnitude. ChaMPlane uses follow-up optical imaging slightly differently than most other surveys: if narrow-band imaging reveals optical objects in the X-ray fields with  $H\alpha$  excesses, these are targeted for spectroscopic follow-up, *regardless of whether they are positionally coincident with a Chandra source* (Rogel et al., 2006)<sup>16</sup>. To date, Rogel et al. (2006) have obtained spectroscopy for 1069 sources; because of the faintness of many of these counterparts ( $R \leq 24 \text{ mag}$ ), classifications are possible for only about 60% of these targets. Of the 612 optical objects currently identified, 437 are K and M stars (71%!); 182 of these have spectra with obvious  $H\alpha$  emission, a sure sign of activity (Rogel et al., 2006).

Similar efforts are underway with data from *XMM-Newton*, which is sensitive to X rays in the 0.2 – 12 keV range. The Serendipitous Sky Survey (Watson et al., 2001) is cataloging new X-ray sources at a rate of close to 50,000 a year, and a number

---

<sup>15</sup>In addition, this fraction should only be considered a lower limit on the number of stellar ChaMP sources, since the spectroscopic follow-up is not completed (P. J. Green 2006, private communication) and is presumably biased toward photometrically selected candidate quasars.

<sup>16</sup>Ironically, the five new cataclysmic variables discovered to date as part of the ChaMPlane follow-up do not currently have *Chandra* detections (Rogel et al., 2006).



of follow-up optical programs are designed to identify the counterparts to (some of) these sources (e.g., Motch et al., 2003; Dietrich et al., 2006). There is also at least one dedicated *XMM* survey program, the *XMM* Galactic Plane Survey (XGPS; Hands et al., 2004). The fraction of stellar X-ray emitters found in these different surveys varies as a function of the area of the sky they cover and in any case will probably not be known for some time—while frequently only one spectrum is needed to reveal the nature of a cataloged *XMM* or *Chandra* X-ray source, the proposed optical counterpart is often very faint, and the spectroscopic follow-up therefore requires significant time and resources (e.g., for ChaMPlane to date, 17 nights with the Hydra multi-object spectrograph on the WIYN 3.5-m telescope, Kitt Peak, AZ; Rogel et al., 2006).

### **1.3 The RASS and SDSS, and a Thesis Preview**

As mentioned above, no more than 10% of RASS sources have had their counterparts identified and fully characterized (Mickaelian et al., 2006). A major obstacle to identifying more RASS sources was the absence of a large-area optical survey of equivalent sensitivity with which to correlate the RASS catalogs. However, the RASS and SDSS are very well matched, making SDSS an ideal tool for identifying large numbers of *ROSAT* sources. For example, previous programs to identify RASS counterparts indicate that roughly 40% will be quasars and related active galactic nuclei (AGN; e.g., Bade et al., 1998; Zickgraf et al., 2003), and we have demonstrated the effectiveness of the SDSS photometry and spectroscopy in finding the optical counterparts to these RASS sources. With about one-fifth of the SDSS survey completed, we identified  $\sim 1200$  X-ray-emitting AGN using a combined RASS/SDSS approach (Anderson et al., 2003). Our high efficiency for finding quasar counterparts arises because the limiting X-ray flux of RASS is such that even the optically faintest counterparts of typical RASS AGN are likely to be detected in the SDSS photometric survey and can be targeted in the spectroscopic survey. The most X-ray luminous (relative to optical) quasars have  $\log(f_X/f_{opt}) \sim 1$  (see Table 1.1; Maccacaro et al., 1988). At the typical limiting RASS X-ray fluxes, this implies that even unusually faint optical AGN will be

brighter than  $m \sim 20$  mag—well within the SDSS photometric limit and accessible to routine SDSS spectroscopy.

Roughly another third of RASS counterparts are expected to be Galactic stars (e.g., Bade et al., 1998; Gioia et al., 2003; Zickgraf et al., 2003). However, unlike quasars, the vast majority of stellar X-ray emitters cataloged in the RASS are unlikely to be discovered from routine SDSS spectroscopy. Relative to their optical output, the most X-ray luminous normal stars (i.e., coronal emitters) have  $\log (f_X/f_{opt}) \sim -1$  (Maccauro et al., 1988) and so almost all are optically *brighter* than the  $m \approx 15$  SDSS spectroscopic limit.

In order to identify these bright stellar X-ray emitters included in the RASS and falling within the footprint of the SDSS Data Release 1 (DR1; Abazajian et al., 2003), I have therefore used the SDSS photometric data, combined with infrared data from the Two Micron All Sky Survey (2MASS; Skrutskie et al., 2006), to select a sample of bright stars near BSC/FSC positions. I then used the Astrophysical Research Consortium 3.5-m telescope at the Apache Point Observatory<sup>17</sup> to obtain spectroscopy for objects in about 900 of these RASS fields (the total number of spectra collected is close to 1200). A spectral-template fitting code was then used to type the likely X-ray counterparts. The cataloged magnitudes are used to obtain estimated  $f_X/f_{opt}$  ratios for these stars; the ratios are then compared to those of known X-ray emitters of the same spectral type, thereby verifying that these stars are indeed plausible RASS source counterparts. I present the results of this work in Chapter 2.

In addition, I have worked on identifying other, rarer types of stellar X-ray emitters in the SDSS spectroscopic footprint. Among these are cataclysmic variables (CVs) and white dwarfs (WDs), for which the typical optical counterpart magnitudes are within the SDSS spectroscopic target range. Accordingly, the SDSS spectroscopic survey is used to confirm the nature of these RASS sources; because they have relatively low surface densities, the entire SDSS survey area is searched for these objects. I have contributed to a series of papers (Szkody et al., 2002, 2004a, 2005, 2006) that

---

<sup>17</sup>The Apache Point Observatory 3.5-m telescope is owned and operated by the Astrophysical Research Consortium.

include descriptions of the X-ray properties of SDSS CVs, and this work is summarized in Chapter 3. I have also correlated the SDSS white dwarf catalogs (Kleinman et al., 2004; Eisenstein et al., 2006) with the RASS to identify X-ray emitters, and used the high quality and uniformity of the SDSS spectra to create composite WD spectra. These will eventually be used to search for unexpected WD spectral features by comparing the composite spectra for X-ray emitters to those from the much larger sample of “ordinary” WDs, for example. I present this work in Chapter 4.

Finally, I used RASS/SDSS correlations to search for new candidate isolated neutron stars (INSs), probably the most elusive stellar X-ray sources in the RASS. Stellar evolution predicts that the number of detected pulsars in the Galaxy ( $\sim 2000$ ) should be dwarfed by the number of older, inactive neutron stars, most of which are too cool to be visible in the X-ray and rotate too slowly to generate radio pulses. However, some of these stars may reheat by accreting material from the interstellar medium, and *ROSAT* was expected to detect hundreds to thousands of rejuvenated NSs (e.g. Treves & Colpi, 1991; Blaes & Madau, 1993). These INSs were predicted to have blackbody spectra that would place strong constraints on the NS equation of state (EOS). Yet only seven INSs are currently known (the “Magnificent Seven”), a sample that manages to be both too small and too diverse in detail to address the EOS definitively. Clearly, obtaining a larger sample is highly desirable. This work is presented in Chapter 5.

I summarize my findings in Chapter 6, where I also discuss a few research questions I plan to pursue that build on this thesis.

## Chapter 2

# A CATALOG OF X-RAY-EMITTING STARS FROM THE *ROSAT* ALL-SKY SURVEY AND THE SLOAN DIGITAL SKY SURVEY DATA RELEASE 1

## 2.1 Introduction

X-ray data obtained since the 1970s have shown definitively that stellar X-ray emitters are present among almost all stellar classes (e.g., Harnden et al., 1979; Cassinelli & Swank, 1983; Stocke et al., 1983; Schmitt et al., 1995; Motch et al., 1998; Zickgraf et al., 2003; Rogel et al., 2006), with the emission mechanism being different for early and late-type stars; only evolved K and M stars and perhaps A stars do not appear to be X-ray emitters (e.g., Ayres et al., 1981; Antiochos et al., 1986; Haisch et al., 1991; Daniel et al., 2002). However, within a given stellar class—particularly among late-type stars—the strength of the X-ray emission varies immensely. A given G5 star may be much brighter in the X-ray regime than its apparent twin, suggesting that the physics of X-ray emission is intimately linked to detailed stellar properties<sup>1</sup>. X-ray spectroscopy with the *Chandra X-ray Observatory* and *XMM-Newton X-ray Observatory*, occasionally in conjunction with observations at other wavelengths, is providing unprecedented insight into these connections (e.g., Osten et al., 2005; Smith et al., 2005). Before such detailed studies can be conducted, however, catalogs of confirmed X-ray-emitting stars from all areas of the Hertzsprung–Russell diagram need to be compiled and broadly characterized.

In this Chapter, we describe an effort to identify a complete sample of X-ray selected normal stars falling within the footprint of the Sloan Digital Sky Survey (SDSS; York et al., 2000) Data Release 1 (DR1; Abazajian et al., 2003). We begin with an overview of the mechanisms for X-ray production from stars, focusing in particular

---

<sup>1</sup>Individual stars also can also be X-ray variables.

on coronal emission and flares from Sun-like stars (Section 2.2). In Section 2.3, we outline the process by which we identified our candidate DR1 stellar counterparts to *ROSAT* All-Sky Survey (RASS; Voges et al., 1999) sources. In Section 2.4, we describe how we made our stellar identifications and obtained our sample of stellar X-ray sources. We produced two catalogs; one is of 322 stars that are typically very bright (the median  $V \approx 9$  mag) and are included in SIMBAD and occasionally in the NASA/IPAC Extragalactic Database (NED)<sup>2</sup>. The other is of 492 new stellar X-ray source identifications made on the basis of spectroscopic observations with the Apache Point Observatory (APO) 3.5-m telescope. In the Appendix we excerpt data from both catalogs, which include the X-ray, optical, and infrared information for our proposed stellar X-ray sources. The full catalogs are available on-line at <http://www.astro.washington.edu/agueros/pub>.

## **2.2 Mechanisms for Stellar X-ray Emission**

### *2.2.1 Coronal emission from late-type stars*

#### *The solar corona and RTV models*

Any discussion of our understanding of X-ray emission for stars later than spectral type F requires a detour into the history of models of the solar corona. Early on, the prevailing view was that solar X rays were produced in a hot inner region of the solar wind. High-resolution imaging data from *Skylab* (1972–74) were essential in overthrowing this picture of the corona as a relatively simple structure, revealing it instead to be a highly complicated collection of loops formed as the Sun’s magnetic field emerges from the photosphere (e.g., Poletto et al., 1975).

Spherically symmetric acoustic heating models, in which the dissipation of sound waves originating within the Sun powered the corona, were then replaced by a far more complicated theoretical picture. First outlined by Rosner et al. (1978) and Craig

---

<sup>2</sup>This research has made use of the SIMBAD database, operated at CDS, Strasbourg, France, and of the NASA/IPAC Extragalactic Database, operated by the Jet Propulsion Laboratory, California Institute of Technology, under contract with the National Aeronautics and Space Administration.

et al. (1978), the new models, generally referred to as the Rosner, Tucker, and Viana (RTV) models, treat the aforementioned loops as the basic building blocks for the corona. Each loop is described as a miniature atmosphere, self-contained and one-dimensional. Input energy is distributed through thermal conduction and eventually radiated away, mainly in spectral lines. The loops are short-lived; they become visible as heated chromospheric material is evaporated and fills them, and are maintained as long as the input energy and radiative losses are in rough equilibrium.

The RTV loop models include scaling relationships, and are therefore an extremely useful starting point for coronal studies of other stars; in particular, the length of the loops can be derived from the X-ray luminosity. Schrijver et al. (1984) applied these relations to a sample of *Einstein* spectra to determine that, in general, the surface of inactive main-sequence (MS) stars such as the Sun is covered almost entirely by relatively small, cool loops ( $R \sim 0.1R_*$  and  $T \sim 2 \times 10^6$  K). By contrast, the loops on moderately active MS stars are hotter ( $\sim 2 \times 10^7$  K), more compact, denser, and require larger heating rates. Finally, the most active MS stars may have additional extended loops of lengths  $\sim R_*$ .

### *The connection with rotation*

As noted earlier, while it is likely that every late-type star is an X-ray emitter at some level, an individual late-type star can have a very different X-ray luminosity compared to other members of its spectral class. The groundbreaking study of *Einstein* stellar sources by Pallavicini et al. (1981) identified a relationship between the X-ray luminosity and the projected rotational velocity  $v \sin i$ :  $L_X \approx 10^{27} (v \sin i)$ , where  $v$  is measured in  $\text{km s}^{-1}$ . Over time, a low-mass star loses angular momentum through its wind, and therefore spins down. As a consequence, its magnetic dynamo is weakened, reducing activity and X-ray emission (a sequence of events originally described by Skumanich, 1972, who used CaII emission strength as a measure of magnetic activity). Observations of fast rotators show that they do have higher X-ray luminosities, but only up to the point, known as saturation, when  $L_X$  reaches  $\sim 10^{-3} L_{bol}$  (a fraction 1,000 times

greater than in the Sun; Haisch & Schmitt, 1996; Robrade & Schmitt, 2005). Increased activity implies that a larger fraction of the stellar surface is covered by coronal loops, which, for a given stellar type and therefore stellar radius, sets the saturation limit. Less obviously, the existence of the saturation limit suggests that there is a limit to how much heating energy a star can deposit into its corona, and therefore sets a maximum efficiency for the underlying magnetic dynamo. This efficiency is described by the Rossby number, which is defined as the ratio of the rotational period and the convective turnover time (Robrade & Schmitt, 2005)<sup>3</sup>.

The relationships described above between  $L_X$ ,  $L_{bol}$ , and  $v \sin i$  imply that the rotational velocity at which a given star will saturate depends on its spectral class. Indeed, in their study of 110 field stars and 149 members of open clusters detected by *ROSAT*, Pizzolato et al. (2003) found that the saturation period varies from one day for early G stars to roughly four days for early M stars. For non-saturated stars in that same spectral range, they confirmed that rotation is an excellent predictor of activity.

### *Some unresolved problems*

While the RTV formalism has withstood the test of time rather well, it suffers from our still far-from-perfect understanding of magnetic fields<sup>4</sup>. The loops observed on the Sun vary significantly in shape and size, suggesting that the magnetic mechanisms responsible for their production are not quite as uniform as RTV models would indicate (e.g., Aschwanden et al., 2000). More sophisticated hydrostatic models that produce emission spectra one can compare directly to observations have also muddied the waters, in particular by implying that several types of magnetic loops may have to co-exist on a given star to explain the X-ray data (see Güdel, 2004, and discussion therein). However, since these models also rely on a set of assumptions (they require some *a priori* knowledge of the statistical distribution of loop parameters within a

---

<sup>3</sup>There is also observational evidence for super-saturation: when rotational velocities exceed  $100 \text{ km s}^{-1}$  (i.e., when the Rossby number becomes very small), the  $L_X/L_{bol}$  ratios begin to decrease slightly. Why this should be is still not well understood (Güdel, 2004).

<sup>4</sup>RTV models also do not identify the origin of the loop input energy, whose source remains elusive (e.g., Pevtsov et al., 2003).

corona, for example), they have not yet definitively supplanted the RTV picture.

Furthermore, while the presence of an active corona implies the constant generation of a magnetic field, the processes responsible for its production are still poorly understood. Solar-type stars are thought to host dynamos created by a combination of bulk motion in the stellar interior, rotation, and a pre-existing magnetic field. These dynamo are generally described in terms of two effects: the twisting of the magnetic field due to convective eddies (the  $\alpha$  effect) and the shearing of the toroidal component of the magnetic field due to differential rotation (the  $\Omega$  effect). Helioseismic observations of the Sun and theoretical predictions place its  $\alpha$ - $\Omega$  dynamo at the boundary between the radiative core and the convective envelope (Favata & Micela, 2003).

We still lack a predictive, self-consistent model for the solar dynamo, however. In addition, stars later than mid M are thought to be fully convective; extending the solar dynamo model to these stars (and to slow rotators) would predict that they should show little to no activity. Observations find instead that the fraction of active M stars *increases* from spectral type M0 to M8 (Hawley et al., 1996; West et al., 2004). While some models suggest that convective eddies are sufficient to generate a so-called  $\alpha^2$  dynamo in these stars (e.g., Durney et al., 1993), recent work argues that various feedback mechanisms may in fact generate turbulent dynamos that are comparable to the  $\alpha$ - $\Omega$  dynamos in earlier-type stars (e.g., Dobler et al., 2006). In short, we are far from having a complete picture of how the Sun’s magnetic field forms, is maintained, and produces the magnetic loops responsible for coronal emission, or of how universal those mechanisms are. For example, Schrijver (1987) identified a “basal flux density” due to some form of magnetic activity in X-ray, ultraviolet, and optical observations of a sample of inactive F through K stars. This emission is unrelated to the corona, and may well be due to acoustic heating (e.g., Bercik et al., 2005).

Finally, the connection between  $L_X$  and rotation, if any, is not evident for M and later-type stars. As mentioned earlier, later M stars tend to be more active as a class than early M stars, with no obvious correlation with rotation; the even later L and T dwarfs are faster rotators than typical M dwarfs (e.g., Bailer-Jones, 2004) yet show weak activity at best (e.g., Reid et al., 2000).



### 2.2.2 *Flares from late-type stars*

Coronal X-ray emission from the Sun and other late-type stars is highly variable. Over time periods of minutes to hours, this variability is mainly due to flares, events in which an individual coronal loop or group of loops suddenly brightens; the largest stellar flares have been observed to have decay times of several days. These events can dominate the observed X-ray emission, significantly outshining the rest of the observed corona<sup>5</sup>. The intensities of flares in active stars can be orders of magnitude greater than those of solar flares, with peak plasma temperatures of over  $10^8$  K (Favata & Micela, 2003). Such a flare's effect can be measured across the electromagnetic spectrum, and in the case of the Sun, in the ejection of high-energy particles. Observations of flares can be used to determine the physical size of the flaring region, the strength of the local magnetic field, and the density of the plasma, among other things. They also give us insight into the most extreme forms of coronal activity, and thereby provide useful constraints on, for example, heating of the stellar corona.

Most flare models start from the assumption that the energy released in a flare is converted magnetic energy produced by the sudden and catastrophic reconnection of stressed magnetic loops. Solar data have been used to build upon this starting point and develop the widely accepted models for the production of a flare (e.g., Dennis & Schwartz, 1989). The reconnection region, situated high in the corona, accelerates electrons to energies on the order of tens of keV. These travel along the magnetic field lines down into the chromosphere, emitting synchrotron (radio) radiation; collisions with ions along the way also produce hard bremsstrahlung X rays. Once in the chromosphere, they heat the cooler ambient gas to coronal temperatures, thereby evaporating some of it upwards into the corona, and produce optical continuum and line emission. Meanwhile, as the evaporated chromosphere fills the coronal loop, it generates soft X rays. This sequence of events predicts a spatial and temporal correlation between the appearance of hard X rays and optical emission during a flare, with the emission of

---

<sup>5</sup>For all but the youngest and most active stars, however, the energy emitted in flares remains a very small fraction of the total energy budget (Favata & Micela, 2003).

soft X rays reaching a later peak. The soft and hard X-ray emission are connected by the Neupert effect (Neupert, 1968), which predicts that the flux in soft X rays should be equal to the time-integrated flux in hard X rays—an effect measured in 80% of the solar flares studied by Dennis & Zarro (1993).

While observations of flares on other stars have detected the Neupert effect (e.g., Hawley et al., 1995), other details of this scenario are harder to verify, and do not appear to be consistent from flare to flare. In any case, our models of the corona and chromosphere during a flare are imperfect, and much work is underway to produce better radiative models of the flare emission for both the Sun and other stars (e.g., Allred et al., 2005, 2006). See Favata & Micela (2003) and Güdel (2004) for extensive discussions of current flare models and comparisons to flare data<sup>6</sup>.

### 2.2.3 X rays from other stars

#### *Early type stars*

*Einstein* found that *all* stars of spectral type B5 or earlier are X-ray emitters, with  $L_X$  varying between  $10^{30}$  and  $10^{34}$  erg s<sup>-1</sup> (e.g., Harnden et al., 1979). The X-ray properties of these stars, however, are very different from those of later-type stellar sources. In particular, there is a nearly linear relationship between the bolometric and X-ray luminosities for early type stars; this is not observed in late-type X-ray sources. From their survey of O stars detected by *Einstein*, Sciortino et al. (1990) determined that  $L_X \approx 4.2 \times L_{bol}^{1.08}$ . This relationship is consistent with the previously developed picture of X-ray emission originating in hot, shocked regions of the radiatively driven winds commonly found around these stars (e.g., Cassinelli & Swank, 1983).

Interestingly, the fact that X-ray emission from early type stars requires the presence of winds while that from late-types is reliant on the existence of a magnetic dynamo leads to the prediction that there should be a gap in the X-ray-emitting main sequence. Stars less massive than B are not expected to generate the needed winds,

---

<sup>6</sup>While we have focused this discussion on flares from late-type stars, flares are in fact observed in all coronally active stars, including, for example, giant and post-He-flash stars (e.g., Ayres et al., 2005).

while stars more massive than early F or late A lack a convective outer layer and therefore an  $\alpha$ - $\Omega$  dynamo. This prediction has largely been confirmed by observations, with a few exceptions. The most likely explanation for these is the presence of an unresolved late-type companion responsible for the X-ray emission. For example, in their study of the Pleiades, Daniel et al. (2002) find five binary systems where the low-mass companion to an early type star is the coronal X-ray emitter—but fail to detect two other known A stars lacking a late-type companion.

### *Evolved stars*

One of the curious results to emerge from studies of X-ray emission from giants and supergiants is the existence of the so-called dividing line separating (hotter) G giants from (cooler) K and M giants. This was first observed in observations with the *International Ultraviolet Explorer* (Linsky & Haisch, 1979), and confirmed by later *Einstein* and *ROSAT* observations (e.g., Ayres et al., 1981; Haisch et al., 1991). G giants, which are to the left of the dividing line in a classic Hertzsprung–Russell diagram, can have X-ray luminosities up to  $\sim 3 \times 10^{30} \text{ erg s}^{-1}$ . However, by the time they migrate to the right of the line, observations indicate a drop in X-ray luminosity of these stars to  $\leq 3 \times 10^{25} \text{ erg s}^{-1}$ ! The reason for this sudden drop-off in X-ray emission is not understood, particularly since late-type giants should still host a magnetic dynamo.

Some work has suggested that the stellar winds these stars generate hold the key. These winds are cooler (20,000 K), slower ( $\leq 100 \text{ km s}^{-1}$ ), and much more massive ( $10^{-10}$  to  $10^{-7} M_{\odot} \text{ yr}^{-1}$ ) than those produced by the Sun ( $> 10^6 \text{ K}$ ,  $450 \text{ km s}^{-1}$ ,  $2 \times 10^{-14} M_{\odot} \text{ yr}^{-1}$ ) and presumably by other main-sequence stars (Haisch & Schmitt, 1996). It may be that these winds—combined with changes in the dynamo that reduce the loop sizes—suppress X-ray emission in these stars. This view has been strengthened by recent detections of weak X rays from the K1 giant Arcturus, which had previously been thought to be X-ray dark. Arcturus appears to have an emission region analogous to a hot corona, powered by magnetic processes, but buried below a thick chromosphere that acts as a barrier to X-ray emission (Ayres et al., 2003).

This overview of X-ray emission from normal stars demonstrates that the field of stellar X-rays, considered unpromising only a few years ago, is rich in unresolved questions and active research areas. Collecting samples of X-ray-emitting stars is therefore essential to explore the connections between stellar interiors, atmospheres, and coronae. In the remainder of this Chapter we describe our efforts to identify such a sample from the RASS and SDSS.

### **2.3 Selection of X-ray Emitting Stars from the RASS and SDSS DR1**

Our version of the merged *ROSAT* All-Sky Survey Bright and Faint Source Catalogs (Voges et al., 1999, 2000) includes 124,730 X-ray sources (Anderson et al., 2003). We began by matching the X-ray source positions listed in this merged catalog to those of the SDSS Data Release 1 (DR1; Abazajian et al., 2003) stripes, using a code kindly provided by B. Willman. The survey uses great circle coordinates as one of its two coordinate systems, and in this system, the stripes are great circles with a common crossing point; in practice, each SDSS stripe is a 2.5-deg-wide rectangle of sky. We found 7464 RASS sources, or just under 6% of the cataloged X-ray sources, within 1' of the stripe edges. Since the DR1 area is 2099 deg<sup>2</sup> (Abazajian et al., 2003), or roughly 5% of the entire sky, this number is consistent with a naive surface density expectation; Figure 2.1 shows the DR1 area, in Galactic coordinates<sup>7</sup>.

In order to identify bright stars near these RASS sources, we first queried the SDSS photometric database using the SDSS Query Analyzer (sdssQA)<sup>8</sup>. The following is our sdssQA query, composed using Structured Query Language:

```
SELECT ra, dec, psfMag_u, psfMag_g, psfMag_r, psfMag_i, psfMag_z, type
FROM PhotoObjAll
WHERE psfMag_g < 16 OR psfMag_r < 16
AND (flags & dbo.fPhotoFlags('BRIGHT')) = 0
AND (flags & dbo.fPhotoFlags('DEBLENDED')) = 0
```

---

<sup>7</sup>The quoted DR1 area is for the imaging survey; the DR1 spectroscopic area is 1360 deg<sup>2</sup>.

<sup>8</sup>See <http://cas.sdss.org/dr4/en/help/download/sdssQA/default.asp> for a description.

`OR (flags & dbo.fPhotoFlags('SATURATED')) > 0`

`OR (flags & dbo.fPhotoFlags('SATURATED_CENTER')) > 0`

This query returns the coordinates, PSF magnitudes<sup>9</sup>, and automatically assigned type (star or galaxy) for objects brighter than 16 mag in either the  $g$  or  $r$  band, subject to a (small) number of tests of the objects' photometric flags. Very bright objects detected by the SDSS photometric pipeline have their properties measured twice before being cataloged—once with a global sky background, and once with the local sky. Setting the BRIGHT flag equal to 0 removes the first set of measurements from consideration; these are almost never used for analysis. The photometric pipeline attempts to deblend composite objects automatically, and the final SDSS database includes entries for so-called children, the various components of a deblended object. At the very bright end, where objects are saturated and stars can be confused with extended galaxies, deblending is often done inaccurately; requesting that objects have DEBLENDED = 0 rejects the children while keeping the parent object. By contrast, we request that the SATURATED or SATURATED\_CENTER flag be set; this occurs if there are saturated pixels in any of the five SDSS images ( $u, g, r, i, z$ ) of a given object (for a detailed discussion of the SDSS flags, see Stoughton et al., 2002).

The number of objects meeting this set of criteria is very large (several million objects), and, as discussed below, also highly contaminated. This is unsurprising, since we are seeking to identify the objects that the SDSS pipeline is least well equipped to handle, and are therefore very unrestrictive in our use of the photometric flags. The survey's goal is to obtain high-quality photometry and spectroscopy for objects fainter than have previously been cataloged, not to characterize very bright stars.

The final output from sdssQA was then matched to the RASS sources determined to be in the DR1 footprint<sup>10</sup>. This matching produced a list of slightly fewer than 5000 RASS sources with a bright/saturated SDSS object within 1', a very large fraction of

---

<sup>9</sup>PSF fitting typically provides better estimates of isolated star magnitudes; see Stoughton et al. (2002).

<sup>10</sup>Here and elsewhere we made use of the various TABLE routines in IRAF. IRAF (Image Reduction and Analysis Facility) is distributed by the National Optical Astronomy Observatories, which are operated by the Association of Universities for Research in Astronomy, Inc., under cooperative agreement with the National Science Foundation.

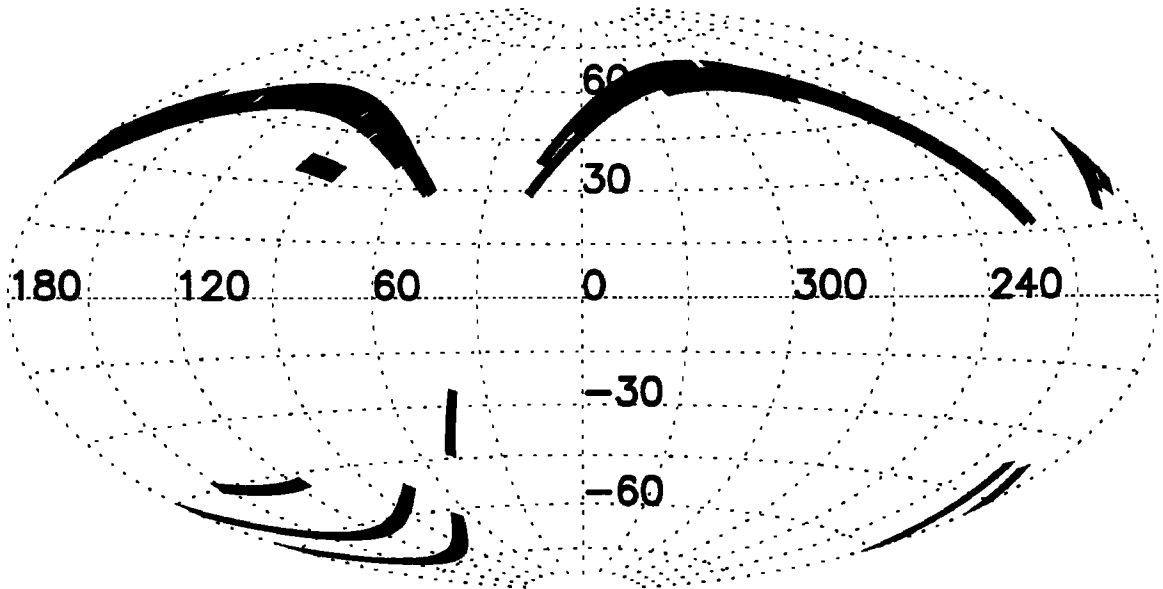


Figure 2.1: The SDSS DR1 imaging area, in Galactic coordinates. The DR1 spectroscopic area is smaller; spectroscopic targets are selected largely based on their photometric properties, and the spectroscopic survey trails the imaging one.

the total number of RASS/DR1 sources (about two-thirds!). However, visual inspection of the SDSS cut-out images for these 5000 sources discovered that a significant fraction did not in fact have a bright object in the field<sup>11</sup>. This contamination was presumably due to the presence of numerous objects with cataloged magnitudes of  $-9999$  (i.e., too faint for the photometric pipeline to assign a magnitude) in our `sdssQA` output. While a more conservative set of cuts using the photometric flags would have eliminated the bulk of these objects, it might also remove the real but saturated objects in which we are interested. We therefore chose instead to use the Two Micron All Sky Survey (2MASS; Skrutskie et al., 2006) to confirm the existence of a bright SDSS object. SDSS is a much deeper survey than 2MASS, whose  $J$ ,  $H$ , and  $K_S$  limits are  $14 - 15$  mag, and previous studies have shown that less than 10% of SDSS objects have a 2MASS counterpart (Finlator et al., 2000). At the bright end ( $r \leq 16$ ), however, the two surveys are

---

<sup>11</sup>Here and elsewhere we use the SDSS image list tool to examine our fields (Nieto-Santisteban et al., 2004).

in fact well matched, and our target sample of bright/saturated SDSS objects should be detected by 2MASS, while faint interlopers should lack 2MASS counterparts.

Accordingly, the 2MASS catalog was queried for matches to the 5000 SDSS objects. The typical positional uncertainties for point sources in both surveys are on the order of a fraction of an arcsecond (e.g., Finlator et al., 2000), but here we defined a match as occurring when a 2MASS object fell within  $10''$  of the SDSS position. We used this large matching radius to account for possible positional inaccuracies due to the large spatial extent of the brightest objects in our sample. The median separation between the SDSS objects for which we found matches and their 2MASS counterparts, however, was only  $0.22''$ . This matching left us with a list of roughly 2500 bright/saturated SDSS objects with a nearby 2MASS counterpart within  $1'$  of a RASS source.

We also wished to examine the SDSS spectroscopic data available for these RASS fields. At that time (September 2003), roughly 680,000 SDSS spectra were available, a sample that we defined for these purposes as making up the DR1 spectroscopic survey. As expected, only a very small fraction of the 2500 SDSS objects had an SDSS spectrum, since the spectroscopic survey does not target objects whose brightness might cause bleeding from one fiber to another. The spectroscopic target's position is within  $3''$  of the photometrically cataloged object for fewer than 70 of our objects. An additional 390 fields have at least one SDSS spectrum within  $1'$  of the X-ray source position. As a result, less than 20% of the RASS sources have an SDSS DR1 spectrum (as defined here) within  $1'$ , so that a significant fraction of these X-ray sources cannot be directly identified from SDSS spectroscopy. Furthermore, most of these identifications are likely to be of quasars and other active galactic nuclei, since these tend to be fainter optical sources compared to X-ray-emitting stars, and are therefore more likely to be targeted for SDSS spectroscopy.

Finally, the 2520 X-ray sources with SDSS/2MASS candidate counterparts were fed into SIMBAD and NED, with which we searched for cataloged objects within  $1'$  of the RASS positions. This allowed us to identify 425 potential known extragalactic counterparts to RASS sources, including 191 previously known quasars and active galactic nuclei, 139 Seyfert 1 galaxies, and 65 clusters of galaxies.

## 2.4 The RASS/SDSS DR1 Catalogs of Stellar X-ray Sources

### 2.4.1 The known stellar X-ray sources

Of the remaining 2095 RASS sources, 416 had a star cataloged in SIMBAD *with an associated spectral type*. If no spectral type was given, the source was not considered “known” and was not included in this sample, which makes up 16.5% of the total number of RASS/SDSS DR1 sources<sup>12</sup>. The average separation between the RASS sources and these bright SIMBAD stars is  $15 \pm 12''$ ; this is equivalent to  $1 \pm 0.7\sigma$ , where  $\sigma$  is the separation between the RASS source and the SIMBAD object divided by the RASS positional uncertainty. In Figure 2.2, the distribution of positional offsets for these stars is plotted in the left panel; in the right panel, the  $\sigma$  distribution is presented. In the rest of this discussion we focus on the 384 stars for which  $\sigma \leq 2$ .

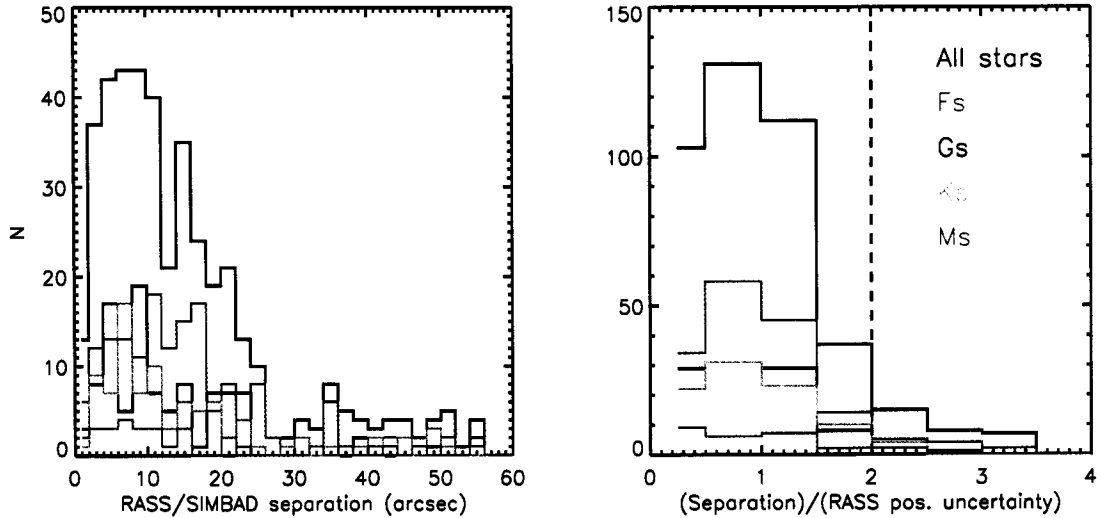


Figure 2.2: *Left panel:* Distribution of positional offsets between the RASS sources and the candidate bright SIMBAD stellar counterparts. *Right panel:* The same distribution, expressed in terms of the cataloged X-ray positional uncertainty. In both panels the colored histograms show the distribution by spectral type. Our discussion focuses on those stars to the left of the dashed line in the right panel.

<sup>12</sup>This does not mean that the SIMBAD object has previously been suggested as the RASS counterpart.



Unsurprisingly, these stars tend to be optically very bright. For the 370 stars that have cataloged  $V$  magnitudes,  $5.2 \leq V \leq 16.6$  mag, with the median being 8.9 mag; for the 360 that have cataloged  $B$  magnitudes,  $5.7 \leq B \leq 15.7$  mag, and the median is 9.5 mag. In addition, these stars are generally near to brighter X-ray sources, with the 384 RASS sources having a median count rate of  $0.040 \pm 0.012$  counts  $\text{s}^{-1}$ ; by contrast, the median count rate for the entire sample of 2520 sources is  $0.026 \pm 0.010$  counts  $\text{s}^{-1}$ . Figure 2.3 displays the RASS count rate versus SIMBAD  $V$  magnitude for these stars. As expected, the bulk of these proposed X-ray counterparts are normal F, G, K, and M stars, although there are a few proposed A star counterparts (see later discussion). There are also a handful of white dwarfs and cataclysmic variables (for which  $B$  was used), which stand out because of their relative optical faintness but X-ray brightness. We discuss these objects briefly later in this section; for an extensive discussion of the X-ray properties of white dwarfs and of cataclysmic variables, see Chapters 3 and 4. The brightest X-ray source in this sample is the famed X-ray binary Hercules X-1, among the first extrasolar X-ray sources to be detected.

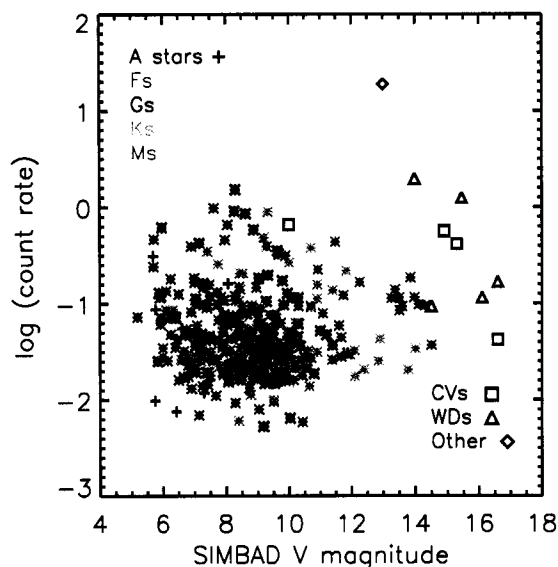


Figure 2.3: Cataloged X-ray count rate versus optical magnitude for the stars for which  $\sigma \leq 2$ ;  $V$  was used for all the stars for which they were available. The brightest X-ray source is Hercules X-1.

The proximity of these stars to the RASS sources and their optical brightnesses strongly suggest that they are indeed the X-ray sources. To confirm that these are plausible associations, we need to calculate the X-ray-to-optical flux ratios for these stars and compare them to those of known X-ray emitters from the same spectral class. While, as mentioned earlier, the X-ray flux from two seemingly similar stars can be very different, previous studies have shown that there is a typical *range* of X-ray-to-optical flux ratios for each stellar type (e.g., Stocke et al., 1991; Krautter et al., 1999; Zickgraf et al., 2003). In order to determine the best photometry to use for these calculations, we collected their cataloged SIMBAD, 2MASS, and SDSS magnitudes. (The 20 objects belonging to luminosity classes III or IV are not included in this analysis; see later discussion and Table 2.2.) To obtain  $K_S$  magnitudes, we searched for 2MASS objects within  $10''$  of the SIMBAD positions; for the 350 stars for which we obtained a match, the median separation is  $0.14''$ . We also fed the SIMBAD positions into the SDSS Imaging CrossID<sup>13</sup> and requested the PSF magnitudes for the nearest cataloged object. For the 359 objects near an SDSS object with a cataloged  $u$  magnitude, the median separation is  $0.28''$  (based on the SDSS filter transmission curves, the  $u$  band is less likely to saturate than the  $g$ ,  $r$ , or  $i$  bands for these bright stars).

In the left panel of Figure 2.4, the 2MASS  $K_S$  versus SDSS  $u$  magnitude is plotted for the 345 matched stars that are cataloged in both surveys, with the color-coding indicating spectral class. The dashed lines represent the best fit to the predicted  $K_S$  versus  $u$  magnitudes when  $u$  is estimated from the measured  $K_S$  using the median ( $J - K_S$ ) color and the appropriate 2MASS to SDSS transformation for F, G, K, and M stars (K. Covey 2006, private communication). This plot suggests that a significant fraction of these stars—those with measured  $K_S$  magnitudes between 4 and 8 and SDSS  $g \approx 14$ —have suspect photometry either in 2MASS or, more likely, in SDSS, which is not designed to study objects this bright. In fact, the surprise is that a significant fraction of these stars *do* appear to have reliable SDSS photometry.

In the right panel of Figure 2.4, the 2MASS  $K_S$  is plotted versus the SIMBAD  $V$

---

<sup>13</sup><http://cas.sdss.org/dr4/en/tools/crossid/upload.asp>.

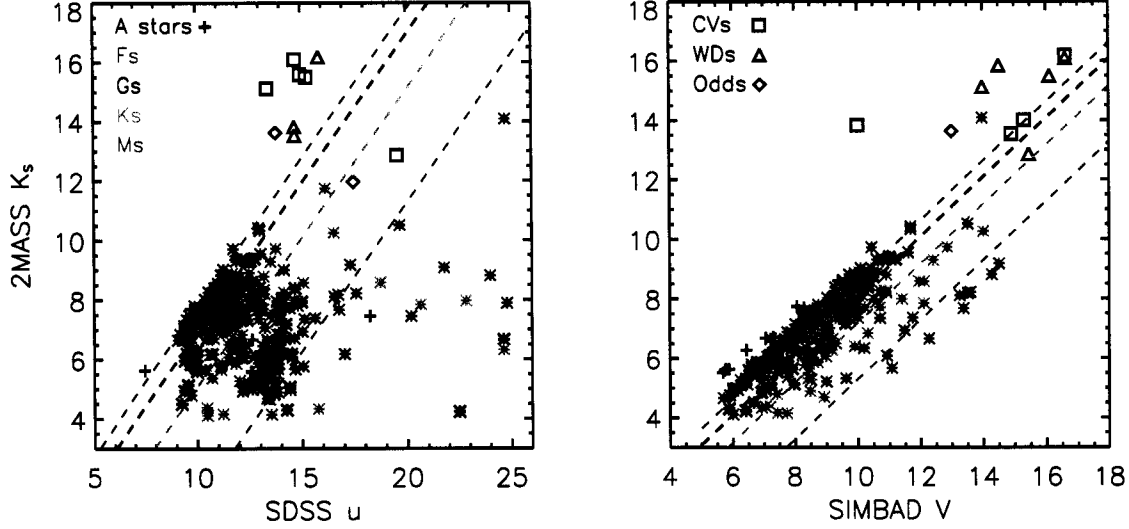


Figure 2.4: *Left panel:* 2MASS  $K_S$  versus SDSS  $u$  for the SIMBAD bright stars within  $2\sigma$  of a RASS source in DR1. The clump of stars with  $u \approx 14$  and  $4 < K_S < 8$  is probably due to bad photometry, as those stars are not well characterized by the dashed lines, which correspond to the predicted  $u$  given the  $K_S$  magnitude. *Right panel:* The 2MASS  $K_S$  versus SIMBAD  $V$  plot is much cleaner, suggesting that the SDSS photometry is indeed suspect for many of these bright stars.

for 342 stars, with the color-coding being identical to that in the left panel. There are still a few outliers relative to the predicted  $K_S$  versus  $V$  relation for F, G, K, and M stars (calculated as above, using standard  $(V - K_S)$  transformations; Cox, 2000), but this plot suggests that the SIMBAD  $V$  magnitude, rather than any SDSS magnitude, should be used for the  $f_X/f_{opt}$  calculations. Accordingly, we calculated  $f_X/f_V$  for these stars using the classic Maccacaro et al. (1988) formula:

$$\log (f_X/f_{opt}) = \log f_X + 0.4 V + 5.37, \quad (2.1)$$

assuming that on average 1 count  $s^{-1}$  translates to an X-ray flux of  $10^{-11}$  erg  $cm^{-2}$   $s^{-1}$  in the 0.1 – 2.4 keV energy range (e.g., Motch et al., 1998; Voges et al., 1999). In Figure 2.5, the  $\log (f_X/f_V)$  histograms for the 330 F, G, K, and M stars in this sample are shown. For the F, G, and K stars, empirical  $2\sigma$  ranges for the flux ratios were estimated from the mean  $\log (f_X/f_V)$  and are presented. Our sample of 20 M stars with a cata-

logged  $V$  is too small to draw useful conclusions about the overall distribution of their flux ratios, and instead we used our (large) sample of M stars with APO spectroscopy (described in §2.4.2) to determine the  $\log (f_X/f_{opt})$  range for X-ray-emitting M stars.

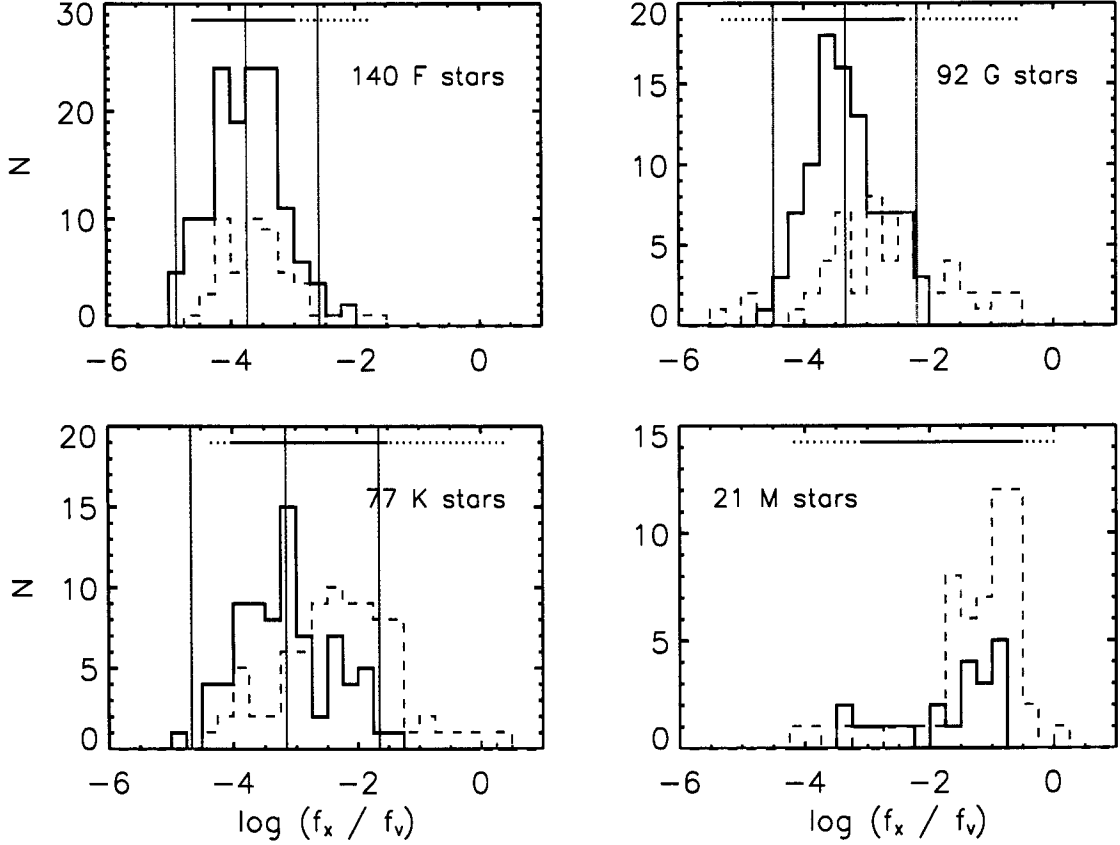


Figure 2.5:  $\log (f_X/f_V)$  histograms for the SIMBAD F, G, K, and M stars. The dashed blue histograms are the Krautter et al. (1999) observed distributions. In the first three panels, the red vertical line corresponds to the mean flux ratio, and the green vertical lines bracket the  $2\sigma$  range, for SIMBAD stars of that spectral class. The horizontal lines are ratio ranges from the literature: the solid lines are from the Maccacaro et al. (1988) *Einstein* survey, while the dotted extensions are from Krautter et al. (1999). In each panel, we indicate the number of stars with a cataloged  $V$ .

For comparison, we show the flux ratio distributions and limits (also calculated using the Maccacaro et al. formula) for each class as observed by Krautter et al. (1999); they identified 274 stellar X-ray emitters in an area-limited survey of RASS BSC and FSC sources. Their catalog includes  $\log (f_X/f_V)$  data for 53 F stars, 54 G stars, 84 K

stars (a third of which are Ke stars), and 55 M stars, 49 of which are dMe stars. The classic Maccacaro et al. (1988) *Einstein* limits are also included in each panel. The flux ratio distributions and ranges for the bright stars are consistent with those found in these earlier studies; only a handful of our stars have unusual  $\log(f_X/f_V)$ . This suggests that, as expected, the vast majority of these SIMBAD stars (including the M stars) are in fact RASS source counterparts. Furthermore, the flux ratio ranges calculated from our own distributions for these stellar types give us limits slightly more generous than the *Einstein* values (which are known to be quite conservative; Stocke et al., 1991), but generally more conservative than those of Krautter et al. (1999).

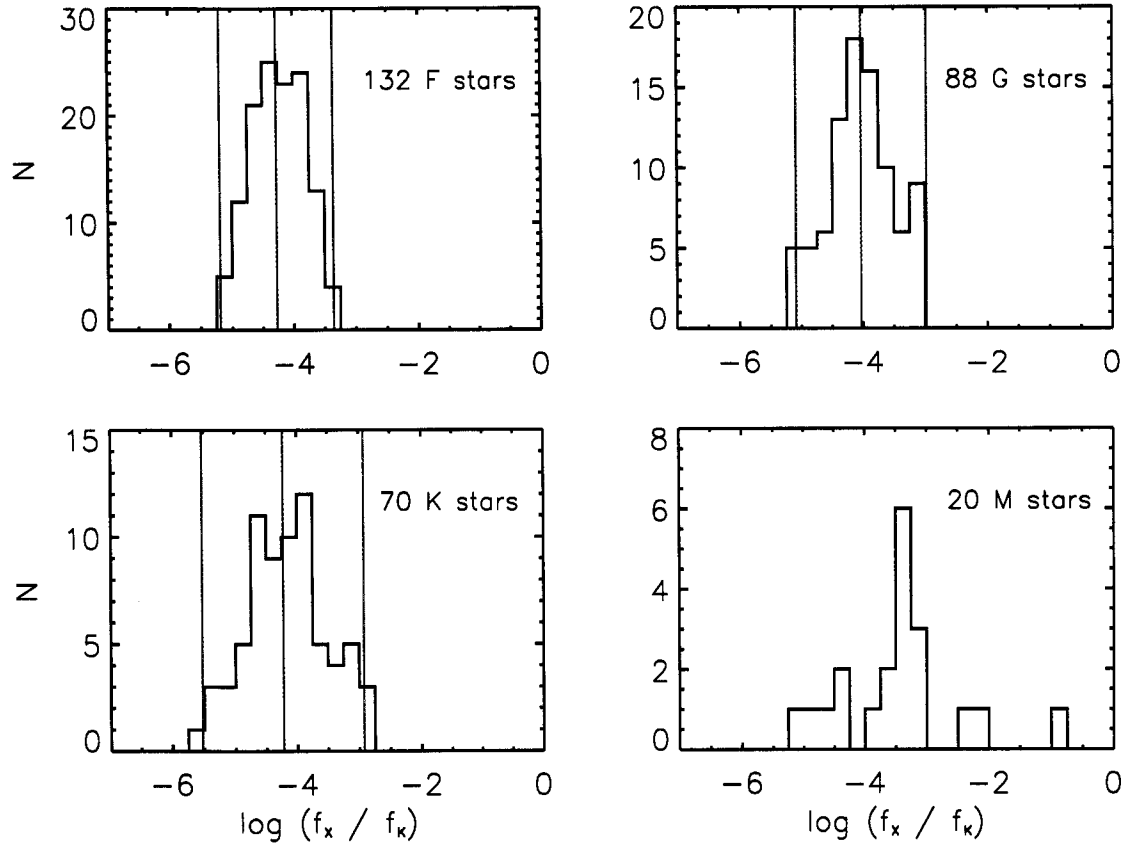


Figure 2.6:  $\log(f_X/f_K)$  ratios for the SIMBAD F, G, K, and M stars. As in Figure 2.5, the red vertical lines are the mean flux ratios, and the green vertical lines bracket the  $2\sigma$  ranges. The number of stars from Figure 2.5 used to calculate these  $2\sigma$  ranges is indicated in the first three panels; 20 M stars have a  $K_S$  magnitude.

We therefore choose to use our empirically determined flux ratio ranges as the basis for later comparisons. We take the 132 F, 90 G, and 74 K stars whose  $\log (f_X/f_V)$  falls within the  $2\sigma$  range for that stellar class and calculate their  $\log (f_X/f_{opt})$  using  $K_S$  rather than  $V$ . We then obtain the mean flux ratio and  $2\sigma$  limits for each stellar type (see Figure 2.6 and Table 2.1). This is *not* equivalent to calculating the infrared-to-X-ray flux ratios for these stars, and the obtained flux ratio ranges can therefore not be directly compared to those found in other samples (e.g., Feigelson et al., 2004). We are simply interested in the statistical distribution of the  $\log (f_X/f_K)$  values. Since the majority of the candidate stellar X-ray emitters identified in this program are too faint to have been cataloged in SIMBAD, but all were selected to have 2MASS counterparts, these ranges allow us to make flux ratio comparisons for our larger sample of proposed counterparts without having to introduce possible uncertainties (e.g., when using a color transformation to obtain  $V$  from  $g$ ).

Table 2.1: Log ( $f_X/f_K$ ) ratios derived from the RASS/SIMBAD stars.

Type	$2\sigma$ Min	$2\sigma$ Max	Mean	Notes
F	−5.19	−3.36	−4.28	
G	−5.10	−2.98	−4.04	
K	−5.53	−2.92	−4.23	
M	−4.65	−1.58	−3.11	Derived from APO sample

Table 2.2 summarizes the properties of this sample of the 364 SIMBAD bright stars in DR1 within  $2\sigma$  of a RASS sources (the Appendix contains sample data from our on-line catalog for the sample). We list the number of stars of each spectral type among the 364, and the number identified as X-ray sources based on positional proximity and X-ray-to-optical flux ratio. We also include the minimum, maximum, and mean  $\log (f_X/f_V)$  for these stars ( $V$  was unavailable for the cataclysmic variables; instead,

$f_X/f_B$  was calculated when a  $B$  was cataloged<sup>14</sup>). Unless otherwise specified, the stars were assumed to be on the main sequence; the 20 stars cataloged as belonging to other luminosity classes were not included in the flux ratio calculation for their stellar class.

The number of variable stars ( $V^*$ ) within a given class is indicated, but should be considered a lower limit. For example, it is likely that nearly all of the M stars flare, and are therefore variable at some level. Likewise, the number of stars with measured emission is indicated (e.g., Ke); these were included in the flux ratio calculations for the relevant class and not treated separately since their total number is small (and the definition of emission is presumably not uniform). Among the atypical stars included in this sample we note the presence, in addition to Hercules X–1, of three non–magnetic peculiar A (Am) stars and of PG 0205+13, a UV emission source that may be an O subdwarf. Below we comment on whether the A stars are likely to be the RASS sources, touch on the properties of the white dwarfs and cataclysmic variables in this sample, and discuss the relative number of F/G and K/M stars among these RASS/SIMBAD stars.

### *The A stars*

The total number (13) and relative fraction ( $\sim 3.5\%$ ) of A stars in this sample are relatively large. Krautter et al. (1999), for example, reported only three A stars (1% of the total) among the 274 stellar counterparts they identified in their survey of RASS sources. As discussed in §2.2.3, A stars are not generally predicted to be X–ray emitters; an unseen, young, active later–type companion is usually thought to be the source for the observed X rays (Güdel, 2004). While some of the A stars in this sample have been previously associated with a RASS source (e.g., HD 139493 with 1RXS J153556.8+543753), it is unlikely, therefore, that *all* of the A stars in this sample are X–ray emitters. However, examination of the available SDSS data does not allow us to propose a different counterpart to these X–ray sources. The stars are simply too bright for the imaging or spectroscopic data to be useful.

---

<sup>14</sup>Here we used the Zickgraf et al. (2003) relation for  $f_X/f_{opt}$  calculations based on  $B$ , which is the Maccaro et al. (1988) formula with a different constant.

Table 2.2: RASS/SIMBAD stars. The full  $f_X/f_V$  ranges are given.

Type	Total Number	RASS Sources	$\log (f_X/f_V)$			Notes
			Min	Max	Mean	
A	13	0?	−5.34	−3.20	−4.06	∈ 3 Am & 2 V*
F	141	132	−4.93	−2.18	−3.74	∈ 17 V*; ∋ 2 FIII & 8 FIV
G	92	90	−4.73	−2.13	−3.34	∈ 9 V*; ∋ 5 GIII & 1 GIV
K	82	74	−4.78	−1.50	−3.16	∈ 7 V* & 4 Ke; ∋ 4 KIII
M	24	16	−3.37	−0.82	−1.77	∈ 5 flare & 2 Me
WD	6	6	−0.86	+0.65	+0.03	∈ 5 DA
CV	4	4	−2.04	−0.12	−0.73	∈ 3 DN; used $f_X/f_B$
other	2	2?				∈ 1 sdO(?) & Hercules X−1

The presence of three chemically peculiar non-magnetic A stars in this sample is quite intriguing, since there is active debate about whether these types of stars can in fact be X-ray emitters (see discussion in Güdel, 2004). For all of these A stars, however, follow-up X-ray and/or optical observations (to search for a late-type companion, for example) are required to test whether they are in fact the RASS sources.

#### *The white dwarfs and cataclysmic variables*

The matches to SIMBAD-cataloged white dwarfs and cataclysmic variables are listed in Table 2.3. All of the cataclysmic variables are known X-ray emitters, and three of the four have had their spectra taken by SDSS (only EI UMa has not). PHL 1242 was identified as a polar in recent work by Szkody et al. (2002) and Schmidt et al. (2005b); see Chapter 3.

Four of the six white dwarfs are explicitly listed as X-ray sources in SIMBAD. A fifth, WD 1125−025, was included in the Marsh et al. (1997b) catalog of ultraviolet-selected *ROSAT* white dwarfs, while the last, WD 1520+525, was recently proposed as a soft X-ray source by Chu et al. (2004). Overall, the X-ray sources near the white



Table 2.3: The white dwarfs (first six objects) and cataclysmic variables among the RASS/SIMBAD matches. For the white dwarfs  $V$  is given, except for WD 1125–025. For this object and the four cataclysmic variables  $B$  is listed.

1RXS J	Counts s <sup>-1</sup>	SIMBAD name	Offset	mag	Type
034850.1–005823	$1.965 \pm 0.158$	WD 0346–01	8''	13.98	DA
112814.4–024950	$0.051 \pm 0.015$	WD 1125–025	37''	15.32	DA
152146.6+522215	$0.168 \pm 0.016$	WD 1520+525	11''	16.60	DO
165008.0+370130	$0.115 \pm 0.019$	WD 1648+371	22''	16.10	DA
165020.4+403723	$0.094 \pm 0.016$	WD 1648+407	3''	14.50	DA
172642.8+583726	$1.247 \pm 0.028$	WD 1725+586	7''	15.45	DA
015543.3+002817	$0.042 \pm 0.012$	PHL 1242	10''	16.60	Polar
083821.6+483800	$0.565 \pm 0.042$	V* EI UMa	4''	14.90	DN
085343.5+574846	$0.414 \pm 0.035$	V* BZ UMa	7''	15.30	DN
113826.8+032210	$0.659 \pm 0.061$	V* T Leo	3''	10.00	DN

dwarfs have very soft X–ray spectra, as measured by their hardness ratios (HRs). By definition,  $HR1 = \frac{(0.5-2.0)-(0.1-0.4)}{(0.1-0.4)+(0.5-2.0)}$  and  $HR2 = \frac{(1.0-2.0)-(0.4-1.0)}{(1.0-2.0)}$ , where, for example, (0.5–2.0) indicates the number of counts in the 0.5–2.0 keV energy range (Motch et al., 1998). For these sources,  $HR1 \approx -1$ , which is typical for X–ray–emitting white dwarfs (e.g., Fleming et al., 1996; Zickgraf et al., 1997), confirming that their counterparts are indeed likely to be these white dwarfs. Only one of these objects has an SDSS spectrum: WD 1725+586 (see Chapter 4).

#### *F/G versus K/M stars*

A peculiarity of this sample is its relative fraction of F/G and K/M stars. F and G stars represent nearly 68% of the proposed stellar X–ray emitters, while K and M stars are only 29% of the total. By comparison, the Krautter et al. (1999) distribution is 40% F/G stars and 54% K/M stars. And in their catalog of Hamburg/RASS identifications

(described in §1.2), Zickgraf et al. (2003) find that 74% of their stellar identifications are M or K stars, and only 10% of the 454 confirmed stellar emitters are F or G stars<sup>15</sup>.

In all likelihood, the relative imbalance in our sample simply reflects the fact that F and G stars are more commonly found in classic catalogs of bright stars (e.g., the Henry Draper catalog). Our sample of spectroscopically confirmed stellar X-ray emitters, discussed below, does not show this same strong bias toward F and G stars.

#### 2.4.2 *The APO spectroscopic sample*

In addition to the 416 sources with nearby SIMBAD bright stars described above, we identified 1430 RASS sources with no obvious likely counterparts cataloged in either SIMBAD or NED; here again,  $1'$  was used as a search radius for cataloged objects. Some sources with matches within  $1'$  were nevertheless included in this sample; for example, if a star was listed in SIMBAD without a spectral type, as is the case for some of the stars in the Guide Star Catalog (GSC)<sup>16</sup>, or if NED returned a galaxy included in the Automatic Plate Measuring survey (APMUKS; Maddox et al., 1990). The  $2 \times 10^6$  galaxies listed only in the APMUKS are generally faint (the limiting magnitude is  $m \sim 20.5$ ), and absent any spectroscopic information, should not be considered strong candidate counterparts to the RASS sources. By contrast, GSC stars are often relatively bright, and are strong candidate counterparts—but without spectral information, the likelihood that they are the RASS X-ray sources cannot be tested.

For the purposes of defining a sample to target for spectroscopic follow-up, we separated the proposed SDSS counterparts to these 1430 RASS sources between those  $\leq 30''$  and  $> 30''$  from the X-ray positions. The roughly 800 objects less than  $30''$  from a RASS source made up the list of primary targets for our spectroscopic campaign. We used the Dual Imaging Spectrograph (DIS) on the APO 3.5-m telescope to obtain spectra for  $\sim 95\%$  of these objects, and also for over 100 of the objects with separations  $> 30''$ , over

---

<sup>15</sup>However, the number of typed stars in their sample is dwarfed by the number of bright stars of unknown type, 1219. Presumably identifying M and K stars with their  $R \approx 100$  spectra is easier because of the relatively common, strong emission features visible in these stars' spectra.

<sup>16</sup>Produced by the Space Telescope Science Institute & Osservatorio Astronomico di Torino (2001).

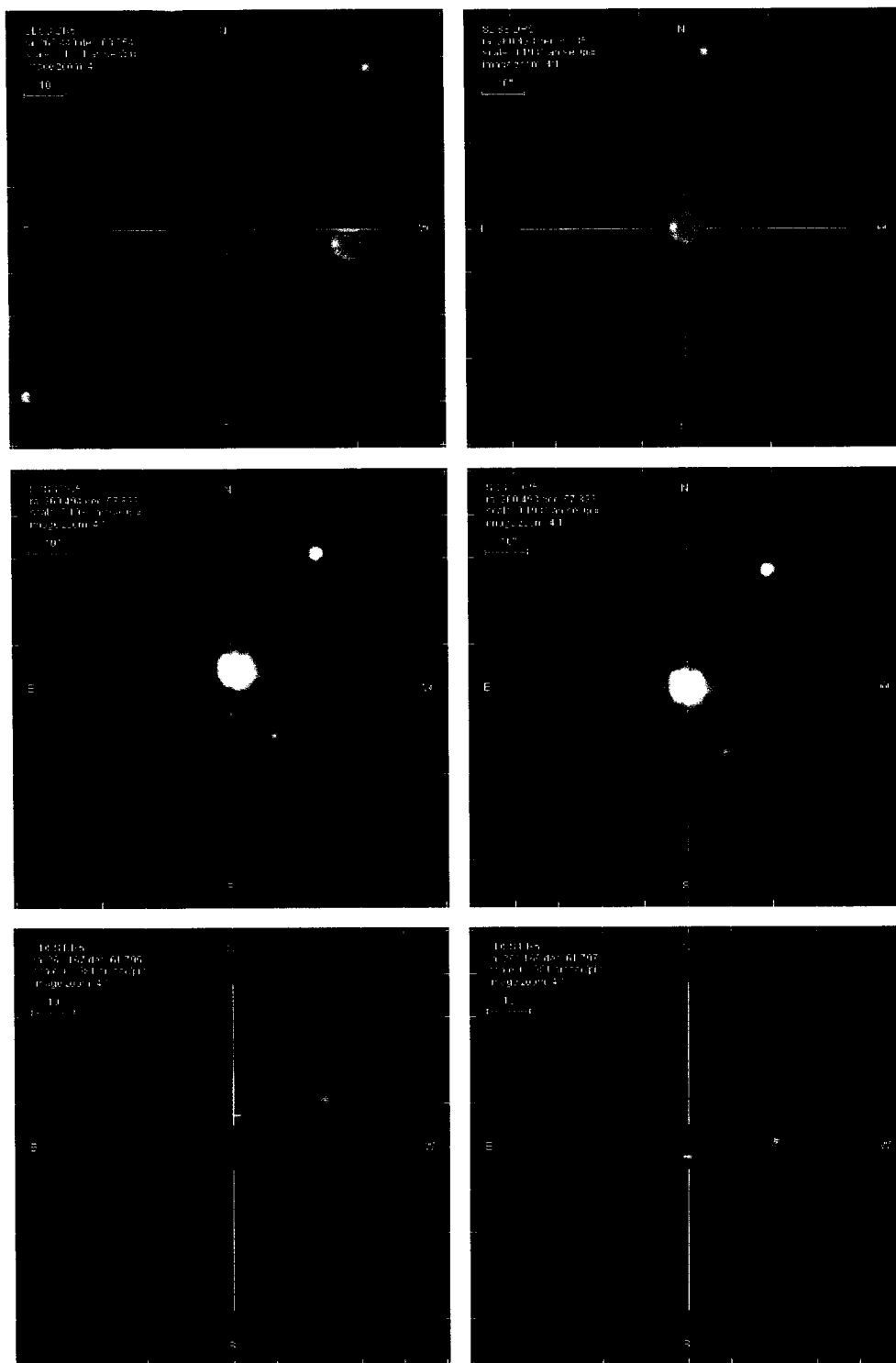


Figure 2.7: SDSS images of three RASS fields (left column) and of the proposed stellar counterpart for which an APO spectrum was obtained (right column).

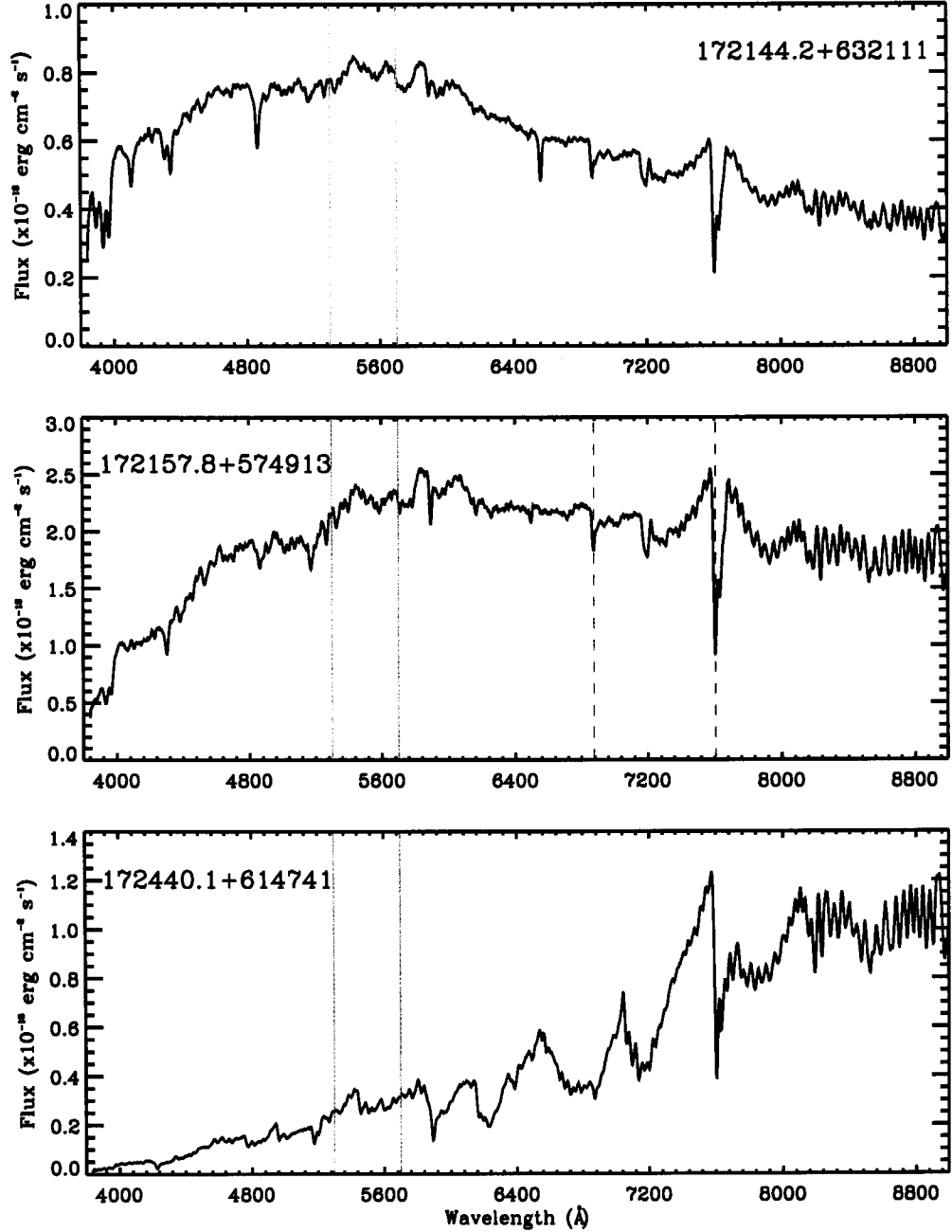


Figure 2.8: APO spectra of the three stars in Figure 2.7. The green lines delimit the overlap between the DIS blue and red spectrum for each object. The prominent features visible in this area in the top and bottom panels are due to the dichroic. The red dashed lines in the middle panel indicate the positions of two telluric features, the Fraunhofer A (7600 Å) and B (6800 Å) bands. The fringing to the red of the Fraunhofer A band is due to the red DIS CCD, which is a thinned chip. For each spectrum, the name of the corresponding RASS source is included.

the course of 50 half nights from 2003 Sept to 2006 May. In our standard low-resolution set-up, the DIS blue CCD is centered on 4500 Å, with a dispersion of 2.4 Å per pixel, while its red CCD is centered on 7600 Å, with a dispersion of 2.3 Å per pixel. In Figure 2.7, we show the SDSS cut-out images of three randomly selected RASS X-ray source fields and of the associated stars targeted for APO spectroscopy; Figure 2.8 presents the DIS spectra for these stars.

In most cases, a single observation was sufficient to obtain a spectral type for the proposed counterpart; we thus have 682 fields with a unique spectrum. In another 124 fields we took at least two spectra of the same target, sometimes because the original spectrum had an insufficient signal-to-noise ratio to allow for confident typing, or because the spectrum suggested that there was something unusual about the star (for example, it appeared to be flaring in the initial spectrum; see later discussion). Finally, in an additional 91 RASS fields we took spectra for more than one target, usually because of the presence of an apparent companion to our primary target. The total number of spectra we collected is about 1200 in 897 RASS fields. Our initial discussion focuses on the 806 RASS fields for which we targeted only one object, whether once or multiple times. We treat the 91 fields in which we took multiple spectra separately, since in these cases there are nominally several candidate counterparts.

To obtain spectral types for our targets, we used the Hammer, an Interactive Data Language code developed by K. Covey<sup>17</sup>. The Hammer automatically analyzes each spectrum and predicts its Morgan-Keenan (for stars earlier than M) or Kirkpatrick (for later stars) spectral type on the basis of a fit to a set of 30 spectral indices. In addition to this automated typing, the Hammer allows the user to interactively modify the assigned spectral type. Every spectrum was therefore checked by eye before a final type was assigned; this allowed us, for example, to identify a handful of interloping quasars in our sample. As mentioned above, in 124 cases we obtained at least two spectra of a proposed RASS counterpart. Generally this was because the target was relatively faint<sup>18</sup>, or the weather uncooperative, and the first spectrum was of insufficient quality

---

<sup>17</sup>Publicly available from <http://www.astro.washington.edu/covey/>.

<sup>18</sup>Almost all of our observing was done in bright time, and our integrations were typically no more than

to allow for confident typing of the star. Nevertheless, in almost four out of five cases, the stellar types assigned for a given star from the different spectra agree to within two stellar subclasses. For those cases where the difference is more significant, we examined the spectra to determine which had the highest signal-to-noise ratios and assigned the corresponding spectral types.

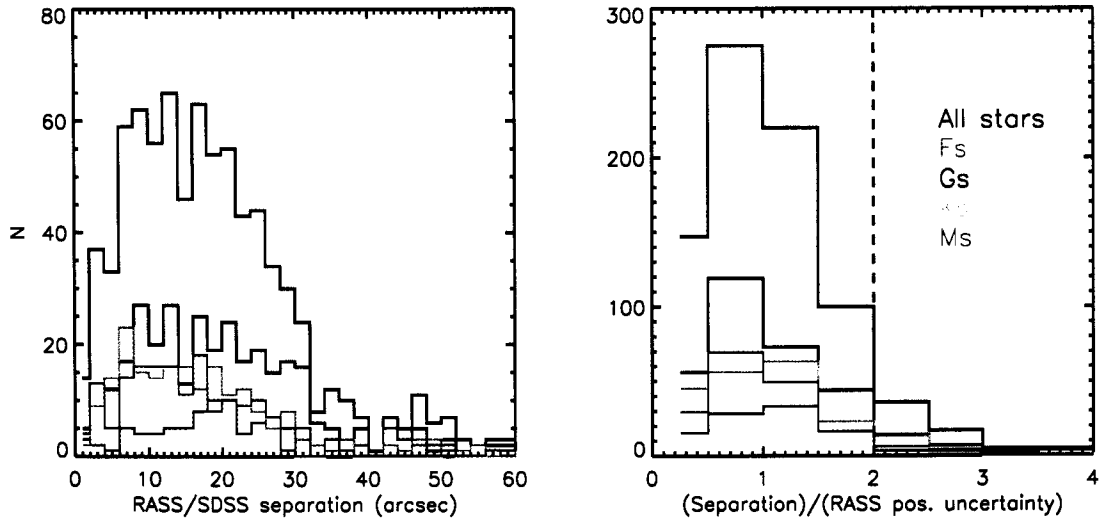


Figure 2.9: *Left panel:* Distribution of positional offsets between the RASS sources and 800 candidate SDSS stellar counterparts with APO spectra. *Right panel:* The same distribution, expressed in terms of the cataloged X-ray positional uncertainty. In both panels the colored histograms show the distribution by spectral type.

In Figure 2.9 we present the positional offset and  $\sigma$  (as defined earlier) distributions for 800 stars in RASS fields where we selected only one target. Of the six objects not included in this analysis, two are quasars, and four are stars whose spectra are too poor for confident typing. 737 (92%) of the 800 stars have separations  $\leq 2\sigma$ ; for these calculations, we updated the positional (and photometric) data for the SDSS stars to the more recent Data Release 5 (DR5) values<sup>19</sup> (the average change in the

---

five minutes long; faint in this context is  $g \approx 16$ .

<sup>19</sup>The DR5 database does not include photometric data for seven stars. For three we use the DR1 data; four others lack data in both DR1 and DR5. Two of these fall on one of the survey edges, while the others were not processed by the pipeline for unknown reasons. Two RASS sources have positional

SDSS position from DR1 to DR5 for our entire sample of APO targets was  $0.36''$ ).

The  $\log(f_X/f_K)$  distributions for the 734 F, G, K, and M stars in our spectroscopic sample with separations  $\leq 2\sigma$  are plotted in Figure 2.10. We also include the equivalent distributions for 320 RASS/SIMBAD stars, along with the means and  $2\sigma$  ranges derived from those distributions for the F, G, and K stars (see Table 2.1). For the M stars we derive the mean and  $2\sigma$  range directly from our spectroscopic sample, which is eight times larger than our RASS/SIMBAD sample.

These plots clearly show that the probability that a spectroscopic target is a RASS counterpart increases as we move to later spectral types. Only 34 of the 92 spectroscopically identified F stars fall within the  $2\sigma$   $\log(f_X/f_K)$  range derived from the RASS/SIMBAD F stars. For the G stars, the fraction is slightly higher: 136 of 292 (47%). For K stars and M stars the fraction is much higher: 132 of 187 K stars (71%) and 159 of 163 M stars (98%)<sup>20</sup> have  $\log(f_X/f_K)$  within their respective  $2\sigma$  ranges; the overall fraction for these stars is 66%.

In Figure 2.11 we compare the bulk optical and X-ray properties of all 461 SDSS F, G, K, and M stars within  $2\sigma$  of a RASS position and with appropriate  $f_X/f_{opt}$  ratios to those of the SIMBAD stellar counterparts, described in the previous section, which meet the same criteria. In the left panel of the figure, we reproduce Figure 2.3 for 312 of the RASS/SIMBAD stars, and in the right panel we plot the SDSS  $g$  versus RASS count rate for the spectroscopic targets. As expected, the latter sample is both fainter optically and in X rays. In addition, there is a clear difference in the spectral distribution of the stars; there are proportionally far more K and M stars in the APO spectroscopic sample than in the SIMBAD bright star sample.

The X-ray, optical, and infrared properties of these stellar X-ray sources are included in an on-line master catalog (see the Appendix). Below we discuss the fields for which we obtained multiple APO spectra, the proposed A star counterparts in our spectroscopic sample, and our candidate flare stars.

---

uncertainties of  $0''$ ; these were changed to  $30''$ .

<sup>20</sup>Note that if we use instead the broader  $2\sigma$  range derived from the SIMBAD sample, the same four M stars have flux ratios outside of the expected range for M star X-ray source counterparts.

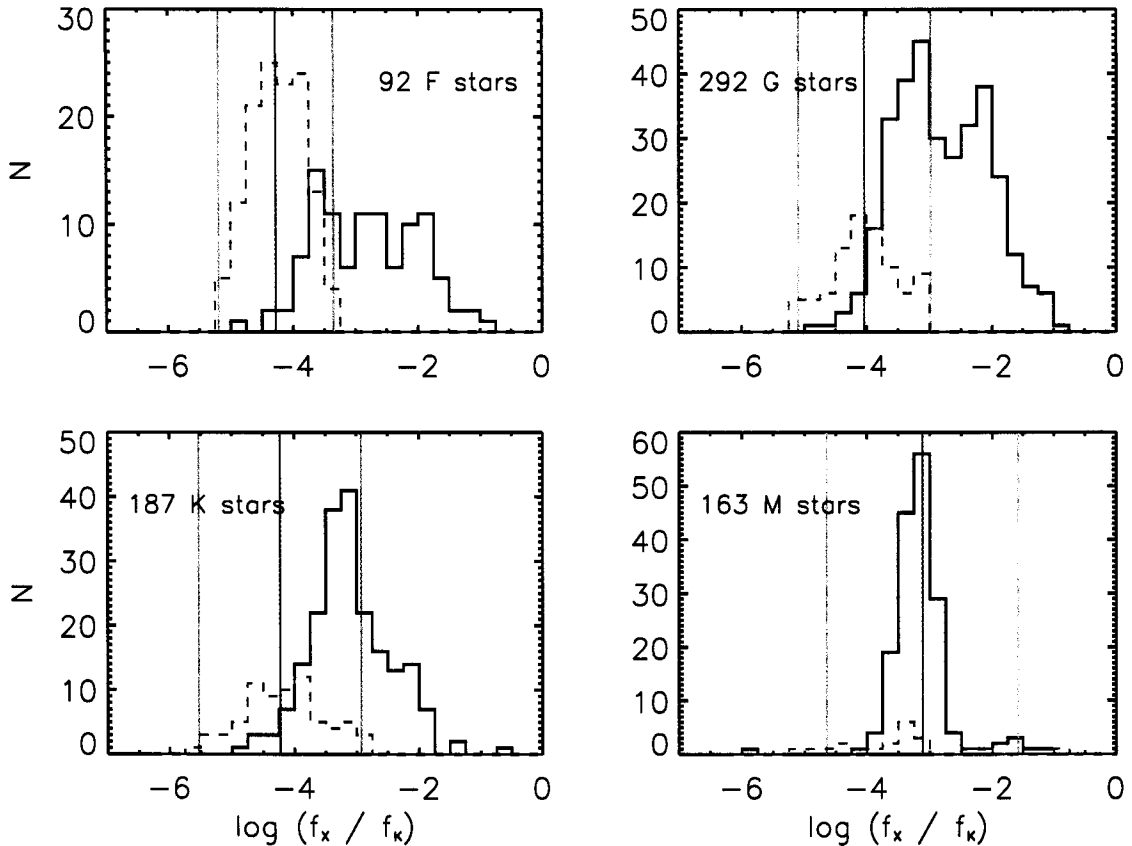


Figure 2.10:  $\log(f_X/f_K)$  ratios for the proposed SDSS counterparts with APO spectroscopy (black), along with the distributions for the RASS/SIMBAD F, G, K, and M stars (dashed blue), within  $2\sigma$  of a RASS source. In the first three panels, the red vertical lines are the mean flux ratios, and the green vertical lines bracket the  $2\sigma$  ranges, derived from the RASS/SIMBAD sample. The mean and  $2\sigma$  range are derived directly from the APO sample for the M stars. The number of stars with an APO spectrum is indicated in each panel.

### *The fields with multiple spectra*

For the 91 fields in which we have APO spectra for several targets, we calculated the separation and  $\log(f_X/f_K)$  ratio and obtained a spectral type for each. The best candidate counterpart in each field was then identified on the basis of its proximity (only stars  $\leq 2\sigma$  from the RASS source were considered) and the appropriateness of its  $f_X/f_K$  given its spectral type. In 31 fields we identified a single stellar counterpart



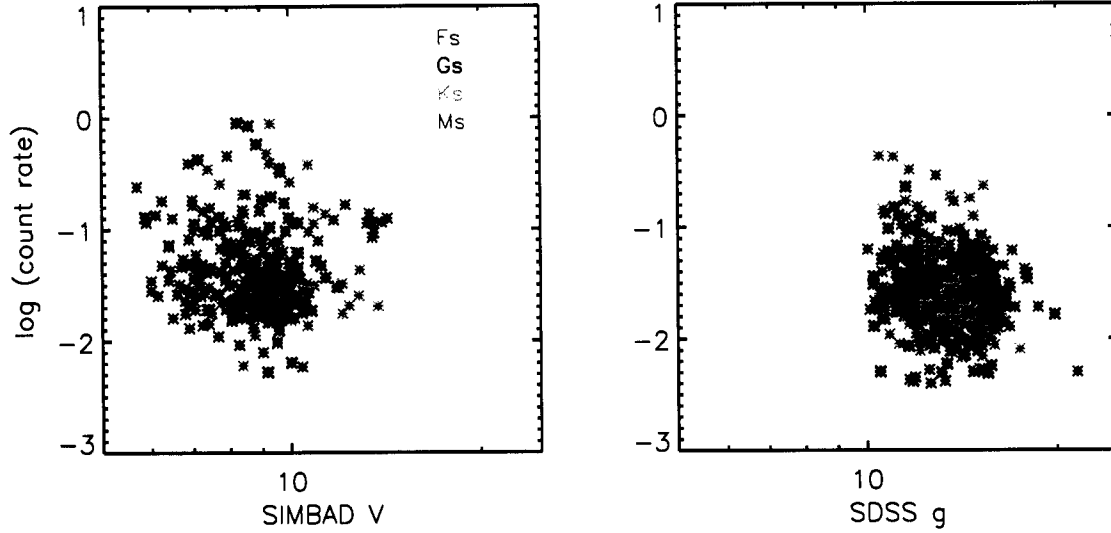


Figure 2.11: Cataloged X-ray count rate versus optical magnitude for the F, G, K, and M stars X-ray emitters. *Left*: RASS/SIMBAD stars. *Right*: RASS/SDSS stars.

(1 F, 10 G, 8 K, and 12 M stars); these are included in our master catalog.

In another 29 fields, two stars met our criteria; in 17 of these cases our target has an apparent close companion (separations of  $\sim 5''$  or less), making it difficult to avoid photometric uncertainties in the SDSS and 2MASS catalogs and sometimes to obtain clean spectra with our  $1.5''$  slit. We list these fields separately in Table 2.4; the table includes the RASS source name and count rate, the SDSS counterpart name and  $g$  magnitude, the 2MASS  $K_S$  and  $f_X/f_K$ , and the spectral type. Higher resolution X-ray observations are required to determine which of the possible counterparts is in fact the X-ray source; it is also possible, of course, that both stars are X-ray emitters.

### *The A stars*

In three RASS fields, our proposed counterpart is identified as a late A star on the basis of its APO spectrum. The bright star coincident with 1RXS J004518.4+151001, however, is in fact the F3IV star HD 4270, according to SIMBAD. This field should therefore not have been among our spectroscopic targets; the APO spectrum was taken

Table 2.4: X-ray, optical, and infrared data for RASS fields with multiple candidate stellar counterparts. 2MASS magnitudes with an asterisk indicate problematic PSF fitting. “CC” is short for close companion.

1RXS J	Counts s <sup>-1</sup>	SDSS J	$\sigma$	$g$	$K_S$	$\log(f_X/f_K)$	Comments
015119.8+132459	0.172 ± 0.023	015119.97+132452.2	0.6	14.85 ± 0.08	7.67 ± 0.02	-3.33	M3
		015119.97+132512.4	0.9	11.86 ± 0.00	8.39 ± 0.02	-3.04	G9
020910.2+010047	0.035 ± 0.012	020910.14+010038.7	0.6	16.75 ± 0.02	10.86 ± 0.04	-2.74	M4; CC
		020909.96+010036.4	0.9	18.06 ± 0.17	11.87 ± 0.03	-2.33	M4; CC
033625.3+005045	0.016 ± 0.007	033625.45+005127.1	1.2	15.76 ± 0.02	9.88 ± 0.02	-3.49	G6
		033627.67+005131.2	1.6	11.00 ± 0.00	9.26 ± 0.02	-3.74	G7
075053.1+442829	0.051 ± 0.013	075053.64+442818.4	1.1	13.60 ± 0.02	8.30 ± 0.01*	-3.60	M1; CC
		075053.77+442816.9	1.3	15.47 ± 0.14	8.30 ± 0.01*	-3.60	M3; CC
083203.9+530354	0.020 ± 0.010	083203.74+530359.6	0.3	12.33 ± 0.02	9.73 ± 0.02	-3.44	K1; CC
		083202.66+530400.0	0.6	13.48 ± 0.13	9.74 ± 0.02	-3.44	G0; CC
085921.0+503256	0.022 ± 0.009	085922.79+503311.4	1.5	16.61 ± 0.24	12.17 ± 0.04	-2.43	M0
		085922.99+503307.6	1.5	12.63 ± 0.00	10.37 ± 0.03*	-3.15	G8
091140.6+493319	0.018 ± 0.008	091140.92+493325.8	0.5	15.36 ± 0.02	10.85 ± 0.02	-3.04	M1
		091139.52+493326.7	0.9	17.63 ± 0.02	11.94 ± 0.02	-2.60	M4
092455.1+575649	0.130 ± 0.023	092456.44+575652.8	0.9	14.09 ± 0.02	8.98 ± 0.02	-2.92	M3; CC
		092455.33+575700.0	0.9	14.62 ± 0.08	7.81 ± 0.02	-3.39	M2; CC

Table 2.4: (continued) The RASS flags are set to 1 for 133524.8+595455, indicating that its X-ray data are poor.

1RXS J	Counts s <sup>-1</sup>	SDSS J	$\sigma$	$g$	$K_S$	$\log(f_X/f_K)$	Comments
114213.1-012237	0.072 ± 0.022	114213.08-012207.3	1.3	15.19 ± 0.02	8.70 ± 0.02	-3.30	M3
		114213.04-012154.2	1.9	13.42 ± 0.00	7.97 ± 0.02	-3.59	M4
115822.6-002006	0.144 ± 0.023	115823.31-002011.3	1.2	13.57 ± 0.03	8.77 ± 0.02	-2.96	M0; CC
		115823.17-002018.9	1.6	16.58 ± 0.25	10.53 ± 0.03	-2.26	M3; CC
120435.2+681854	0.018 ± 0.007	120435.80+681840.1	0.7	16.66 ± 0.034	11.08 ± 0.04	-2.95	M3; CC
		120436.14+681836.6	0.9	17.20 ± 0.06	11.90 ± 0.02	-2.61	M2; CC
121357.5+663753	0.024 ± 0.010	121358.01+663809.6	0.9	15.51 ± 0.10	9.53 ± 0.02*	-3.43	G6; CC
		121357.70+663811.8	1.1	15.75 ± 0.14	9.53 ± 0.02*	-3.43	K1; CC
123247.7-010419	0.024 ± 0.011	123247.68-010419.8	0.1	14.38 ± 0.20	9.60 ± 0.03	-3.41	G6; CC
		123247.29-010423.7	0.6	15.37 ± 0.15	10.30 ± 0.03	-3.13	G8; CC
132339.1+641635	0.021 ± 0.009	132338.98+641630.2	0.3	15.10 ± 0.07	10.54 ± 0.03	-3.09	M0; CC
		132339.64+641630.4	0.4	13.90 ± 0.03	9.90 ± 0.04	-3.35	M1; CC
132828.5+051424	0.076 ± 0.018	132828.90+051435.4	1.1	12.45 ± 0.00	8.95 ± 0.03	-3.17	K3
		132830.10+051423.4	2.0	17.06 ± 0.02	11.74 ± 0.02	-2.05	M3
133524.8+595455	0.033 ± 0.009	133524.39+595455.5	0.3	15.84 ± 0.68	8.15 ± 0.03	-3.85	G1; CC
		133524.79+595500.4	0.4	15.13 ± 0.03	8.03 ± 0.05	-3.90	K1; CC

Table 2.4: (continued) “U” indicates that  $K_S$  is an upper limit. No 2MASS error estimates are available for 140148.47+001024.7 and 140148.68+001025.5. 152351.62+532942.1 does not have a 2MASS counterpart.

1RXS J	Counts s <sup>-1</sup>	SDSS J	$\sigma$	$g$	$K_S$	$\log(f_X/f_K)$	Comments
135902.2+591754	0.067 ± 0.013	135903.24+591747.4	1.0	16.21 ± 0.07	10.73 ± 0.03	-2.51	M3; CC; U
		135902.75+591744.4	1.0	12.32 ± 0.00	8.66 ± 0.02	-3.34	K5; CC
140148.9+001008	0.024 ± 0.011	140148.47+001024.7	0.6	14.35 ± 0.11	9.59	-3.41	K4; CC; U
		140148.68+001025.5	0.6	14.42 ± 0.02	9.52*	-3.44	M0; CC
145626.1+560341	0.019 ± 0.007	145626.46+560324.6	0.9	13.55 ± 0.01	9.94 ± 0.02	-3.37	K5
		145628.49+560321.9	1.6	10.96 ± 0.00	9.26 ± 0.02	-3.64	G0
150521.8+595810	0.010 ± 0.005	150523.09+595755.2	0.8	15.69 ± 0.18	9.54 ± 0.02	-3.82	G6
		150520.38+595755.4	0.8	11.25 ± 0.00	9.31 ± 0.02	-3.91	G6
150656.8+011533	0.025 ± 0.010	150656.87+011532.7	0.1	15.37 ± 0.02	9.98 ± 0.05	-3.25	M3; CC
		150656.90+011527.1	0.5	16.65 ± 0.12	10.49 ± 0.03	-3.04	M3; CC
152350.6+533009	0.018 ± 0.007	152351.62+532942.1	1.3	18.91 ± 0.02	N/A	+0.19	z= 2.58 QSO; $f_X/f_g$
		152348.90+532959.3	1.7	13.72 ± 0.01	8.45 ± 0.02	-4.00	M3
153826.3+523407	0.010 ± 0.005	153826.02+523414.0	0.4	17.88 ± 14.97	8.56 ± 0.02	-4.21	K3; CC
		153826.38+523418.2	0.7	14.38 ± 0.16	8.29 ± 0.03	-4.32	K3; CC
160207.9+534105	0.013 ± 0.006	160206.85+534039.9	0.4	12.25 ± 0.00	7.01 ± 0.02	-4.70	G9
		160208.40+534122.5	1.1	13.84 ± 0.02	10.77 ± 0.02	-3.20	K1

Table 2.4: (continued)

1RXS J	Counts s <sup>-1</sup>	SDSS J	$\sigma$	$g$	$K_S$	$\log(f_X/f_K)$	Comments
164129.8+400617	0.022 ± 0.009	164129.47+400602.9	0.7	10.15 ± 0.00	8.48 ± 0.03	-3.90	G5; CC
		164129.54+400559.5	0.9	20.02 ± 13.33	8.48 ± 0.03	-3.90	G8; CC
171017.5+632135	0.052 ± 0.006	171016.46+632133.9	0.8	19.96 ± 6.98	9.32 ± 0.03	-3.19	M0; CC
		171017.05+632141.1	0.8	13.23 ± 0.07	9.15 ± 0.03	-3.25	K4; CC
171702.0+561220	0.047 ± 0.007	171702.12+561219.2	0.2	13.99 ± 0.01	8.11 ± 0.03	-3.71	K2
		171702.55+561235.6	1.6	13.40 ± 0.02	8.85 ± 0.02	-3.42	G6
172713.4+593324	0.013 ± 0.004	172714.59+593338.5	1.3	10.63 ± 0.00	8.50 ± 0.02	-4.13	G8
		172715.10+593315.1	1.4	15.42 ± 0.02	10.95 ± 0.02	-3.15	G7
235942.7-011325	0.029 ± 0.011	235943.68-011322.7	1.2	15.85 ± 0.11	9.21 ± 0.02	-3.48	K7; CC
		235943.80-011325.6	1.3	14.18 ± 0.03	9.10 ± 0.04*	-3.53	K3; CC

when we were still developing our algorithm.

SIMBAD lists RXS J165711.6+392028 as near CAIRNS J165712.56+392017.7, a galaxy in a cluster of galaxies, suggesting that the cluster may be the X-ray source. However, the RASS source is not extended, and its hardness ratios ( $HR1 = 0.49 \pm 0.36$ ;  $HR2 = -0.2 \pm 0.32$ ) are more consistent with those of stars (e.g., Voges et al., 1999), although the associated uncertainties are large. It is probable that a galaxy in the cluster is in fact the X-ray source, but further X-ray observations are needed to confirm this.

Finally, the SDSS spectrum of SDSS J095220.07+531455.6, a galaxy 33.5'' away from the third RASS source, reveals it to be a  $z = 0.12$  quasar. While the proposed stellar counterpart is closer (19.2''), the RASS hardness ratios ( $HR1 = -0.05 \pm 0.34$ ;  $HR2 = -0.15 \pm 0.46$ ) are consistent with those commonly found for active galactic nuclei (although here again the uncertainties are large), and it therefore seems most likely that the quasar is in fact the RASS source.

### *The candidate flare stars*

Of the 124 stars for which we obtained multiple spectra, 32 were M stars with what appeared to be stronger-than-average emission lines. Figure 2.12 shows the spectra for the target with the largest number of observations, the proposed counterpart to 1RXS J080826.7+434745. The initial spectrum suggested that we had caught this M4 star flaring, and we returned to it regularly over the course of the next two years to obtain quiescent spectra to which we could compare the flare (and because we hoped to capture another flare!). All of the spectra include the Balmer and Ca II H & K emission lines typical of M star spectra. However, these features are much stronger in the initial spectrum than in any of the others, as can be clearly seen in the bottom panel of Figure 2.12, where the spectra have been normalized to the value of their flux at 4600 Å. In addition, an emission feature at 4471 Å is evident in the initial spectrum and absent in the quiescent spectra. During a flare, the amount of material emitting at chromospheric temperatures increases, and lines due to high-excitation species such

as HeI, which is responsible for this feature, appear (Reid & Hawley, 2005). The blue continuum visible in the initial spectrum is also typically observed in flare events (e.g., Hawley & Pettersen, 1991). In a forthcoming paper (Hilton et al., 2006, in preparation) we describe the properties of M stars for which we detected similar changes to the emission lines and continuum.

Spectra for another proposed counterpart are presented in Figure 2.13. This K4 star, associated with 1RXS J171456.2+585130, shows strong, persistent Balmer emission. The emission lines are clearly broader than for the M star in Figure 2.12, suggesting that what we are observing is accretion rather than flaring, and there is therefore a currently invisible companion to the K4 star. This binary may be a cataclysmic variable; in those systems the spectra are typically (but not always) dominated by the white dwarf onto which accretion is occurring, or by the accretion disk around the white dwarf (see Figure 3.3 for sample cataclysmic variable spectra). Here the spectrum is clearly not that of a white dwarf or of a disk-dominated system, and the binary could therefore be a symbiotic system. Typically in such systems a white dwarf accretes material from the wind of a companion red giant; in some cases, the accreted material forms a disk around the white dwarf, much as in cataclysmic variables. However, symbiotics have much longer orbital periods (on the order of years), and their relatively small optical outbursts tend to occur every few years to decades (Sokoloski, 2003). With high-resolution spectroscopy the nature of this system may become obvious (e.g., cataclysmic variables tend to have broader emission lines than symbiotics); further study will then allow us to characterize it.

## **2.5 Appendix: The Catalogs**

Two separate catalogs of stellar X-ray sources are available on-line. One is for the sample of RASS counterparts identified with APO spectroscopy; representative data for the first 19 objects in this catalog are shown in Table 2.5. We give the RASS source name, count rate, hardness ratios, and detection likelihood (DL), a maximum likelihood measure of source significance. We also include the SDSS counterpart name, the

offset between the X-ray position and SDSS position expressed in terms of the X-ray positional uncertainty ( $\sigma$ ), the  $g$  magnitude and  $(g - r)$  color. From 2MASS we list the  $K_S$  magnitude and  $(J - K_S)$  color, along with  $\log(f_X/f_K)$ , calculated using equation 2.1 (Maccacaro et al., 1988; Voges et al., 1999) and substituting  $K_S$  for  $V$ . Finally, we give the date of the APO spectroscopic observations and the stellar type derived from our DIS spectra. Comments are also included, for example, if the RASS or 2MASS data have relevant flags set (the full set of SDSS flags is available in the on-line catalog), or if several objects were targeted within the RASS field. In total this catalog includes data for 492 stars, including 35 F stars, 146 G stars, 140 K stars, and 171 M stars.

A similar catalog is available for 322 sources with SIMBAD-cataloged counterparts. In addition to the six white dwarfs and four cataclysmic variables listed in Table 2.3, we include 132 F, 90 G, 74 K, and 16 M stars. The F, G, and K stars fall within  $2\sigma$  of the mean  $\log(f_X/f_V)$  calculated for their spectral class, while the M stars fall within  $2\sigma$  of the mean  $\log(f_X/f_K)$  calculated for the APO M stars. Data from the first 18 entries in this catalog are shown in Table 2.6.

### ***Acknowledgments***

We are grateful to the APO time allocation committee at the University of Washington for providing us with the nights needed to complete our spectroscopic program. We thank the telescope operators at the observatory for their assistance with our observations. We also thank Michelle Cash, Kevin Covey, Nick Cowan, Suzanne Hawley, Lee Mannikko, Anil Seth, Nicole Silvestri, and Kristine Washburn for using some of their APO observing time to obtain data for this program. Finally, we thank Beth Willman for sharing her matching code, and Kevin Covey for making available his DISpipeline script for reducing DIS data and for developing the Hammer spectral typing program.



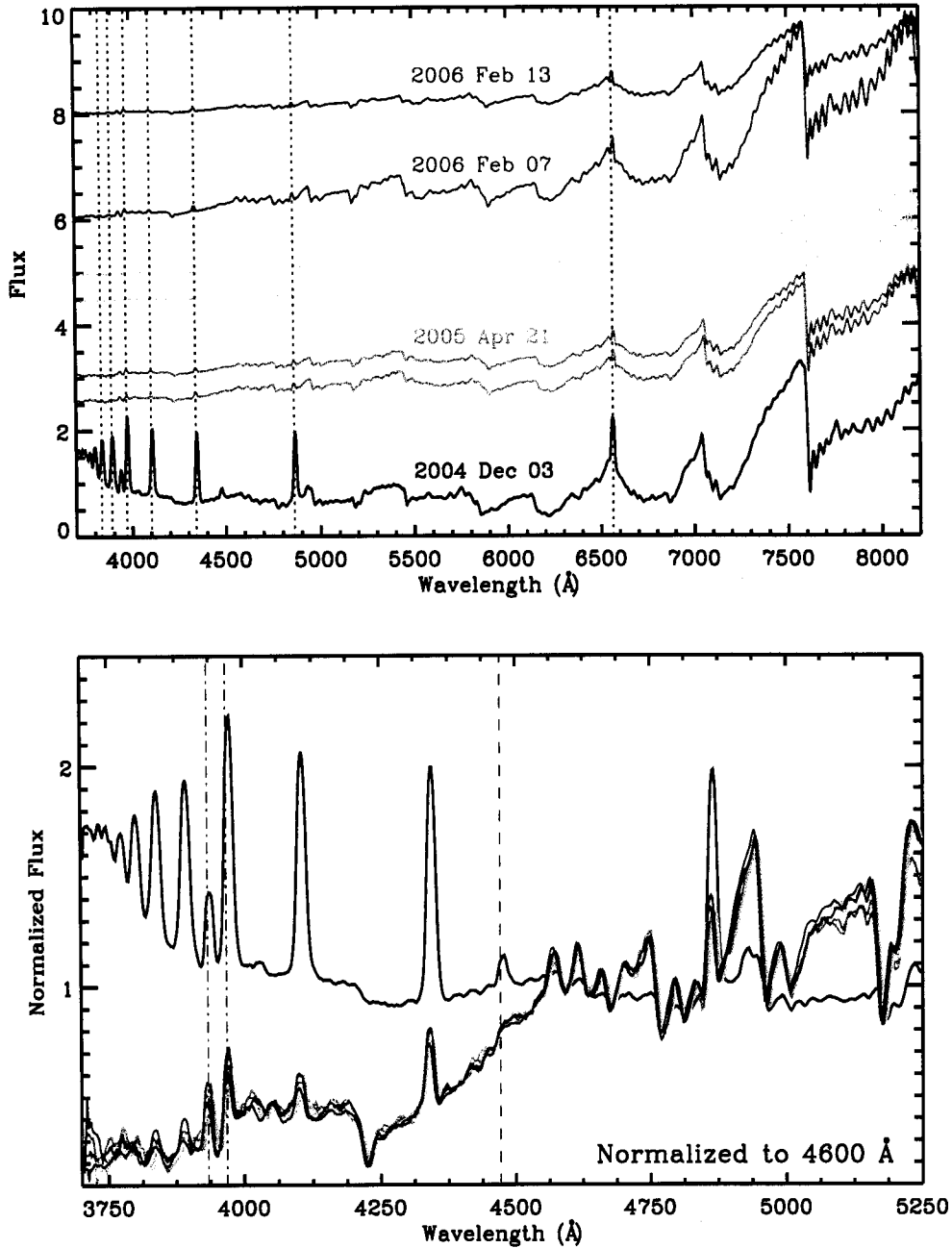


Figure 2.12: APO spectra of the proposed stellar counterpart to 1RXS J0808+4347. *Top*: The spectra are artificially offset from each other in flux; two spectra were obtained on 2005 Apr 21 and Dec 20. The dotted lines indicate the positions of the Balmer lines. *Bottom*: The blue continuum and strong Balmer emission visible in the 2004 Dec 03 spectrum are even more apparent when all of the spectra are normalized to their flux value at 4600 Å. The dot-dashed lines indicate the positions of the Ca H & K lines (at this resolution, Ca H is blended with H $\epsilon$ ), while the dashed line is He I at 4471 Å.

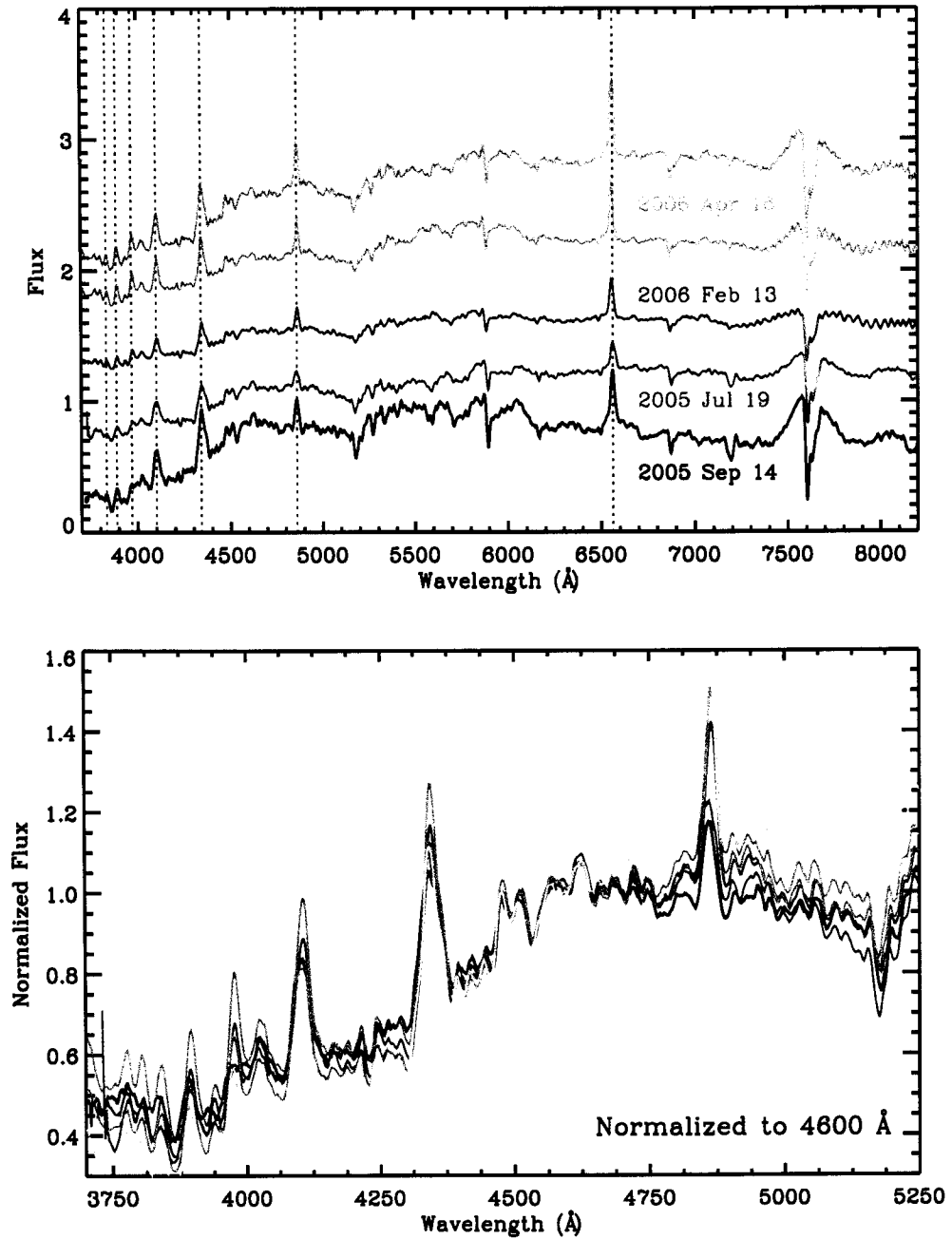


Figure 2.13: APO spectra of the proposed stellar counterpart to 1RXS J1714+5851. The spectra are presented as in Figure 2.12. Two spectra were obtained on 2006 Apr 16.

Table 2.5: X-ray and optical data for the first 18 RASS/APO stars.

1RXS J	Counts s <sup>-1</sup>	HR1	HR2	DL	SDSS J	$\sigma$	$g$	$(g-r)$
000053.1+002205	0.025 ± 0.011	0.02 ± 0.42	0.52 ± 0.74	8	000051.96+002216.4	0.9	12.79 ± 0.00	0.86 ± 0.00
000312.8-001444	0.025 ± 0.011	-0.20 ± 0.38	-1.00 ± 0.88	8	000312.64-001504.5	0.8	14.37 ± 0.02	1.08 ± 0.02
000659.3-000351	0.023 ± 0.009	0.79 ± 0.39	-0.08 ± 0.39	13	000658.40-000344.0	1.2	12.59 ± 0.00	0.80 ± 0.00
000714.2-103634	0.062 ± 0.016	-0.20 ± 0.24	0.08 ± 0.39	28	000714.07-103628.8	0.5	12.60 ± 0.00	1.39 ± 0.00
000803.1-002736	0.041 ± 0.012	0.18 ± 0.29	0.17 ± 0.36	19	000803.42-002740.5	0.4	15.92 ± 0.03	1.47 ± 0.03
000921.2+003809	0.114 ± 0.019	-0.01 ± 0.16	0.18 ± 0.21	76	000921.80+003806.5	0.9	12.09 ± 0.01	-4.00 ± 0.03
002203.7-101628	0.135 ± 0.024	-0.18 ± 0.16	0.44 ± 0.25	69	002204.48-101619.1	1.3	12.98 ± 0.01	-2.56 ± 0.17
002552.2-095756	0.055 ± 0.016	0.01 ± 0.28	0.38 ± 0.38	17	002550.98-095740.1	1.1	14.80 ± 0.03	1.45 ± 0.03
003038.1+002435	0.023 ± 0.007	0.11 ± 0.31	0.60 ± 0.33	21	003038.37+002439.3	0.5	14.41 ± 0.02	1.29 ± 0.02
003058.7+000358	0.011 ± 0.005	1.00 ± 0.93	1.00 ± 0.78	10	003059.20+000356.4	0.6	13.13 ± 0.00	1.07 ± 0.00
003215.1-000600	0.018 ± 0.007	0.01 ± 0.36	0.11 ± 0.47	10	003214.39-000613.1	1.1	14.82 ± 0.03	1.31 ± 0.03
003225.7-103123	0.018 ± 0.009	0.83 ± 0.38	-0.17 ± 0.48	8	003225.15-103122.5	0.4	13.06 ± 0.00	0.79 ± 0.00
003257.2+160943	0.038 ± 0.013	0.27 ± 0.33	-0.69 ± 0.39	13	003255.84+161001.7	1.5	14.10 ± 1.09	6.71 ± 1.09
003403.7+010558	0.124 ± 0.020	-0.03 ± 0.15	0.06 ± 0.21	83	003404.33+010547.8	1.6	11.58 ± 0.00	0.70 ± 0.00
003459.7-094555	0.026 ± 0.011	-0.70 ± 0.29	-1.00 ± 2.06	9	003458.74-094536.6	0.8	14.04 ± 0.03	1.12 ± 0.03
003651.2+145929	0.056 ± 0.014	0.29 ± 0.24	-0.15 ± 0.33	31	003650.14+145950.7	1.5	12.05 ± 0.01	2.72 ± 0.01
003934.4+145424	0.045 ± 0.012	-0.42 ± 0.24	-0.52 ± 0.86	24	003933.54+145419.0	1.0	15.10 ± 0.02	1.06 ± 0.03
004222.8-094033	0.024 ± 0.010	-0.37 ± 0.47	1.00 ± 9.99	10	004225.12-094033.3	1.8	10.55 ± 0.00	0.30 ± 0.00

Table 2.5: (continued) Infrared and APO data for the first 18 RASS/APO stars.

1RXS J	SDSS J	$K_S$	$(J - K_S)$	$\log (f_X/f_K)$	Observed	Notes
000053.1+002205	000051.96+002216.4	$9.55 \pm 0.02$	$0.75 \pm 0.03$	-3.41	2003 Nov 08	K4
000312.8-001444	000312.64-001504.5	$10.54 \pm 0.02$	$0.75 \pm 0.03$	-3.01	2003 Dec 07	K7
000659.3-000351	000658.40-000344.0	$9.74 \pm 0.02$	$0.65 \pm 0.03$	-3.37	2004 Oct 04	K2
000714.2-103634	000714.07-103628.8	$7.99 \pm 0.02$	$0.84 \pm 0.03$	-3.64	2003 Sept 03	M1
000803.1-002736	000803.42-002740.5	$10.09 \pm 0.02$	$0.82 \pm 0.03$	-2.98	2004 Oct 04	M3
000921.2+003809	000921.80+003806.5	$8.71 \pm 0.02$	$0.73 \pm 0.03$	-3.09	2003 Dec 07	K3
002203.7-101628	002204.48-101619.1	$8.67 \pm 0.02$	$0.37 \pm 0.04$	-3.03	2003 Nov 08	K7e; multiple targets
002552.2-095756	002550.98-095740.1	$8.95 \pm 0.03$	$0.84 \pm 0.03$	-3.31	2003 Sept 03	M4
003038.1+002435	003038.37+002439.3	$9.96 \pm 0.02$	$0.93 \pm 0.04$	-3.28	2003 Nov 08	K7
003058.7+000358	003059.20+000356.4	$9.46 \pm 0.02$	$0.77 \pm 0.03$	-3.82	2004 Oct 04	K4
003215.1-000600	003214.39-000613.1	$10.44 \pm 0.02$	$0.74 \pm 0.04$	-3.20	2005 Sept 16	K7; RASS flags set
003225.7-103123	003225.15-103122.5	$10.08 \pm 0.02$	$0.85 \pm 0.03$	-3.35	2003 Nov 08	G9
003257.2+160943	003255.84+161001.7	$5.74 \pm 0.02$	$0.58 \pm 0.03$	-4.76	2004 Oct 04	F7
003403.7+010558	003404.33+010547.8	$8.85 \pm 0.02$	$0.26 \pm 0.03$	-2.99	2003 Nov 08	K1
003459.7-094555	003458.74-094536.6	$10.28 \pm 0.02$	$0.64 \pm 0.03$	-3.10	2003 Nov 08	K5
003651.2+145929	003650.14+145950.7	$7.67 \pm 0.02$	$0.78 \pm 0.03$	-3.82	2003 Dec 15	K2
003934.4+145424	003933.54+145419.0	$9.12 \pm 0.02$	$0.45 \pm 0.03$	-3.33	2004 Oct 04	M4
004222.8-094033	004225.12-094033.3	$9.06 \pm 0.02$	$0.84 \pm 0.03$	-3.62	2005 Sept 16	F8

Table 2.6: X-ray and optical data for the first 18 RASS/SIMBAD stars.

1RXS J	Counts s <sup>-1</sup>	HR1	HR2	DL	SIMBAD name	$\sigma$	V	log ( $f_X/f_V$ )
000447.9-095206	0.051 ± 0.015	-0.29 ± 0.28	-0.49 ± 0.91	14	HD 225263	1.7	10.00	-2.92
001308.9-002548	0.082 ± 0.016	-0.10 ± 0.18	0.12 ± 0.27	64	DENIS J001309.3-002551	0.7	N/A	N/A
001745.3-010255	0.097 ± 0.019	-0.05 ± 0.18	-0.12 ± 0.27	53	HD 1353	0.4	9.83	-2.71
002246.7-091332	0.065 ± 0.016	0.45 ± 0.25	0.16 ± 0.29	32	V* BD Cet	1.4	7.97	-3.63
003409.5+151136	0.105 ± 0.019	0.20 ± 0.18	-0.05 ± 0.22	67	BD+14 65	1.1	9.27	-2.90
003942.9-110937	0.048 ± 0.016	0.03 ± 0.34	0.93 ± 0.38	14	HD 3708	0.6	6.83	-4.22
004510.2+001522	0.166 ± 0.026	-0.08 ± 0.14	0.06 ± 0.21	94	NLTT 2476	1.5	7.00	-3.61
005119.6-092444	0.013 ± 0.007	-0.36 ± 0.47	-0.37 ± 0.60	7	HD 4939	1.3	6.90	-4.75
005659.6+002727	0.024 ± 0.010	0.23 ± 0.38	-1.00 ± 0.86	8	HD 5520	0.6	8.36	-3.90
010637.9+135302	0.027 ± 0.010	-0.67 ± 0.32	0.23 ± 1.75	12	HD 6566	1.0	7.30	-4.28
011125.4+152625	0.094 ± 0.018	-0.08 ± 0.20	-0.47 ± 0.26	62	GJ 3076	0.3	13.59	-1.22
013418.2-082724	0.016 ± 0.007	0.46 ± 0.63	1.00 ± 0.66	11	CCDM J01343-0827AB	1.0	8.06	-4.20
014008.7-001441	0.097 ± 0.024	0.06 ± 0.23	0.24 ± 0.29	34	HD 10232	1.9	7.28	-3.73
014149.4-000920	0.039 ± 0.016	-0.28 ± 0.35	0.77 ± 1.52	13	BD-00 262	1.3	9.66	-3.18
014920.7+003615	0.020 ± 0.009	-0.29 ± 0.37	-0.04 ± 0.63	14	BD-00 279	0.6	9.87	-3.38
015404.1+001037	0.026 ± 0.010	0.72 ± 0.26	0.26 ± 0.39	12	CCDM J01541+0011AB	0.8	10.18	-3.15
015543.3+002817	0.042 ± 0.012	0.36 ± 0.28	0.44 ± 0.30	29	PHL 1242	1.0	16.60	-0.59

Table 2.6: (continued) Infrared data for the first 18 RASS/SIMBAD stars. “U” indicates that  $K_S$  is an upper limit. HD 225263 does not have a 2MASS counterpart; no 2MASS error estimates are available for PHL 1242.

1RXS J	SIMBAD name	$K_S$	log			Notes
			$(J - K_S)$	$(f_X/f_K)$	$(f_X/f_K)$	
000447.9-095206	HD 225263	N/A	N/A	N/A	N/A	K0; double star system
001308.9-002548	DENIS J001309.3-002551	$11.32 \pm 0.03$	$0.85 \pm 0.04$	-2.19	-2.19	M5.5
001745.3-010255	HD 1353	$8.26 \pm 0.02$	$0.42 \pm 0.04$	-3.34	-3.34	G5
002246.7-091332	V* BD Cet	$5.13 \pm 0.02$	$0.77 \pm 0.03$	-4.76	-4.76	G5; RS CVn
003409.5+151136	BD+14 65	$7.79 \pm 0.02$	$0.37 \pm 0.03$	-3.49	-3.49	G0
003942.9-110937	HD 3708	$5.68 \pm 0.02$	$0.26 \pm 0.03$	-4.68	-4.68	F5; RASS flags set
004510.2+001522	NLT 2476	$5.63 \pm 0.02$	$0.35 \pm 0.03$	-4.16	-4.16	F8; high proper motion star
005119.6-092444	HD 4939	$5.67 \pm 0.02$	$0.30 \pm 0.03$	-5.25	-5.25	F2
005659.6+002727	HD 5520	$7.46 \pm 0.02$	$0.19 \pm 0.04$	-4.26	-4.26	F2V
010637.9+135302	HD 6566	$6.18 \pm 0.02$	$0.18 \pm 0.03$	-4.73	-4.73	F6V
011125.4+152625	GJ 3076	$8.21 \pm 0.03$	$0.87 \pm 0.04$	-3.38	-3.38	M5; flare star
013418.2-082724	CCDM J01343-0827AB	$6.85 \pm 0.03$	$0.26 \pm 0.04$	-4.68	-4.68	F5; multiple star system
014008.7-001441	HD 10232	$6.17 \pm 0.02$	$0.24 \pm 0.03$	-4.17	-4.17	F5
014149.4-000920	BD-00 262	$7.61 \pm 0.02$	$0.56 \pm 0.03$	-4.00	-4.00	K2
014920.7+003615	BD-00 279	$8.39 \pm 0.02$	$0.38 \pm 0.03$	-3.98	-3.98	G5
015404.1+001037	CCDM J01541+0011AB	$8.62 \pm 0.03$	$0.37 \pm 0.03$	-3.77	-3.77	G0; multiple star system
015543.3+002817	PHL 1242	0.33	16.17	-0.54	-0.54	Polar; U; $f_X/f_B$

## Chapter 3

### **A CATALOG OF X-RAY-EMITTING CATAclySMIC VARIABLES FROM THE *ROSAT* ALL-SKY AND SLOAN DIGITAL SKY SURVEYS**

*The data discussed in this chapter and presented in Table 3.2 and Figure 3.3 are culled from a series of papers which appeared in the Astronomical Journal (Szkody et al., 2002, 2003, 2004a, 2005, 2006, all © the American Astronomical Society). In addition, Section 3.3.2 of this chapter and the associated figures and table data originally appeared in the Astronomical Journal (Szkody et al., 2002, © the American Astronomical Society). The inclusion of these materials in this chapter is by permission of the American Astronomical Society. Where necessary, they have been edited to conform to University of Washington's requirements for doctoral theses.*

#### **3.1 Introduction**

Cataclysmic variables (CVs) are binary systems in which a white dwarf (WD) accretes material from its companion, typically a late-type star. These systems are characterized observationally by their variability, and CVs are accordingly divided into novae, dwarf novae, and nova-likes. Classical novae, which are thought to be produced by thermonuclear runaway events, have the largest increase in brightness (10 to 20 magnitudes), but are not periodic, or at least have only one *observed* eruption (classical novae that are found to repeat their outbursts are known as recurrent novae; Warner, 1995). Dwarf novae undergo quasi-periodic changes in their brightness of order 2 to 7 magnitudes on timescales of weeks to years; these are usually thought to be due to instabilities in the accretion disk around the WD. Finally, nova-likes have unpredictable increases in their brightness of order a few magnitudes. These events are thought to reflect changes in the mass-transfer process (and hence stronger/weaker accretion onto the WD; Szkody et al., 2002). Both dwarf novae and nova-likes are further di-

vided according to their properties (e.g., Verbunt et al., 1997); see Table 3.1 for details. Essentially CVs are characterized by the rate of the mass transfer from the donor onto the WD and by the latter’s magnetic moment (Kuulkers et al., 2003).

Table 3.1: Cataclysmic variable nomenclature.

Class	Differentiating characteristic	Subclass
Dwarf novae	Occasional super-outbursts	SU UMa
	Brightness plateaus before quiescence	Z Cam
	All others	U Gem
Nova-likes	Strong B field locks WD to orbit	AM Her/polar
	Strong B field, no locking	DQ Her/intermediate polar
	No evidence for WD B field	UX UMa
Either	Donor is also WD	AM CVn/double degenerate

Before the Sloan Digital Sky Survey (SDSS; York et al., 2000) began taking data,  $\sim 1000$  CVs were known (Downes et al., 2001). Most of these systems include a (faint) M-dwarf companion and are fairly faint in quiescence—but have prominent accretion disks or strong outbursts. The result is a bright and blue object that is fairly easy to detect, but is probably not representative of the overall population of Galactic CVs. Evolutionary models predict that aging CVs will have very low mass-transfer rates and cool, optically faint secondary stars, but this harder-to-detect population was under-sampled before the advent of SDSS. As a result, questions such as the true number of CVs in the Galaxy and their age distribution are difficult to answer (Szkody et al., 2002). These questions are directly related to broader questions about our Galaxy: for example, there is currently much debate about the abundance in the Galactic Center of high-mass X-ray binaries and of CVs (e.g., discussion in Munro et al., 2005). These abundances reflect the Galactic star formation history: the presence of high-mass X-ray binaries, in which matter from a 10 or 20  $M_{\odot}$  star accretes onto a degenerate companion, implies recent episodes of massive star formation. By contrast, CVs, where



the donor is a low-mass star, are longer-lived. If they dominate the stellar population detected at hard X rays, tidal disruptions of globular clusters, in which CVs form preferentially, might be the main process shaping the central Galactic stellar population (Laycock et al., 2005, and references therein).

While designed as a galaxy survey, SDSS is in fact an ideal tool for finding rare Galactic objects such as CVs. The survey's five-color  $u, g, r, i, z$  photometry and faint limiting magnitudes make it useful for selecting both blue objects such as the young CVs and red ones such as the older ones. Furthermore, its spectroscopy renders confirmation of a candidate CV straightforward, as the easily detected presence of hydrogen Balmer and helium emission lines are telltale signs of ongoing accretion (Szkody et al., 2002). Accordingly, the data have yielded more than 150 *new* spectroscopically confirmed CVs to date, with another 30 or so known CVs having been recovered in the SDSS spectroscopic survey (Szkody et al., 2006).

The general properties of these SDSS CVs have been described in a series of discovery papers by P. Szkody and collaborators (Szkody et al., 2002, 2003, 2004a, 2005, 2006). In this chapter we focus on those systems found to be X-ray emitters through correlations with the *ROSAT* All-Sky Survey (RASS) Bright and Faint Source Catalogs (Voges et al., 1999, 2000). In §3.2 we summarize the mechanisms through which CVs are thought to produce X rays. In §3.3, we present and discuss the properties of the published SDSS CVs that are X-ray emitters, and give an example of the follow-up work required to characterize one of these systems. Finally, in §3.4 we describe the handful of candidate X-ray-emitting CVs found in the SDSS spectroscopy since the last SDSS discovery paper was published.

### **3.2 X-ray Emission in Cataclysmic Variables**

Although CVs, which have typical X-ray luminosities between  $10^{29}$  and  $10^{32}$  erg s<sup>-1</sup> (Verbunt et al., 1997), do not belong to a particularly X-ray-bright class of objects, individual CVs were among the earliest known sources of X rays. Several were detected in soft X rays ( $< 1$  keV) by rocket-borne experiments (e.g., SS Cyg by Rappaport et al.,

1974), and one magnetic system, EX Hya, was detected in hard X rays (2.0 – 6.0 keV) by *Uhuru* (Warner, 1972), in the early 1970s. Based on later data from the *Einstein Observatory*, Patterson & Raymond (1985a,b) developed the first observationally supported models for hard and soft X-ray emission from CVs. For highly magnetic CVs, where the white dwarf has  $B \sim 10^7 - 10^8$  G, the emission of hard X rays is probably due to radial accretion onto the magnetic poles—a process that creates a shock above the star’s surface and converts infall energy to hard X rays (Patterson & Raymond, 1985a). This process, however, is unlikely to explain the production of hard X rays in most CVs, where accretion onto the WD takes place through a disk, and where the WD magnetic field is weaker. In those systems, Patterson & Raymond suggested that the boundary between the rapidly rotating disk and the slowly rotating WD is the source of hard X rays, with some fraction of the gravitational energy of infalling matter (which depends on the accretion rate) producing a hot ( $> 10^5$  K), optically thin layer emitting the observed X rays (Patterson & Raymond, 1985a). The emission of soft X rays can then be understood as taking place in the limit of this model, when high accretion rates ( $> 1.5 \times 10^{-10} M_{\odot} \text{ yr}^{-1}$ ) render the boundary layer optically thick (Patterson & Raymond, 1985b).

Polars and intermediate polars are thought to be the most inherently luminous X-ray sources among CVs (e.g., Verbunt et al., 1997). Polars, somewhat surprisingly, are particularly bright at *soft* X-ray energies (below  $\sim 1$  keV) despite the absence of accretion disks in these systems (Warner, 1995). For example, in their study of *ROSAT*-detected CVs, Verbunt et al. found that while seven of the ten brightest sources overall were AM Her-type systems, only two of these polars were among the brightest detected at energies between 0.5 and 2.5 keV—the *ROSAT* hard X-ray energy band (Verbunt et al., 1997). The hard X rays produced in these CVs by the radial accretion mechanism described above are reprocessed in the WD atmosphere, which also intercepts and reprocesses as much as half of the cyclotron radiation emitted by the accretion column into soft X rays (see discussion in Kuulkers et al., 2003). As a result, the ratio of soft to hard X rays in these CVs depends strongly on the relative importance of thermal bremsstrahlung and cyclotron cooling in the WD atmosphere, and therefore on the WD

magnetic field strength (de Martino et al., 2006, and references therein). The accretion rate is also key, as it determines both the main heating and cooling mechanisms for the accretion region (Kuulkers et al., 2003). In any case, because of the interstellar medium’s opacity to soft X rays ( $< 100$  eV), we are largely unable to observe much and perhaps most of the X-ray emission produced by these CVs, with the exceptions being nearby systems. It is therefore possible that the X-ray census of polars is essentially complete for objects with  $V < 20$  mag, with *ROSAT* having detected (if not yet identified) all of these CVs (Warner, 1995). However, even occasionally X-ray-bright polars appear to spend much of their lives in low-accretion states (e.g., Ramsay et al., 2004), and may therefore have evaded *ROSAT*<sup>1</sup>.

Intermediate polars (IPs), with lower magnetic fields and truncated accretion disks, are both harder and brighter X-ray sources than polars. The accretion in these systems occurs over a larger area of the WD (Kuulkers et al., 2003), producing an  $L_X$  roughly ten to one hundred times that of polars (Warner, 1995). Higher intrinsic absorption than in polars may help explain the absence of detected soft X-ray emission from IPs (de Martino et al., 2006). The nature of the possible evolutionary relationship between the polars and IPs is still unclear; a few IPs do in fact emit soft X rays, suggesting that they may be polar progenitors (de Martino et al., 2006).

One consequence of the diversity of CVs and of the inherent variability in their X-ray emission is that the observed ratio of X-ray to optical fluxes (a standard tool in characterizing X-ray sources; see, for example, Chapter 2) is perhaps less useful than for other classes of X-ray emitters. These flux ratios are strongly dependent on the mechanism responsible for the X-ray production and by extension the nature of the CV. Non-magnetic CVs typically have  $-3 < \log(f_X/f_{opt}) < 1$ , while polars have  $0.5 < \log(f_X/f_{opt}) < 2.5$ ; because IPs are optically brighter on average than polars, their  $f_X/f_{opt}$  ratios are similar to those of the non-magnetic systems. Clearly, however, an individual CV’s flux ratio will vary as a function of its state, with dwarf novae, for

---

<sup>1</sup>Also likely to be underrepresented in the RASS data are low-accretion-rate magnetic CVs (Schwope et al., 2002). A few of these systems, thought to be pre-polars, have been discovered in SDSS; they are too faint to have RASS detections, and are barely detected in follow-up X-ray observations (Szkody et al., 2004b; Schmidt et al., 2005a).

example, producing on average three times as much hard X-ray flux during outbursts than at quiescence (Warner, 1995).

### 3.3 Published X-ray-Emitting SDSS Cataclysmic Variables

*ROSAT*, designed to be five times more sensitive than *Einstein*, was expected to discover thousands of new CVs. This prediction has yet to be confirmed (Warner, 1995), although the counterparts to a large fraction of the 124,000 sources included in the RASS Bright and Faint Source Catalogs (Voges et al., 1999, 2000) remain unidentified (see Chapter 1). New magnetic CVs have been found in the RASS, most of them polars, with the number cataloged growing from roughly a dozen before the survey to over 80—a substantial increase, if still a small total number of systems (Kuulkers et al., 2003; Staude et al., 2003; Schmidt et al., 2005a). Because *ROSAT*’s sensitivity does not extend past 2.5 keV, it is not ideally suited to detecting very hard sources such as IPs. Still, follow-up observations of RASS sources has added roughly 20 new IPs to the handful that had been previously cataloged in the X ray (Staude et al., 2003), and identified at least one new variety of CVs, the “soft IPs” (de Martino et al., 2006).

Table 3.2 lists the 40 SDSS CVs found to have X-ray counterparts in the RASS and published as part of the SDSS CV discovery papers (Szkody et al., 2002, 2003, 2004a, 2005, 2006). This is not a complete list of X-ray-emitting CVs in the SDSS/RASS overlap region. Rather, this is a list of *color-selected and spectroscopically confirmed SDSS CVs falling within 1' of a RASS source*<sup>2</sup>; the typical separation was under 45". Because of the survey design, not every candidate CV identified in the SDSS photometry is targeted for spectroscopic follow-up. Conversely, some fraction of the SDSS spectra of CVs are “accidentally” obtained, since CVs share color-space with quasars (QSOs) and are therefore occasionally targeted as part of the SDSS spectroscopic QSO or serendipity surveys (90% of the spectra for the first SDSS CV sample, for example, came from these two surveys; Szkody et al., 2002).

---

<sup>2</sup>One published CV, SDSS J075853.03+161645.2, is more than 1' removed from the RASS position (Szkody et al., 2006). In addition, another CV, SDSS J023322.61+005059.5, was found to have a counterpart in the *ROSAT* catalog of pointed observations, but not in the RASS (Szkody et al., 2002).

Since the space density of both SDSS CVs and RASS sources is low ( $\sim 0.04 \text{ deg}^{-2}$  and  $\sim 3 \text{ deg}^{-2}$ , respectively), the likelihood that a given CV is a RASS source is *a priori* fairly high. The case for the CV/RASS association was strengthened by searching the SDSS spectroscopic databases for other, nearby possible counterparts to the X-ray source. The standard catalogs were also examined for other possible counterparts.

Table 3.2 includes the SDSS name and  $g$  magnitude<sup>3</sup>, the corresponding RASS source, and the separation between the two ( $\sigma$ ) expressed in terms of the X-ray positional uncertainty, for each CV. It also lists the RASS count rate and X-ray flux (calculated assuming a 2 keV bremsstrahlung spectrum; 1 count  $\text{s}^{-1}$  corresponds to a 0.1 to 2.4 keV flux of about  $7 \times 10^{-12} \text{ ergs cm}^{-2} \text{ s}^{-1}$ ).  $\log(f_X/f_{opt})$  was calculated for each of these sources using the Maccacaro et al. (1988) formula adapted to the RASS (equation 2.1; Voges et al., 1999) and substituting  $g$  for  $V$ ; we also include the systems' periods, if known, and their cataloged name, if they were previously published. In several cases the data have been updated to reflect information obtained from follow-up observations; for example, the period of SDSS J085414.02+390537.3 is now known, while 144659.95+025330.3 has been confirmed as an IP (P. Szkody 2006, private communication). The SDSS spectra for the 40 CVs are presented again in Figure 3.3.

Below we discuss the  $\log(f_X/f_{opt})$  distributions for these CVs, and reproduce the classic Patterson & Raymond (1985a)  $\log(f_X/f_{opt})$  versus  $H\beta$  equivalent width plot. In the following section we provide an example of a detailed study of one of these CVs in which we participated (Szkody et al., 2002).

### 3.3.1 Flux ratios and $H\beta$ equivalent width

The left panel of Figure 3.1 is a histogram of the overall  $\log(f_X/f_g)$  distribution for the CVs in Table 3.2. While this distribution is fairly symmetric about the median (0.40), the right panel, which separates the CVs by type where known, shows the expected offset between confirmed polars (median  $\log(f_X/f_g) = 1.13$ ) and dwarf novae (median  $\log(f_X/f_g) = 0.28$ ).

---

<sup>3</sup>We use PSF magnitudes throughout this Chapter.

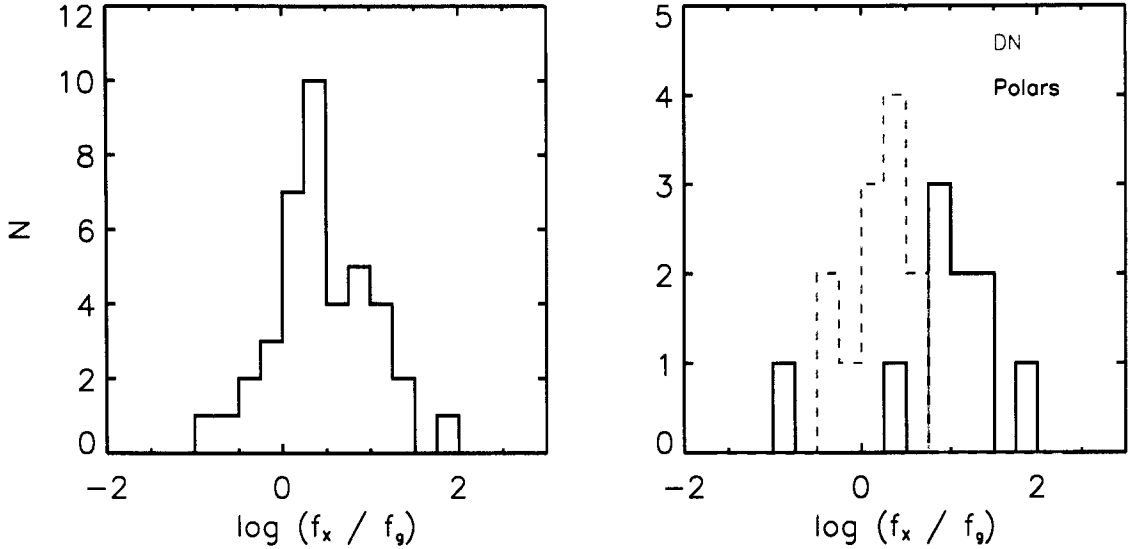


Figure 3.1: *Left panel:* Distribution of  $\log(f_X/f_g)$  for all of the published SDSS/RASS CVs. *Right panel:* The same distribution for the known dwarf novae and polars.

Strong HeII emission in a spectrum indicates that the CV is either magnetic or undergoing high mass transfer. Follow-up polarimetry is generally required to determine whether the system is in fact magnetic and to differentiate between polars and IPs; large circular polarization is observed in polars and not IPs (Wickramasinghe & Ferrario, 2000). Time-resolved photometry and spectroscopy also help to identify the nature of the system: IPs and high-mass-transfer systems both show less polarization than polars, but the WDs in the former are rapidly rotating with spin periods on the order of only a few minutes (Szkody et al., 2005).

Patterson & Raymond (1985a) were the first to identify a correlation between the  $f_X/f_g$  ratio and the equivalent width of the  $H\beta$  emission line, a proxy for the CV's overall emission strength. In Figure 3.2 we plot these two quantities for our CV sample. The  $H\beta$  equivalent widths are reported in Szkody et al. (2002, 2003, 2004a, 2005, 2006) for all but one of these CVs, SDSS J083642.80+532838.1 (SW UMa), for which we measure it directly<sup>4</sup>. The Patterson & Raymond (1985a) relationship holds for the

<sup>4</sup>Here and elsewhere we used IRAF's fitting routines in *splot*.

majority of these CVs, with the scatter around the predicted  $f_X/f_g$  being comparable to that found in other studies (e.g., Richman, 1996). However, there are clear departures from the Patterson & Raymond (1985a) relationship, with the polars in particular appearing to form a distinct population from the dwarf novae and other CVs. Furthermore, because they are relatively faint optically, the SDSS CVs tend to have higher  $f_X/f_{opt}$  ratio than those included in the earlier studies, where only a handful had  $\log(f_X/f_{opt}) \geq 0$  (Richman, 1996).

The  $\log(f_X/f_g) = -0.93$  of SDSS J015543.40+002807.2 makes it a clear outlier relative to the other polars plotted in Figure 3.1, and explains its anomalous position in Figure 3.2. As noted by Szkody et al. (2002), SDSS J0155 was significantly brighter when observed by the survey than in its Digitized Sky Survey (DSS) image. A change in brightness of a few magnitudes—typical for polars entering a phase of stronger accretion—would be sufficient to explain the apparent inconsistency of this system’s  $\log(f_X/f_g)$  relative to that of other polars. Follow-up observations by Schmidt et al. (2005b) confirmed that this an eclipsing polar, with the shortest known period of any such system.

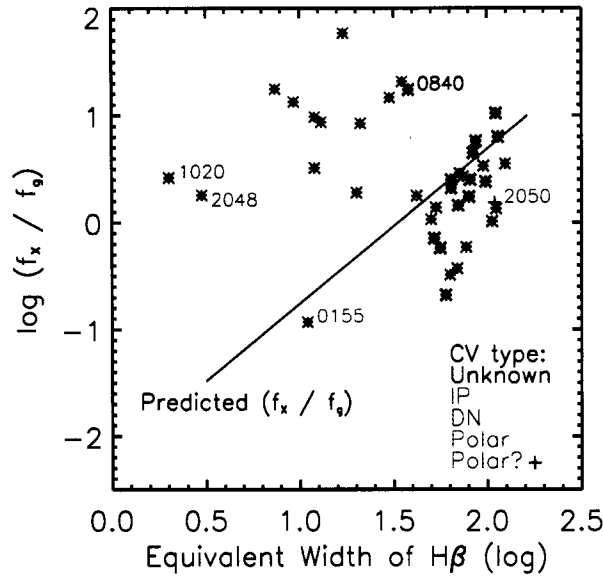


Figure 3.2:  $\log(f_X/f_g)$  versus equivalent width of the  $H\beta$  line for the 40 published SDSS/RASS CVs. The predicted  $f_X/f_g$  is from Patterson & Raymond (1985a).

While the SDSS spectrum of SDSS J205017.84–053626.8, another system highlighted in Figure 3.2, showed HeII emission, initial follow-up observations of this CV could not confirm whether it is a magnetic system (Szkody et al., 2003). It does not appear to have polarized emission to the limits of the current observations, and is considered a candidate intermediate polar (P. Szkody 2006, private communication). Indeed, its  $\log(f_X/f_g)$  of 0.19 is similar to that of other IPs in our sample. As mentioned earlier, because IPs are optically brighter on average than polars, their flux ratios are similar to those of non-magnetic CVs. However, SDSS J2050 has a period of 1.6 hr, much shorter than is typical for IPs, suggesting that this is in fact not a magnetic system.

We investigated the properties of a number of other systems because of their position in Figure 3.2. SDSS J102026.53+530433.1, the dwarf nova KS UMa, has an anomalously low  $H\beta$  equivalent width relative to other dwarf novae; this is because its SDSS spectrum was taken during an outburst and is dominated by the accretion disk. As for SDSS J204827.91+005008.9, its spectrum is very unusual (see Figure 3.3), with a hump apparent between 4000 and 5000 Å and a typical M-dwarf continuum to the red of the hump. Follow-up observations by Schmidt et al. (2005a) led to the conclusion that this is a low-accretion magnetic binary and possibly a pre-polar system.

Interestingly, the X-ray luminosity derived for this CV is an order of magnitude greater than the  $L_X$  for similar SDSS systems, where the X-ray emission is thought to be due to coronal emission from the late-type companion star (Szkody et al., 2004b). Schmidt et al. (2005a) suggest that this weakens the case for SDSS J2048 as an X-ray emitter. Accordingly, on 2005 August 08 we obtained a spectrum for the most obvious potential X-ray counterpart in the RASS field with the APO 3.5-m telescope using DIS in low-resolution mode. The spectrum, of a bright nearby star ( $g = 14.43 \pm 0.00$  mag) was then typed using the Hammer, an IDL code developed by K. Covey (see Chapter 2 for details about our observing set-up and typing procedure). This G6 star has a 2MASS counterpart with  $K_S = 14.85 \pm 0.12$  mag; the resulting  $\log(f_X/f_K)$  of  $-1.55$  is not typical for G stars (see Chapter 2). However, this is a crowded field; pointed X-ray observations are required to confirm that SDSS J2048 is an X-ray source.



Table 3.2: Optical and X-ray properties of the published SDSS CVs; these data originally appeared in Szkody et al. (2002, 2003, 2004a, 2005, 2006). Fluxes are calculated for a 2 keV bremsstrahlung spectrum.

SDSS J	$g$	1RXS J	$\sigma$	counts s <sup>-1</sup>	Flux $\times 10^{-12}$	log ( $f_X/f_g$ )	P hr	Comments
015543.40+002807.2	15.18 $\pm$ 0.02	015543.3+002817	1.0	0.042 $\pm$ 0.012	0.30 $\pm$ 0.09	-0.93	1.45	PHL 1242, P
075117.32+144423.9	14.18 $\pm$ 0.00	075117.6+144434	1.1	2.964 $\pm$ 0.268	20.75 $\pm$ 1.88	0.51	5.19	PQ Gem; IP
075853.03+161645.2	15.33 $\pm$ 0.02	075855.4+161801	0.9	0.321 $\pm$ 0.138	2.25 $\pm$ 0.97	0.01	1.44	DW Cnc; IP
083619.15+212105.4	16.77 $\pm$ 0.02	083620.2+212109	1.8	0.049 $\pm$ 0.019	0.34 $\pm$ 0.13	-0.23	1.76	CC Cnc; DN
083642.80+532838.1	16.89 $\pm$ 0.02	083641.7+532844	1.2	0.254 $\pm$ 0.033	1.78 $\pm$ 0.23	0.53	...	SW UMa; DN
083845.23+491055.5	19.59 $\pm$ 0.02	083845.8+491038	0.8	0.035 $\pm$ 0.013	0.25 $\pm$ 0.09	0.76	...	
084026.16+220446.6	19.89 $\pm$ 0.03	084024.8+220438	0.5	0.082 $\pm$ 0.026	0.57 $\pm$ 0.18	1.24	...	
085344.00+574841.0	16.40 $\pm$ 0.02	085343.5+574846	1.0	0.414 $\pm$ 0.035	2.90 $\pm$ 0.25	0.55	...	BZ UMa; DN
085414.02+390537.3	19.17 $\pm$ 0.01	085413.1+390543	1.6	0.124 $\pm$ 0.021	0.87 $\pm$ 0.14	1.13	1.89	EUVE J0854; P
085909.18+053654.5	18.59 $\pm$ 0.02	085909.5+053703	0.9	0.233 $\pm$ 0.028	1.63 $\pm$ 0.20	1.17	1.10	RX 0859; P
094325.90+520128.8	16.35 $\pm$ 0.03	094327.7+520139	1.4	0.026 $\pm$ 0.009	0.18 $\pm$ 0.06	-0.68	...	
094431.71+035805.5	16.78 $\pm$ 0.02	094432.1+035738	1.4	0.089 $\pm$ 0.022	0.62 $\pm$ 0.16	0.03	...	RX 0944.5; DN
101534.67+090442.1	17.22 $\pm$ 0.02	101534.8+090448	0.8	1.145 $\pm$ 0.098	8.02 $\pm$ 0.69	1.32	1.33	GG Leo; P
102026.53+530433.1	17.43 $\pm$ 0.04	102027.1+530439	1.0	0.119 $\pm$ 0.017	0.83 $\pm$ 0.12	0.42	1.60	KS UMa; DN
105135.15+540436.0	18.39 $\pm$ 0.03	105135.3+540438	0.3	1.109 $\pm$ 0.045	7.76 $\pm$ 0.31	1.77	1.91	EK UMa; P

Table 3.2: (continued) The period for SDSS J1538 is estimated based on a single-night observation (Szkody et al., 2004a).

SDSS J	$g$	1RXS J	$\sigma$	counts s <sup>-1</sup>	Flux $\times 10^{-12}$	log ( $f_X/f_g$ )	P hr	Comments
105657.00+494118.3	17.78 $\pm$ 0.02	105656.9+494111	0.8	0.096 $\pm$ 0.016	0.67 $\pm$ 0.11	0.46	1.63	CY UMa; DN
110014.72+131552.1	18.67 $\pm$ 0.02	110014.7+131608	1.0	0.035 $\pm$ 0.013	0.24 $\pm$ 0.09	0.38	...	...
110425.64+450314.0	15.77 $\pm$ 0.02	110425.6+450319	0.8	1.771 $\pm$ 0.069	12.40 $\pm$ 0.48	0.93	1.91	AN UMa; P
113122.39+432238.6	16.17 $\pm$ 0.03	113121.8+432242	0.6	0.054 $\pm$ 0.015	0.38 $\pm$ 0.10	-0.43	1.53	RX 1131; DN
113215.50+624900.4	18.49 $\pm$ 0.03	113213.3+624903	0.9	0.025 $\pm$ 0.009	0.17 $\pm$ 0.06	0.16	1.40	...
113722.25+014858.6	18.72 $\pm$ 0.03	113723.5+014847	1.1	0.026 $\pm$ 0.010	0.18 $\pm$ 0.07	0.28	...	RZ Leo; DN
113826.73+061919.5	18.85 $\pm$ 0.02	113826.5+061910	0.6	0.031 $\pm$ 0.011	0.21 $\pm$ 0.08	0.40	...	...
113826.82+032207.1	14.86 $\pm$ 0.02	113826.8+032210	0.4	0.659 $\pm$ 0.061	4.61 $\pm$ 0.42	0.13	...	T Leo; DN
114628.80+675909.7	18.76 $\pm$ 0.03	114631.3+675932	1.3	0.023 $\pm$ 0.007	0.16 $\pm$ 0.05	0.24	...	...
124325.92+025547.5	18.33 $\pm$ 0.02	124326.5+025603	0.8	0.125 $\pm$ 0.035	0.87 $\pm$ 0.25	0.80	...	...
124426.26+613514.6	18.76 $\pm$ 0.02	124424.5+613511	0.8	0.023 $\pm$ 0.009	0.19 $\pm$ 0.07	0.32	...	...
125834.77+663551.6	20.53 $\pm$ 0.04	125837.1+663608	1.4	0.027 $\pm$ 0.010	0.19 $\pm$ 0.07	1.02	...	...
130753.87+535130.6	16.53 $\pm$ 0.02	130753.6+535137	1.1	1.859 $\pm$ 0.064	13.01 $\pm$ 0.45	1.25	1.33	EV UMa; P
144659.95+025330.3	18.20 $\pm$ 0.02	144700.9+025344	0.9	0.040 $\pm$ 0.013	0.28 $\pm$ 0.09	0.25	3.80	IP
153817.35+512338.0	18.57 $\pm$ 0.01	153818.5+512348	1.7	0.071 $\pm$ 0.012	0.50 $\pm$ 0.08	0.65	1.60?	1.60?

Table 3.2: (continued)

SDSS J	$g$	1RXS J	$\sigma$	counts s <sup>-1</sup>	Flux $\times 10^{-12}$	log ( $f_X/f_g$ )	P	hr	Comments
154104.67+360252.9	19.70 $\pm$ 0.03	154107.5+360234	2.2	0.049 $\pm$ 0.014	0.34 $\pm$ 0.10	0.94	1.40	1.40	P
162501.75+390926.4	17.20 $\pm$ 0.02	162501.2+390924	0.9	0.077 $\pm$ 0.011	0.54 $\pm$ 0.08	0.14	1.31	1.31	V844 Her; DN
165658.13+212139.3	18.52 $\pm$ 0.01	165658.7+212141	0.8	0.042 $\pm$ 0.010	0.29 $\pm$ 0.07	0.40	...	...	
170053.30+400357.6	19.42 $\pm$ 0.02	170053.7+400354	0.6	0.071 $\pm$ 0.012	0.50 $\pm$ 0.08	0.99	1.90	1.90	P
170324.09+320953.2	18.17 $\pm$ 0.01	170324.6+320935	1.6	0.013 $\pm$ 0.006	0.09 $\pm$ 0.04	-0.24	...	...	
173008.38+624754.7	15.91 $\pm$ 0.02	173008.0+624744	1.6	0.060 $\pm$ 0.006	0.42 $\pm$ 0.04	-0.49	1.95	1.95	DN
204827.91+005008.9	19.38 $\pm$ 0.02	204828.2+005022	0.7	0.014 $\pm$ 0.007	0.10 $\pm$ 0.05	0.26	4.25	4.25	P
205017.84-053626.8	18.15 $\pm$ 0.01	205018.4-053631	0.8	0.036 $\pm$ 0.013	0.25 $\pm$ 0.09	0.19	1.60	1.60	P?
225831.18-094931.7	15.65 $\pm$ 0.02	225834.4-094945	2.4	0.167 $\pm$ 0.038	1.17 $\pm$ 0.26	-0.15	...	...	PB 7412
230351.64+010651.0	18.18 $\pm$ 0.02	230352.0+010645	0.6	0.061 $\pm$ 0.015	0.43 $\pm$ 0.10	0.43	1.67	1.67	DN

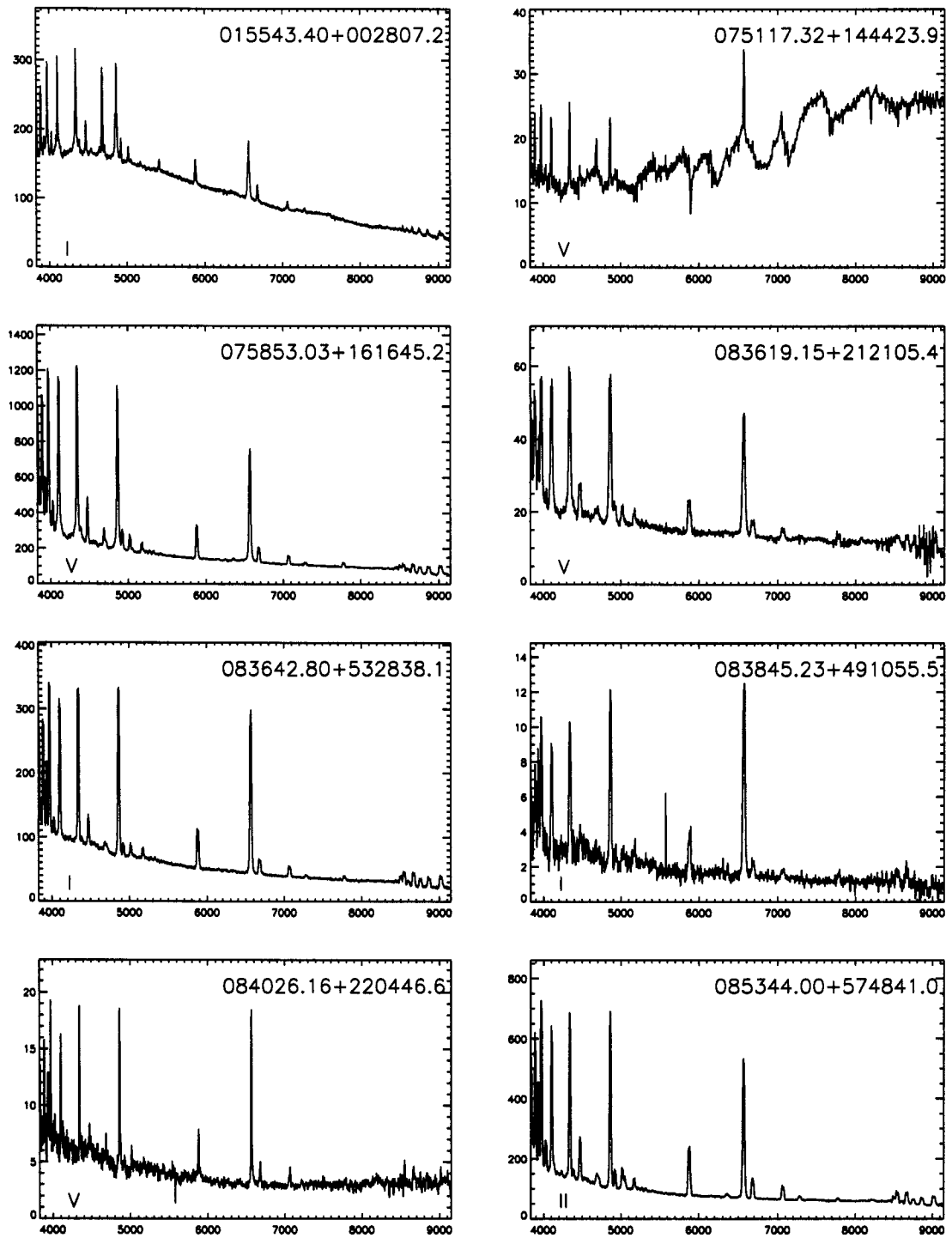


Figure 3.3: SDSS spectra for the X-ray-emitting CVs in Table 3.2. The y axis is flux density ( $10^{-17}$  ergs  $\text{cm}^{-2}$   $\text{s}^{-1}$   $\text{\AA}^{-1}$ ); the x axis is wavelength ( $\text{\AA}$ ).

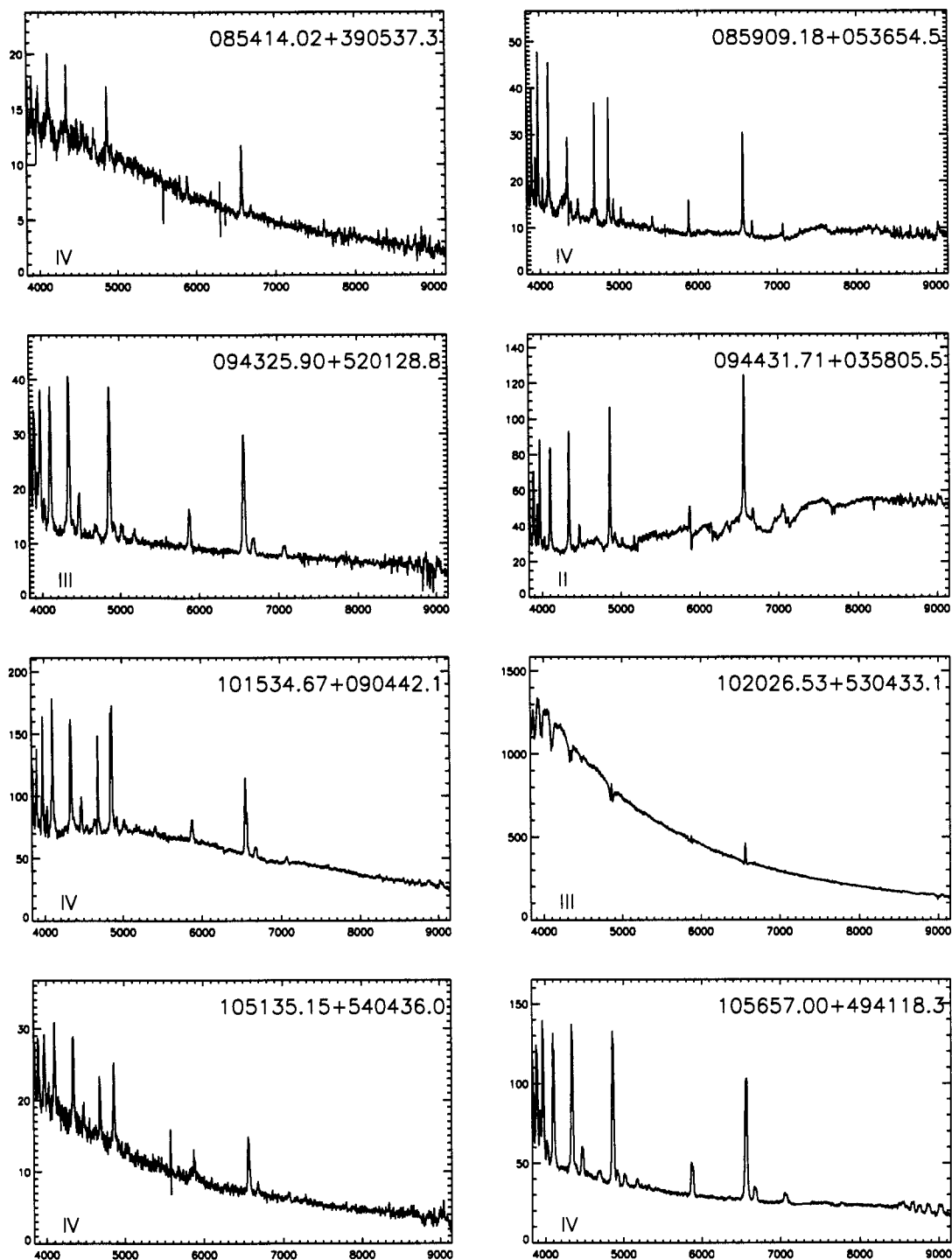


Figure 3.3: (continued) The roman numeral indicates the Szkody et al. paper in which the CV spectrum was published (Szkody et al., 2002, 2003, 2004a, 2005, 2006).

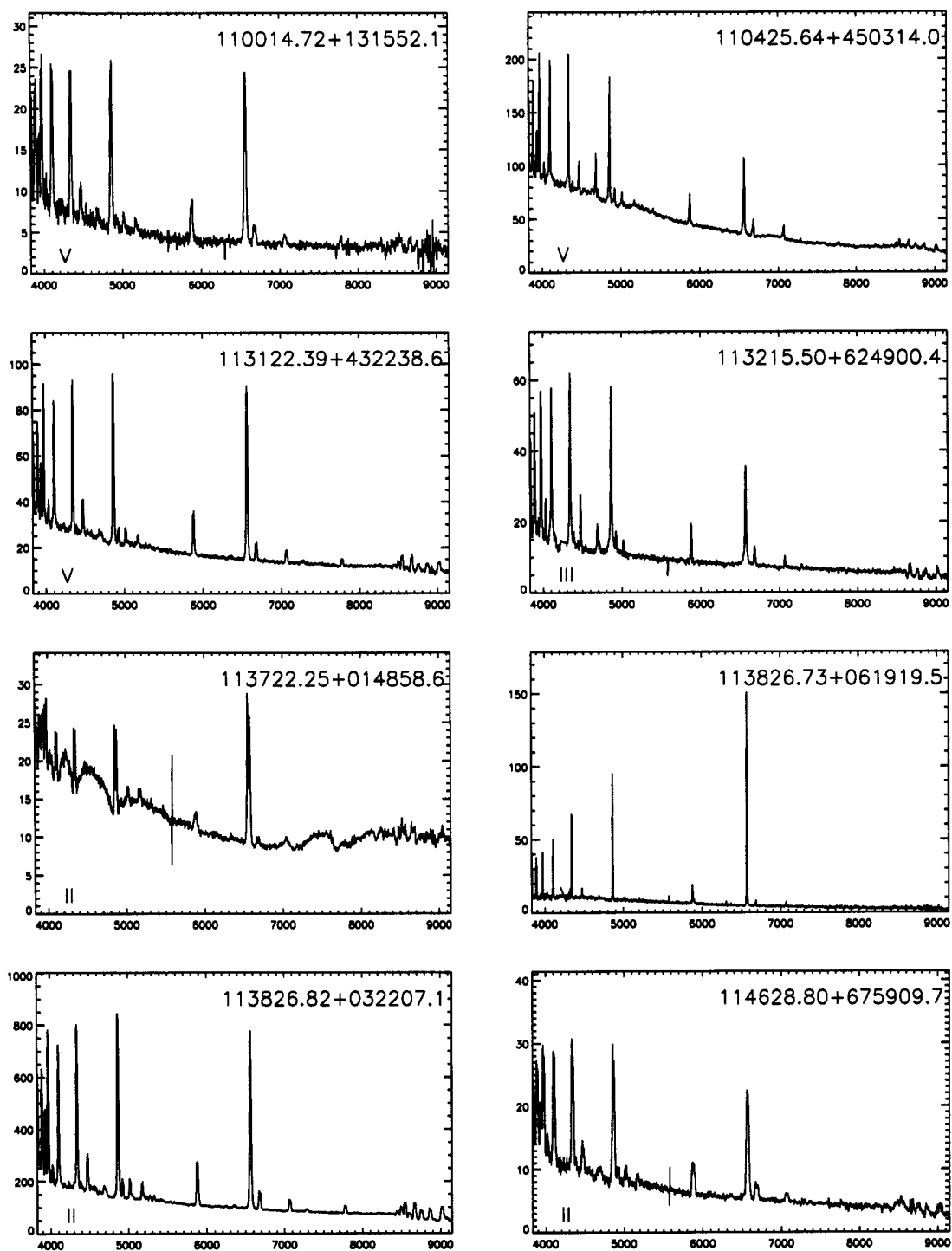


Figure 3.3: (continued)

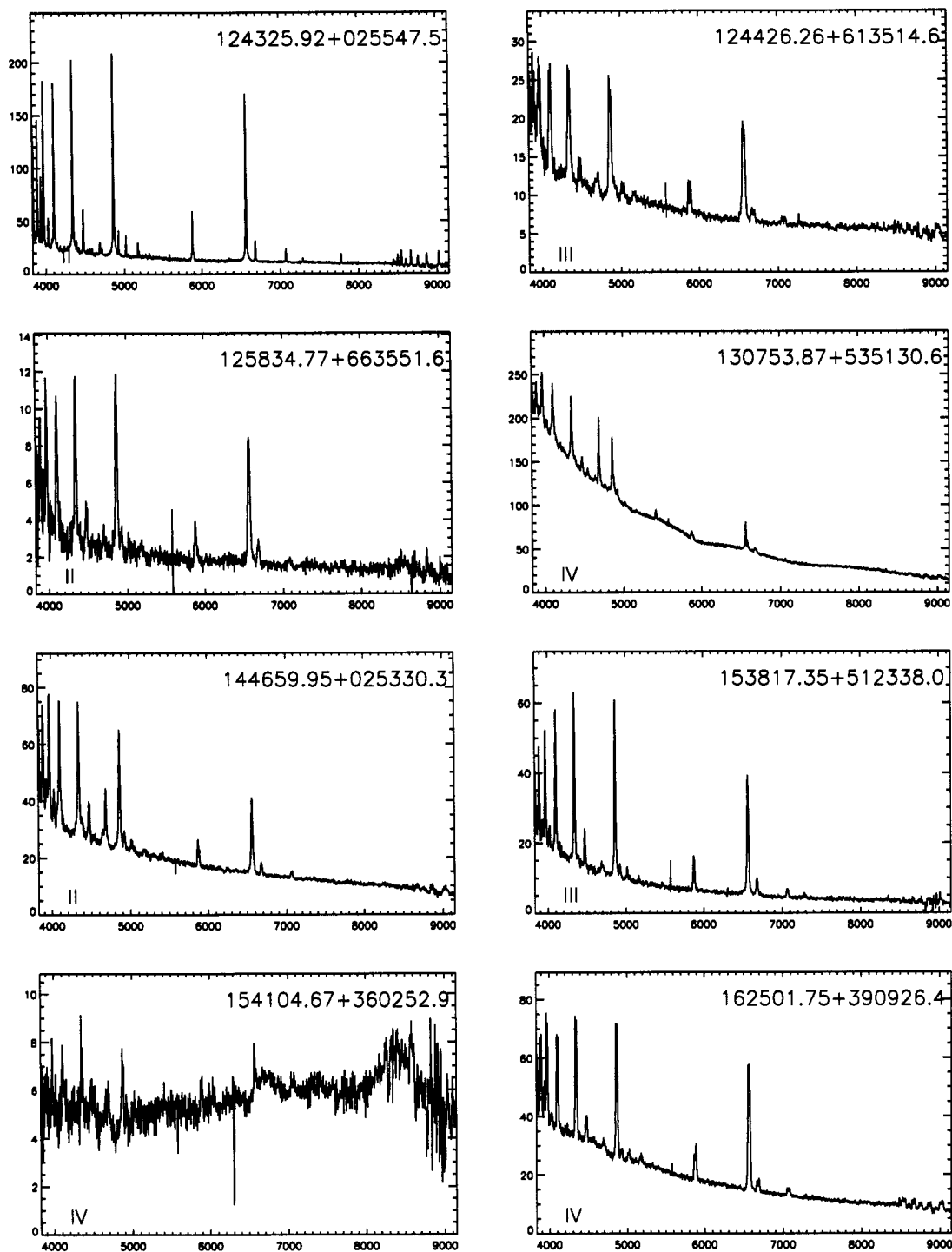


Figure 3.3: (continued)

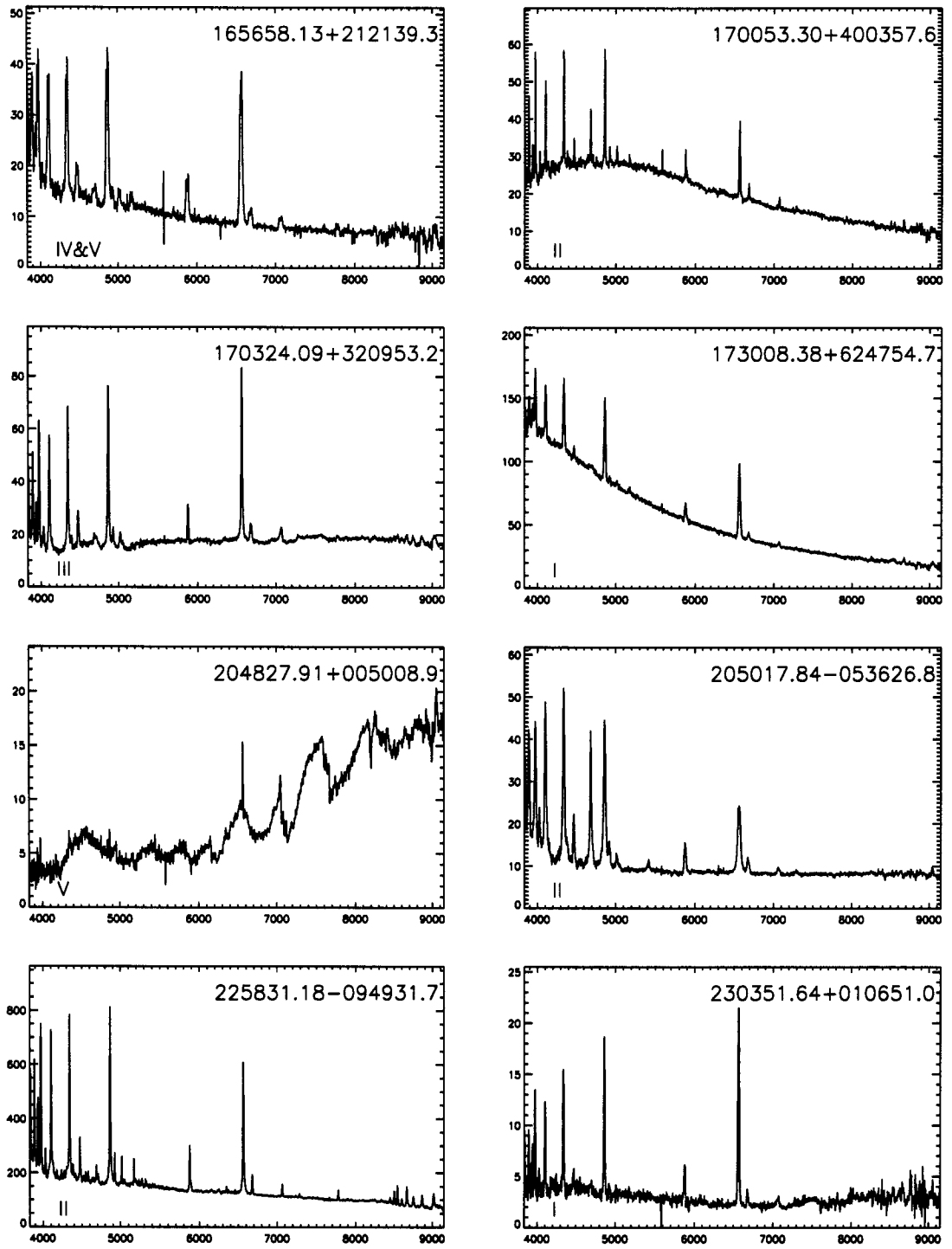


Figure 3.3: (continued) J165658.13+212139.3 was accidentally included in both Szkody et al. 2005 and 2006.



Finally, SDSS J084026.16+220446.6 was not listed as having strong HeII emission in its discovery paper (Szkody et al., 2006), but its  $\log(f_X/f_g)$  and  $H\beta$  equivalent width are very similar to those of the known polar GG Leo. However, definitively classifying this systems and many other SDSS CVs clearly requires more observational data than is provided by the survey. An example of the work needed to characterize one SDSS CV, SDSS J173008.38+624754.7, is given in the following section.

### 3.3.2 *A detailed optical study of one X-ray-emitting SDSS CV: the dwarf nova SDSS J173008.38+624754.7*

While SDSS is not designed primarily to be a variability survey, the SDSS photometric data and spectra are obtained at different times. With the addition of the DSS data, we therefore have three separate measurements of a given object’s brightness—useful for identifying candidate dwarf novae (where the variations indicate that the system is undergoing an outburst) and nova–likes (where the variations are due to changes in the system’s accretion rate). To distinguish between these cases requires spectroscopic follow–up.

Table 3.3: Follow–up data from APO and MRO for SDSS J1730.

UT Date	Site	Interval	Data Obtained
2000 Jun 05	MRO	5.00 hr	<i>V</i> photometry
2000 Jun 16	MRO	1.75 hr	<i>V</i> photometry
2000 Jul 16	MRO	2.40 hr	<i>V</i> photometry
2000 Aug 07	MRO	4.80 hr	<i>V</i> photometry
2000 Aug 08	MRO	47.20 hr	<i>B</i> photometry
2000 Aug 25	MRO	2.00 hr	<i>B</i> photometry
2000 Oct 03	APO	2.20 hr	20 spectra at outburst
2000 Oct 06	APO	0.25 hr	2 spectra at quiescence

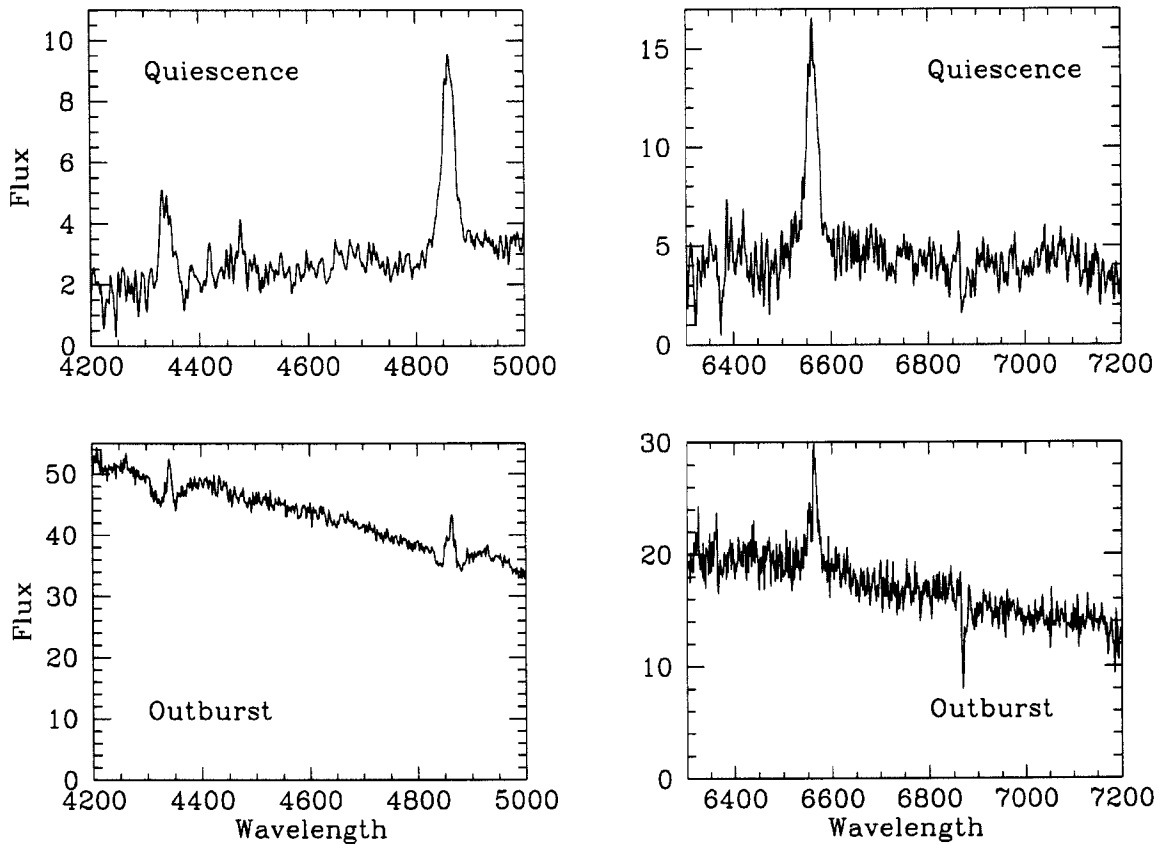


Figure 3.4: APO spectra showing the outburst and quiescence of SDSS J1730. The fluxes have units of  $10^{-16}$  ergs  $\text{cm}^{-2}$   $\text{s}^{-1}$   $\text{\AA}^{-1}$ .

SDSS J173008.38+624754.7 was among the early CVs identified in the survey data (Szkody et al., 2002), and was found to be variable. A summary of the follow-up observations of this system is presented in Table 3.3. Twenty time-resolved spectra of the system were obtained on 2000 October 2 with the 3.5-m telescope at APO, and two more were obtained three nights later, using DIS in high-resolution mode ( $\sim 3$  Å). These spectra revealed that SDSS J1730 was undergoing a dwarf nova outburst, during which the Balmer emission lines turned into absorption lines when the system was several magnitudes brighter than at quiescence.

Figure 3.4 shows typical outburst spectra and the smoothed mean of the two quiescent spectra for the blue and red wavelength regions. At outburst, the overall flux

increased by a factor of 20 in the blue and 4 in the red, with noticeable, broad absorption features surrounding the  $H\beta$  and  $H\gamma$  emission lines. Figure 3.5 shows a closeup of the  $H\beta$  line throughout the orbit. While inspection of the line suggests the possible presence of a narrow component passing from blue (phase 0.48) to red (phase 0.57), careful analysis of the velocity of the peak component did not produce an unambiguous feature which could be associated with the orbital period.

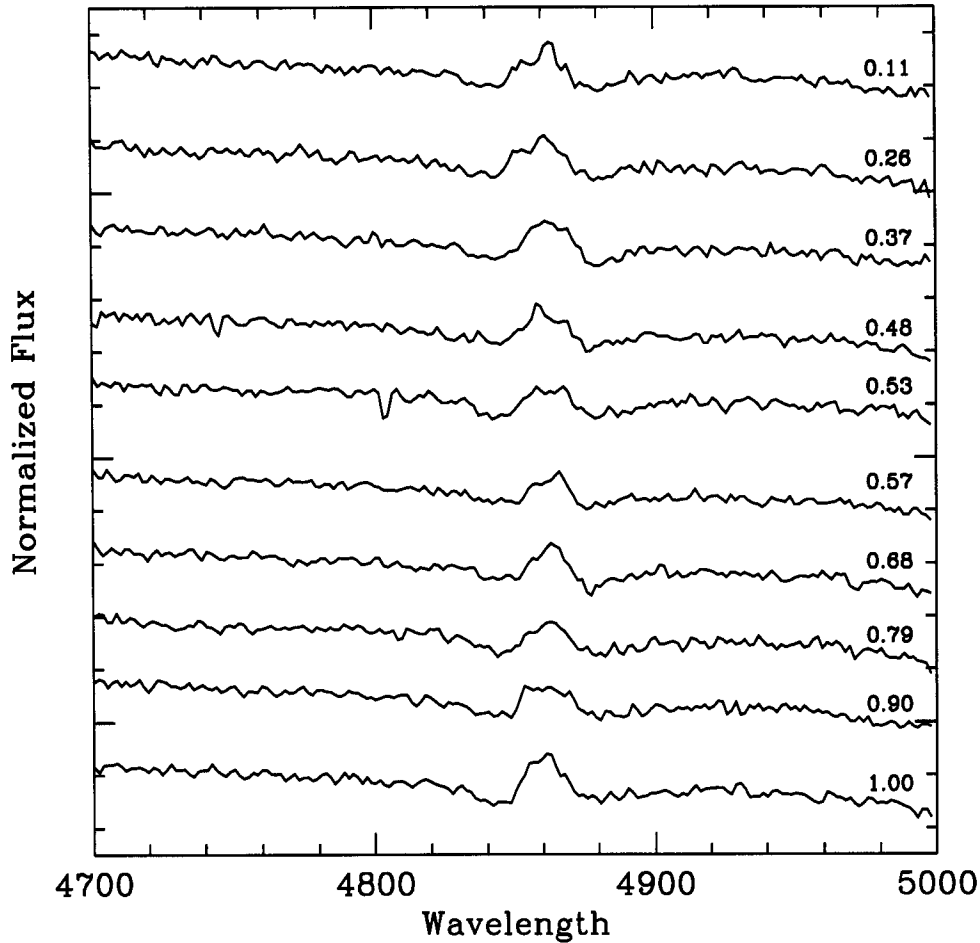


Figure 3.5: APO spectra showing the variation of the  $H\beta$  line profile of SDSS J1730 throughout an orbital period during outburst.

The presence of the underlying absorption features at  $H\beta$  and  $H\gamma$  in SDSS J1730 made it difficult to obtain radial velocities for these two lines, and a reliable solution

was obtained only for the  $H\alpha$  data. We obtained values for the central peak of the  $H\alpha$  line by using IRAF's fitting routines in *splot*. As the line shows a fair amount of structure at outburst, the centroid "e" method returned more consistent answers than did Gaussian fitting. An IDL routine, *CURVEFIT*, was used to fit the radial velocities with a sinusoidal function of the form  $v = \gamma - K \sin[2\pi(t - t_0)/P]$ , where  $\gamma$  (systemic velocity),  $K$  (semi-amplitude),  $P$  (orbital period) and  $t_0$  (time of conjunction) were left as free parameters (see Table 3.4 for the best fit parameters).

Figure 3.6 shows the best fit to the  $H\alpha$  radial velocity curve. Four spectra showed extreme deviations and were not included in the fitting, and are indicated in Figure 3.6 as open circles. We studied these spectra for evidence of shifts in the lines and for other potential sources of error, but were unable to detect any cause. Nevertheless, they provided velocities which were clearly inconsistent with the rest of our measurements. The velocities for these four spectra shown in Figure 3.6 are from measurements of the midpoint of the extremes of the  $H\alpha$  line done by eye. We tested our fitting program while including these spectra, and found that the best fit obtained for the orbital period ( $117 \pm 5$  min) was consistent with the fit excluding these points.

Finally, we used the period obtained from the spectra to look for evidence of variability in the photometry of this system obtained with the 0.76-m telescope at the Manastash Ridge Observatory (MRO) in eastern Washington (see Table 3.3). We folded the differential magnitudes on each of the two longest nights on the orbital period but found no evidence for any significant orbital variability. An average of the two nights' data produces an upper limit for any such variability of 0.04 mag. The absence of variability, along with the lack of line doubling, suggests that SDSS J1730 is a system with a fairly low inclination (Warner, 1995).

Table 3.4: Radial velocity solution for SDSS J1730.

Line	P (min)	$\gamma$	K (km/s)	$\phi$	$\sigma$
$H\alpha$	$117 \pm 5$	$23 \pm 3$	$74 \pm 6$	$0.0 \pm 0.02$	19

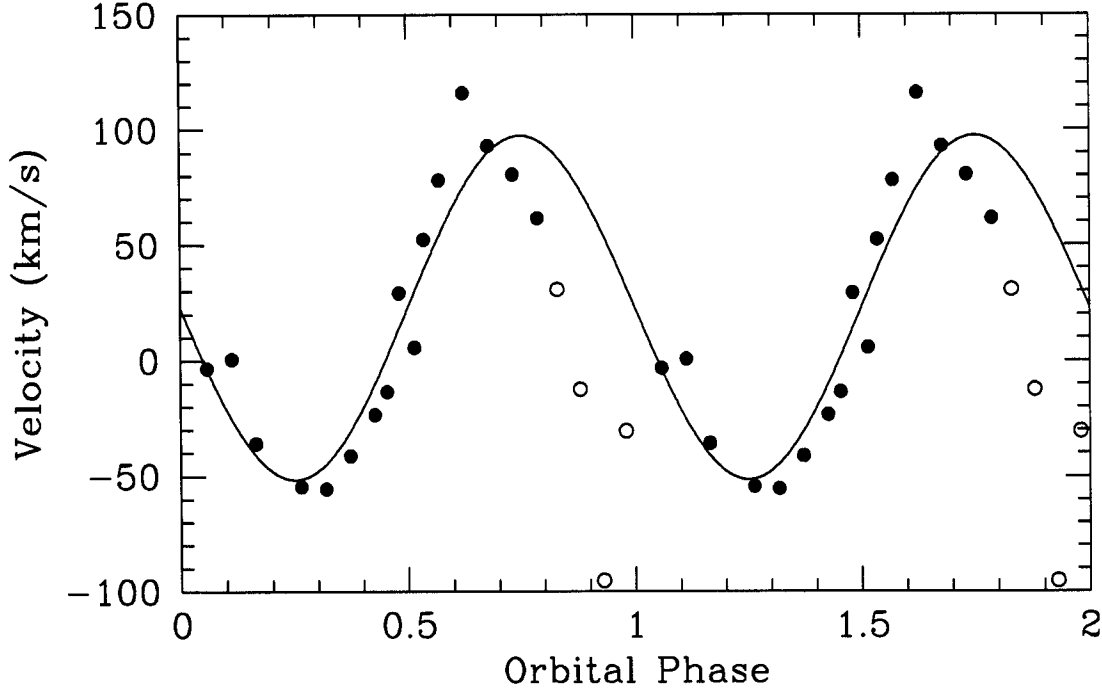


Figure 3.6: Best fit to the radial velocity curve of SDSS J1730 at outburst using the  $H\alpha$  emission line. The open circles produced large deviations to a sine fit and were therefore left out of the best solution, which is shown as the solid line.

### 3.4 New Candidate X-ray-Emitting SDSS Cataclysmic Variables

In the time since the publication of the most recent SDSS CV discovery paper (Szkody et al., 2006), new candidate CVs have been identified from visual inspection of the survey spectra. Among these are eight objects within  $1'$  of a RASS X-ray source position. Four of these are previously cataloged objects: one is a dwarf nova, one is a polar, and the two others are symbiotic stars<sup>5</sup>. The four other objects are SDSS discoveries.

Table 3.5 includes the SDSS name and  $g$  magnitude, the corresponding RASS source, and the separation between the two ( $\sigma$ ) expressed in terms of the X-ray positional uncertainty, for each of these candidates. We also list the RASS count rate, X-ray flux, and  $\log(f_X/f_g)$  (both calculated as for the objects in Table 3.2), and include measure-

---

<sup>5</sup>One of these, Draco C1, is included in the Downes et al. (2004) study of high-latitude carbon stars in SDSS.

ments of the  $H\beta$  equivalent width. Finally, for the first four objects we list the cataloged name. The SDSS spectra for these eight objects are presented in Figure 3.8.

The SDSS photometric data for SDSS J215101.33+123737.9, the symbiotic star AG Peg, are misleading. The star has  $B = 9.81$ ,  $V = 8.65$  according to SIMBAD, and is obviously saturated in SDSS imaging; unsurprisingly, the SATURATED flag is set in its photometric catalog entry. Accordingly, we use its SIMBAD  $V$  to calculate its  $\log(f_X/f_{opt})$  and include this value in Table 3.5.

CVs are typically UV-excess objects for which the SDSS  $(u - g) \leq 0.6$ . By contrast, the candidate CV SDSS J012018.49–102536.1 has  $(u - g) = 2$ . Furthermore, its emission lines are narrower than one would expect for a CV, suggesting that this is possibly a flaring, solitary late-type star. However, the blue upturn that is usually seen in flares (e.g., in Figure 2.12) appears to be absent in this spectrum; further spectroscopic observations are required to confirm whether this star was in fact caught flaring, or is simply very active. In any case, while this object is clearly the RASS source counterpart, it cannot be confidently classified as a CV.

SDSS J100515.38+191107.9 is at a large positional offset from the RASS source 1RXS J100511.9+191105. The SDSS data do not suggest an immediately apparent alternate counterpart to the X-ray source, but a pointed X-ray observation would be useful to confirm that this is indeed the RASS source.

#### 3.4.1 Flux ratios and $H\beta$ equivalent width

We updated Figure 3.2 by adding the  $\log(f_X/f_g)$  and  $H\beta$  equivalent width values of the two previously published CVs and four SDSS discoveries; the new plot is shown in Figure 3.7. The dwarf nova SX LMi and polar RX J1554.2+2721 both appear in the expected regions of the plot, although the  $\log(f_X/f_g)$  of the latter object is lower than one might expect. SDSS J0120, as expected, is unlike the other CVs in our sample.

While the three other candidates all show strong HeII emission, only one, SDSS J094558.24+292253.2, appears to have a larger than usual  $\log(f_X/f_g)$ . This is therefore our strongest candidate to be a new magnetic CV. Follow-up observations will be

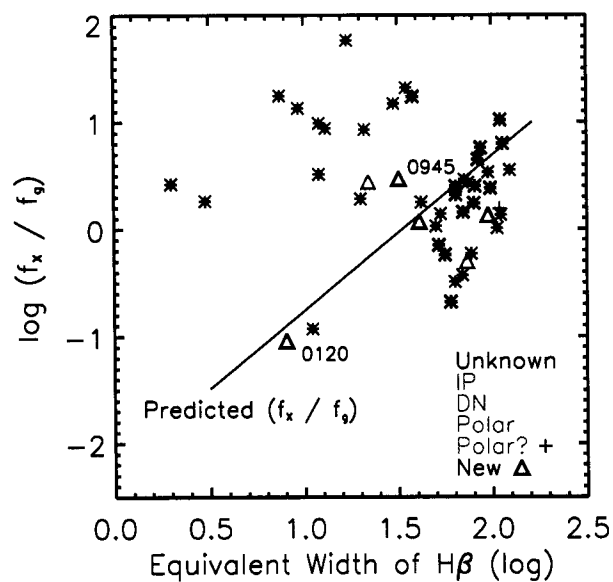


Figure 3.7:  $\log(f_X/f_g)$  versus equivalent width of the H $\beta$  line. The two recently recovered CVs and four new CV candidates have been added.

necessary to verify whether any of these are in fact magnetic systems.

Table 3.5: Optical and X-ray properties of the unpublished SDSS candidate CVs. Fluxes are calculated as in Table 3.2. SDSS J215101.33+123737.9 is saturated; we give its  $\log(f_X/f_V)$  based on its SIMBAD  $V = 8.65$ . The  $H\beta$  EW is measured in Å.

SDSS J	$g$	1RXS J	$\sigma$	counts s <sup>-1</sup>	Flux $\times 10^{-12}$	$\log$ $(f_X/f_g)$	$H\beta$ EW	Comments
105430.43+300610.1	$16.76 \pm 0.02$	105430.9+300620	0.7	$0.042 \pm 0.013$	$0.29 \pm 0.09$	-0.30	73	SX LMi; DN
155412.33+272152.4	$17.55 \pm 0.02$	155412.7+272143	0.7	$0.113 \pm 0.021$	$0.79 \pm 0.15$	0.44	22	RX J1554.2; P
171957.65+575005.5	$17.73 \pm 0.01$	171955.7+574959	1.2	$0.030 \pm 0.006$	$0.21 \pm 0.04$	-0.07	19	Draco C1; Sy
215101.33+123737.9	$25.11 \pm 11.53$	215102.8+123745	2.1	$0.075 \pm 0.018$	$0.52 \pm 0.13$	-3.30	26	AG Peg; Sy
012018.49-102536.1	$14.54 \pm 0.05$	012020.1-102510	1.9	$0.060 \pm 0.014$	$0.42 \pm 0.10$	-1.04	8	
094558.24+292253.2	$19.10 \pm 0.02$	094558.3+292249	0.2	$0.029 \pm 0.010$	$0.20 \pm 0.07$	0.47	32	
100515.38+191107.9	$18.22 \pm 0.03$	100511.9+191105	8.2	$0.026 \pm 0.000$	$0.18 \pm 0.00$	0.07	41	
101947.26+335753.6	$18.39 \pm 0.01$	101946.7+335811	1.2	$0.025 \pm 0.010$	$0.18 \pm 0.07$	0.13	95	



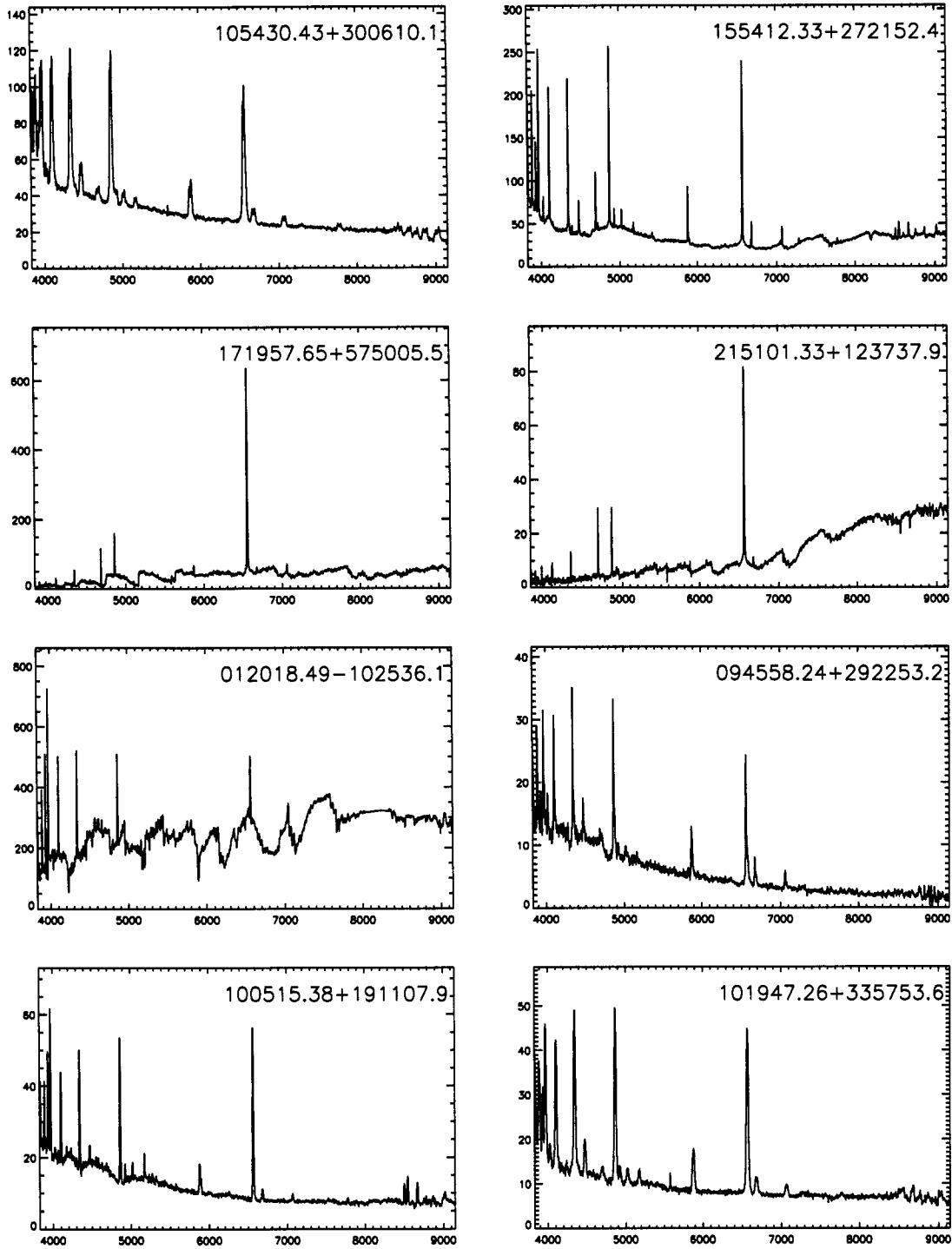


Figure 3.8: SDSS spectra of the unpublished candidate X-ray emitting CVs. The axes are as in Figure 3.2.

## Chapter 4

### A CATALOG OF X-RAY-EMITTING WHITE DWARFS FROM THE *ROSAT* ALL-SKY AND SLOAN DIGITAL SKY SURVEYS

#### 4.1 Introduction

White dwarfs (WDs) are the eventual end point of the lives of low- to medium-mass stars such as the Sun, and are observed in a number of different forms: at the heart of beautiful planetary nebulae, in binary systems such as cataclysmic variables, and as solitary stars, slowly cooling their way to eventual invisibility. Roughly the diameter of the Earth, WDs are very dense: according to theoretical predictions, they can reach up to  $1.44 M_{\odot}$ , although the observed mass function is strongly peaked at  $\sim 0.6 M_{\odot}$  (e.g., Koester et al., 1979; Madej et al., 2004). Observed WD properties are therefore of great interest to those who wish to explore the physics of degenerate matter: white dwarfs are macroscopic objects sustained by microscopic quantum mechanical effects.

Like most stars, WDs are essentially blackbody emitters. DA white dwarfs, which have a pure hydrogen atmosphere and are the most commonly observed WDs, can have temperatures  $\geq 100,000$  K when they form, but cool as they age; generally, they are observed to have effective temperatures  $\approx 10,000$  K (e.g., Kleinman et al., 2004; Eisenstein et al., 2006). At those temperatures, one would not expect a typical DA to be a significant producer of thermal X rays, and so this does not seem a natural regime in which to study WDs. However, Shipman (1976) pointed out that the X rays produced in the hotter interior of a DA WD should travel through its thin hydrogen atmosphere unabsorbed, and should therefore be detected. Early satellite X-ray missions did in fact detect a handful of DAs: five were found with *Einstein*, and another 11 with *EXOSAT*, the European X-ray Observatory (Kahn et al., 1984; Paerels & Heise, 1989).

Since these were targeted observations of previously known WDs, and *Einstein* was not sensitive to the soft X rays the DAs were predicted to emit, the small number of

detections was not considered worrisome. Indeed, the consensus was that *ROSAT*, sensitive to soft X rays and designed to conduct an all-sky survey, would detect upwards of 5000 DAs (e.g., Barstow, 1989). These should be particularly easy to find in the RASS data because of their “super-soft” X-ray spectra: DA X-ray emission should be from the Wein tail of the blackbody spectrum and the detected flux should be below 0.28 keV, so that the sources are detected in soft but not hard RASS images (Fleming et al., 1996). In practice, this means that for DAs the cataloged hardness ratios HR1 and HR2 should equal  $-1$  and  $0$ , respectively, where  $HR1 = \frac{(0.5-2.0)-(0.1-0.4)}{(0.1-0.4)+(0.5-2.0)}$  and  $HR2 = \frac{(1.0-2.0)-(0.4-1.0)}{(1.0-2.0)}$  and, for example,  $(0.5 - 2.0)$  indicates the number of counts in the  $0.5 - 2.0$  keV (hard) energy band (Fleming et al., 1996; Motch et al., 1998).

However, when the *ROSAT* All-Sky Survey (RASS; Voges et al., 1999, 2000) was completed, the number of detected DAs was far smaller than had been predicted. Searching for the super-soft sources among 55,000 RASS sources, Fleming et al. (1996) found only 161 DAs, leading them to conclude that 90% of DAs are in fact opaque to X-ray emission. Still, these data allowed observers to probe beneath the surface of WDs, as well as to explore the composition of these stars. Barstow et al. (1993) were able to show, for example, that WDs cooler than  $\sim 40,000$  K have essentially pure hydrogen atmospheres, while hotter WDs contain significant amounts of heavier elements. It is now thought that WDs are soft X-ray sources if they are hotter than  $23,000$  K and have pure hydrogen atmospheres (Jordan et al., 1994), are between  $23,000$  and  $54,000$  K and have hydrogen atmospheres significantly polluted by heavier elements (Marsh et al., 1997b), or are hotter than  $100,000$  K and have helium-rich atmospheres (i.e., rarer types such as PG 1159 stars and DO WDs; Motch et al., 1993).

#### 4.1.1 SDSS and White Dwarfs

While the number of known X-ray-emitting WDs remains small, with recent RASS identifications programs adding only a few dozen to the Fleming et al. (1996) sample (e.g., Zickgraf et al., 2003), the overall number of known WDs has increased dramatically since the beginning of the Sloan Digital Sky Survey (SDSS; York et al., 2000).

Previous to SDSS, the most extensive WD catalog was that of McCook & Sion (1999), which in its most recent form includes data for 3061 WDs. While the SDSS spectroscopic survey is intended to focus on extragalactic targets, there are sufficient fibers on each of the survey plates to insure that significant numbers of interesting Galactic sources are also targeted<sup>1</sup>. As a result, the SDSS Data Release 1 (DR1; Abazajian et al., 2003) produced a catalog of 2551 spectroscopically confirmed WDs; these are stars selected on the basis of their SDSS colors and spectroscopic properties, as described in Kleinman et al. (2004), and whose spectra are well fit by theoretical WD atmosphere models. Of these WDs, only 108 were included in the McCook & Sion (1999) list (Kleinman et al., 2004). A more recent catalog of WDs in the Data Release 4 (DR4; Adelman-McCarthy et al., 2006), which covers an area roughly 3.5 times larger than DR1, identifies 9309 WDs, of which  $\sim 6000$  are new discoveries (Eisenstein et al., 2006); the vast majority of these WDs are DAs (7999).

In this chapter we begin by cataloging the X-ray-emitting WDs in SDSS from correlations with the RASS (§4.2). We found that SDSS is not adding many *new* WDs to the sample of previously known X-ray emitters. For example, we are able to identify with a high degree of confidence only 14 X-ray-emitting DAs among the 7999 DAs cataloged by Eisenstein et al. (2006) that were not included in the Fleming et al. (1996), McCook & Sion (1999), and Zickgraf et al. (2003) catalogs. This dearth of new X-ray-emitting WDs may be a result of the relative sensitivities of the two surveys. Stellar counterparts to RASS-cataloged sources tend to be optically very bright, and can be identified without requiring the depth of SDSS—while the fainter WDs discovered by SDSS are unlikely to be bright enough in the X-ray regime to have RASS detections (e.g., because they are too distant). However, among these new X-ray emitters are three that, if confirmed, may be the coolest X-ray-emitting DAs detected to date (see §4.2.5), suggesting that these fainter SDSS X-ray-emitting WDs, while small in number, may prove to be very interesting.

---

<sup>1</sup>Because many interesting Galactic sources share color-color space with extragalactic sources and particularly quasars, they are also occasionally inadvertently targeted for spectroscopy. Several WDs were also among the hot stars selected as spectroscopic standards.

We then use the DR1 sample of DA WD spectra to produce high resolution composite white dwarf spectra (§4.3). These composites will allow us to search for heretofore unidentified spectral features, and may eventually help us identify differences in the composition of known DA X-ray emitters and ordinary DAs of the same temperature.

## 4.2 X-ray-Emitting SDSS White Dwarfs

### 4.2.1 Previously known X-ray-emitting DAs

Correlations of the Eisenstein et al. (2006) catalog of DR4 WDs with the RASS Bright and Faint Source Catalogs (Voges et al., 1999, 2000) identified 22 DAs listed in the McCook & Sion (1999) catalog with an X-ray source within  $1'$ . We classified seven of these sources as unlikely WDs. In four cases, a known quasar is in the RASS field and the X-ray source is not super-soft, as measured by its HR1 ( $\text{HR1} = -0.28 \pm 0.43$ ,  $0.62 \pm 0.63$ ,  $-0.78 \pm 0.17$ , and  $0.18 \pm 0.27$ , respectively), which is consistent with the quasars being the X-ray sources. This leaves us with 18 possible associations.

In three ambiguous cases, the sources are not super-soft and at large separations from the RASS source, but the available SDSS data for the RASS fields do not rule out the DA WD as the X-ray source. SDSS J022618.60–083049.3 is in a RASS field with two bright stars ( $g = 12.98 \pm 0.00$  and  $13.19 \pm 0.00$ )<sup>2</sup>. The RASS source is not soft ( $\text{HR1} = 0.22 \pm 0.36$ ) and it is therefore unlikely that the WD is the X-ray source. SDSS J093456.44+023121.1 is in a field with no obvious X-ray source counterparts. There is a very faint, red star closer to the RASS position ( $g = 21.35 \pm 0.06$ ,  $r = 20.06 \pm 0.03$ ), but were it the X-ray counterpart, its  $\log(f_X/f_g)$  (calculated using the updated Maccacaro et al. (1988) formula; Voges et al., 1999) would be much higher than one expects for stars. Again, the RASS source is not soft ( $\text{HR1} = 0.36 \pm 0.52$ ), so perhaps this is a quasar with stellar colors. Finally, SDSS J152349.89+041434.6 is in a field with SDSS J152349.88+041400.8, a  $g = 17.71 \pm 0.02$  galaxy. In these cases follow-up spectroscopy is needed to reveal, for example, whether this galaxy hosts an active galactic nucleus.

---

<sup>2</sup>Because the WDs are cataloged in Eisenstein et al. (2006) with PSF magnitudes, we quote PSF magnitudes throughout this chapter.

Table 4.1: Optical and X-ray properties of the previously known DAs.

SDSS J	PSF $g$	$T_{eff}$	$\log g$	1RXS J	$\sigma$	counts $s^{-1}$	$\log (f_X/f_g)$
090611.00+414114.3	$17.15 \pm 0.02$	$48276 \pm 601$	$8.02 \pm 0.05$	090611.3+414116	0.2	$0.063 \pm 0.019$	0.03
091215.43+011958.8	$17.52 \pm 0.02$	$55691 \pm 1415$	$8.03 \pm 0.09$	091215.5+012003	0.3	$0.041 \pm 0.015$	-0.01
093608.90+382200.5	$17.63 \pm 0.03$	$37809 \pm 397$	$7.80 \pm 0.07$	093609.6+382237	1.6	$0.038 \pm 0.012$	0.00
094022.64+502105.8	$15.70 \pm 0.01$	$36681 \pm 240$	$7.80 \pm 0.03$	094021.7+502116	1.3	$0.085 \pm 0.015$	-0.42
095245.58+020938.9	$16.35 \pm 0.02$	$43114 \pm 443$	$7.80 \pm 0.04$	095244.6+020946	0.6	$0.025 \pm 0.010$	-0.69
100614.75+441906.3	$16.82 \pm 0.01$	$57865 \pm 1196$	$7.82 \pm 0.07$	100615.3+441921	1.0	$0.030 \pm 0.011$	-0.42
101328.16+061207.3	$16.28 \pm 0.02$	$50050 \pm 646$	$7.98 \pm 0.05$	101326.2+061202	2.0	$0.062 \pm 0.015$	-0.33
102945.27+450704.9	$15.88 \pm 0.02$	$36923 \pm 243$	$7.89 \pm 0.03$	102945.3+450717	0.9	$0.091 \pm 0.018$	-0.32
104157.22+630701.6	$14.95 \pm 0.02$	$25727 \pm 66$	$8.48 \pm 0.01$	104155.4+630612	2.7	$0.022 \pm 0.008$	-1.32
104332.61+445328.9	$16.67 \pm 0.01$	$51064 \pm 621$	$7.88 \pm 0.05$	104331.5+445339	1.4	$0.190 \pm 0.026$	0.32
105916.42+512443.1	$16.50 \pm 0.05$	$74446 \pm 1649$	$8.50 \pm 0.06$	105916.6+512452	1.6	$4.180 \pm 0.092$	1.59
143156.60+370630.2	$14.96 \pm 0.02$	$36364 \pm 236$	$7.94 \pm 0.03$	143157.4+370635	1.1	$0.140 \pm 0.018$	-0.50
145600.79+574150.7	$16.19 \pm 0.02$	$31500 \pm 79$	$7.72 \pm 0.03$	145605.0+574132	1.8	$0.021 \pm 0.008$	-0.83
165851.11+341853.2	$16.17 \pm 0.02$	$60000 \pm 1071$	$7.88 \pm 0.06$	165851.0+341852	0.2	$0.149 \pm 0.016$	0.01
172643.38+583732.2	$15.32 \pm 0.01$	$63476 \pm 959$	$8.61 \pm 0.04$	172642.8+583726	1.3	$1.247 \pm 0.028$	0.59
022618.60-083049.3	$20.13 \pm 0.02$	$9692 \pm 153$	$8.16 \pm 0.22$	022615.8-083108	3.3	$0.033 \pm 0.011$	0.94
093456.44+023121.1	$19.69 \pm 0.03$	$20844 \pm 1009$	$7.77 \pm 0.16$	093458.0+023151	2.2	$0.023 \pm 0.011$	0.60
152349.89+041434.6	$18.37 \pm 0.02$	$23852 \pm 542$	$7.93 \pm 0.07$	152351.0+041356	2.2	$0.059 \pm 0.020$	0.49

Table 4.1: (continued) Optical and X-ray properties of the previously known DAs. “F” indicates that the WD is included in the Fleming et al. (1996) catalog; “Z” indicates that it was included in the Zickgraf et al. (2003) catalog.

SDSS J	1RXS J	HR1	HR2	DL	McCook & Sion (1999)	Comments
090611.00+414114.3	090611.3+414116	$-1.00 \pm 0.23$	$0.00 \pm 0.00$	17	WD 0902+418	Z
091215.43+011958.8	091215.5+012003	$-1.00 \pm 0.21$	$0.00 \pm 0.00$	12	WD 0909+015	suspect <i>g</i>
093608.90+382200.5	093609.6+382237	$-1.00 \pm 0.35$	$0.00 \pm 0.00$	13	WD 0933+385	DQ
094022.64+502105.8	094021.7+502116	$-0.99 \pm 0.03$	$-1.00 \pm 3.49$	41	WD 0937+505	F; Z
095245.58+020938.9	095244.6+020946	$-1.00 \pm 0.22$	$1.00 \pm 8.85$	10	WD 0950+023	
100614.75+441906.3	100615.3+441921	$-1.00 \pm 0.16$	$-1.00 \pm 6.75$	9	WD 1003+445	F; suspect <i>g, r, i</i>
101328.16+061207.3	101326.2+061202	$-1.00 \pm 0.13$	$0.00 \pm 0.00$	22	WD 1010+064	Z
102945.27+450704.9	102945.3+450717	$-1.00 \pm 0.04$	$0.00 \pm 0.00$	34	WD 1026+453	F; Z
104157.22+630701.6	104155.4+630612	$-1.00 \pm 0.25$	$0.00 \pm 0.00$	10	WD 1038+633	
104332.61+445328.9	104331.5+445339	$-1.00 \pm 0.03$	$-1.00 \pm 8.00$	86	WD 1040+451	F; Z
105916.42+512443.1	105916.6+512452	$-0.99 \pm 0.00$	$-0.02 \pm 0.91$	7380	WD 1056+516	F; Z
143156.60+370630.2	143157.4+370635	$-1.00 \pm 0.01$	$0.00 \pm 0.00$	89	WD 1429+373	F; Z
145600.79+574150.7	145605.0+574132	$-0.84 \pm 0.15$	$0.00 \pm 0.00$	8	WD 1454+578	
165851.11+341853.2	165851.0+341852	$-1.00 \pm 0.03$	$0.00 \pm 0.00$	141	WD 1657+343	F; Z
172643.38+583732.2	172642.8+583726	$-0.99 \pm 0.00$	$-1.00 \pm 1.12$	5540	WD 1725+586	F; Z
022618.60-083049.3	022615.8-083108	$0.22 \pm 0.36$	$0.62 \pm 0.35$	18	WD 0223-087	
093456.44+023121.1	093458.0+023151	$0.36 \pm 0.52$	$-0.19 \pm 0.55$	8	WD 0932+027	suspect <i>u</i>
152349.89+041434.6	152351.0+041356	$-0.47 \pm 0.27$	$-1.00 \pm 1.89$	12	WD 1521+044	

We list the 15 confident known DA WD/RASS source associations in Table 4.1 and add these three possible associations at the end of the Table. We include the SDSS name, PSF  $g$  magnitude, effective temperature ( $T_{eff}$ ) and surface gravity (expressed as  $\log g$ ), for the DA WDs. We also list the RASS source name, the offset between the WD and the RASS source (expressed as  $\sigma$ , where  $\sigma$  is the separation between the RASS source and the WD divided by the RASS positional uncertainty), the RASS count rate, and the  $\log(f_X/f_{opt})$ , calculated using the Maccacaro et al. (1988) formula and using the SDSS  $g$  magnitude. The RASS source hardness ratios and detection likelihood (DL), a maximum likelihood measure of source significance, are also given. Finally, we list the WD name in the McCook & Sion (1999) catalog and add comments, e.g., if the DA was listed by Fleming et al. (1996) or Zickgraf et al. (2003) as an X-ray source. We also summarize the SDSS flags by indicating if the  $u, g, r, i, z$  magnitudes are suspect.

While all of these WDs are classified as DAs by Eisenstein et al. (2006), we note that SDSS J093608.90+382200.5 is cataloged as a DQ WD. However, the SDSS spectrum does not show the carbon absorption lines typical of DQs, and it seems that this is indeed a DA WD. Furthermore, while these DAs were all previously known, four were previously unidentified as X-ray sources.

#### 4.2.2 *New SDSS X-ray-emitting DAs*

Correlating the Eisenstein et al. (2006) catalog and the RASS data yielded a further 25 SDSS-discovered DA WDs (i.e., not listed in the McCook & Sion (1999) catalog) with an X-ray source within  $1'$ . Five of these sources also have nearby cataloged quasars and are not super-soft. We eliminate these DAs as likely X-ray sources, and have 20 remaining possible associations.

For three other WDs we identify other plausible counterparts to the RASS sources. A UV-excess source with  $(u - g) = 0.00 \pm 0.03$  is positionally coincident with the RASS source for which SDSS J083300.12+272254.5 is proposed as a counterpart. Similarly, another UV-excess source (with  $(u - g) = 0.24 \pm 0.13$ ) is closer than SDSS J094437.72+493815.3 to the RASS source for which the WD is the proposed counter-



Table 4.2: Optical and X-ray properties of the new SDSS DAs.

SDSS J	PSF $g$	$T_{eff}$	log $g$	1RXS J	$\sigma$	counts $s^{-1}$	log ( $f_X/f_g$ )
075106.51+301726.4	15.92 $\pm$ 0.02	33158 $\pm$ 65	7.90 $\pm$ 0.03	075107.4+301719	0.5	0.038 $\pm$ 0.013	-0.69
082346.14+245345.6	15.55 $\pm$ 0.03	34521 $\pm$ 47	7.78 $\pm$ 0.03	082345.4+245344	0.5	0.039 $\pm$ 0.014	-0.81
093006.79+522803.3	16.29 $\pm$ 0.03	36469 $\pm$ 185	7.78 $\pm$ 0.03	093006.7+522752	0.4	0.039 $\pm$ 0.013	-0.53
101339.56+061529.5	20.10 $\pm$ 0.02	14375 $\pm$ 603	7.64 $\pm$ 0.2	101340.6+061556	1.2	0.019 $\pm$ 0.009	0.70
113836.33+475509.8	17.52 $\pm$ 0.02	50602 $\pm$ 1169	7.68 $\pm$ 0.09	113836.9+475459	0.6	0.046 $\pm$ 0.015	0.04
120432.67+581936.9	19.82 $\pm$ 0.03	15725 $\pm$ 545	7.99 $\pm$ 0.12	120428.0+581934	1.8	0.022 $\pm$ 0.010	0.63
125938.08+603900.0	16.85 $\pm$ 0.04	37640 $\pm$ 225	7.70 $\pm$ 0.04	125936.6+603910	1.2	0.039 $\pm$ 0.012	-0.30
132629.58+571131.5	18.59 $\pm$ 0.02	94382 $\pm$ 5479	7.33 $\pm$ 0.27	132634.4+571052	2.0	0.020 $\pm$ 0.009	0.11
154448.25+455039.0	17.22 $\pm$ 0.02	53109 $\pm$ 1119	7.98 $\pm$ 0.08	154449.3+455035	1.0	0.046 $\pm$ 0.011	-0.08
163418.25+365827.1	20.05 $\pm$ 0.03	10080 $\pm$ 216	7.96 $\pm$ 0.3	163421.8+365859	2.0	0.016 $\pm$ 0.007	0.60
074859.06+215445.7	19.93 $\pm$ 0.02	29717 $\pm$ 911	7.66 $\pm$ 0.19	074858.9+215458	0.5	0.026 $\pm$ 0.010	0.75
093307.65+400637.9	18.87 $\pm$ 0.02	9037 $\pm$ 57	8.23 $\pm$ 0.1	093305.6+400553	3.9	0.035 $\pm$ 0.011	0.46
103237.35+512857.9	19.46 $\pm$ 0.02	20983 $\pm$ 585	7.33 $\pm$ 0.12	103236.8+512809	2.7	0.016 $\pm$ 0.007	0.35
112740.90-024638.7	17.40 $\pm$ 0.03	20784 $\pm$ 206	7.40 $\pm$ 0.03	112741.1-024614	1.0	0.017 $\pm$ 0.007	-0.45
165645.49+182437.7	20.30 $\pm$ 0.02	12460 $\pm$ 638	8.44 $\pm$ 0.26	165643.7+182441	1.7	0.015 $\pm$ 0.006	0.66
232658.89-002339.9	19.35 $\pm$ 0.03	8081 $\pm$ 83	8.87 $\pm$ 0.12	232701.2-002337	1.8	0.018 $\pm$ 0.009	0.37
232659.23-002348.0	17.51 $\pm$ 0.02	10622 $\pm$ 47	8.33 $\pm$ 0.04	232701.2-002337	1.6	0.018 $\pm$ 0.009	-0.37

Table 4.2: (continued) Optical and X-ray properties of the new SDSS DAs.

SDSS J	1RXS J	HR1	HR2	DL	Identification	Comments
075106.51+301726.4	075107.4+301719	$-0.77 \pm 0.19$	$-0.39 \pm 1.49$	11	Eisenstein et al. (2006)	suspect $u, g, r, i, z$
082346.14+245345.6	082345.4+245344	$-1.00 \pm 0.26$	$1.00 \pm 9.99$	10	Eisenstein et al. (2006)	
093006.79+522803.3	093006.7+522752	$-1.00 \pm 0.18$	$-1.00 \pm 9.99$	12	Eisenstein et al. (2006)	
101339.56+061529.5	101340.6+061556	$-0.77 \pm 0.33$	$1.00 \pm 4.76$	7	Eisenstein et al. (2006)	
113836.33+475509.8	113836.9+475459	$-1.00 \pm 0.30$	$0.00 \pm 0.00$	15	Eisenstein et al. (2006)	
120432.67+581936.9	120428.0+581934	$-0.98 \pm 0.28$	$0.00 \pm 0.00$	8	Eisenstein et al. (2006)	
125938.08+603900.0	125936.6+603910	$-1.00 \pm 0.10$	$0.00 \pm 0.00$	18	Eisenstein et al. (2006)	
132629.58+571131.5	132634.4+571052	$-1.00 \pm 0.23$	$0.00 \pm 0.00$	7	Eisenstein et al. (2006)	
154448.25+455039.0	154449.3+455035	$-1.00 \pm 0.09$	$0.00 \pm 0.00$	26	Eisenstein et al. (2006)	
163418.25+365827.1	163421.8+365859	$-1.00 \pm 0.23$	$0.00 \pm 0.00$	7	Eisenstein et al. (2006)	
074859.06+215445.7	074858.9+215458	$-0.06 \pm 0.37$	$0.55 \pm 3.56$	9	Eisenstein et al. (2006)	Star?
093307.65+400637.9	093305.6+400553	$-0.02 \pm 0.30$	$0.70 \pm 0.39$	19	Eisenstein et al. (2006)	Galaxy?
103237.35+512857.9	103236.8+512809	$0.61 \pm 0.70$	$0.11 \pm 0.47$	7	Eisenstein et al. (2006)	
112740.90-024638.7	112741.1-024614	$1.00 \pm 0.38$	$-0.79 \pm 0.40$	8	Eisenstein et al. (2006)	Star?
165645.49+182437.7	165643.7+182441	$0.78 \pm 0.37$	$-0.01 \pm 0.43$	9	Eisenstein et al. (2006)	
232658.89-002339.9	232701.2-002337	$0.31 \pm 0.51$	$1.00 \pm 1.48$	8	Eisenstein et al. (2006)	
232659.23-002348.0	232701.2-002337	$0.31 \pm 0.51$	$1.00 \pm 1.48$	8	Kleinman et al. (2004)	

Table 4.3: Optical and X-ray properties of the other new SDSS WDs. The first two objects are DB WDs; the third is a PG 1159 star; the final three are DAM dwarf binaries. The  $T_{eff}$  and  $\log g$  values for the latter four objects are suspect.

SDSS J	PSF $g$	$T_{eff}$	$\log g$	1RXS J	$\sigma$	counts $s^{-1}$	$\log (f_X/f_g)$
093122.86+362209.4	$20.01 \pm 0.03$	$20496 \pm 1050$	$7.97 \pm 0.19$	093119.2+362223	2.3	$0.017 \pm 0.008$	0.60
153225.49+472700.9	$19.39 \pm 0.03$	$17567 \pm 447$	$8.32 \pm 0.22$	153221.7+472648	2.9	$0.012 \pm 0.005$	0.20
114635.23+001233.5	$14.87 \pm 0.03$	$10000 \pm 794$	$5.00 \pm 0.00$	114634.6+001238	0.8	$0.091 \pm 0.020$	-0.72
114312.57+000926.6	$18.17 \pm 0.02$	$9760 \pm 47$	$8.07 \pm 0.06$	114313.8+000955	1.1	$0.038 \pm 0.017$	0.22
134100.03+602610.4	$16.71 \pm 0.01$	$47909 \pm 638$	$7.59 \pm 0.05$	134101.0+602556	0.6	$0.034 \pm 0.009$	-0.42
223051.15+125706.8	$19.53 \pm 0.02$	$6302 \pm 5$	$6.78 \pm 0.34$	223051.6+125713	0.4	$0.023 \pm 0.010$	0.55

Table 4.3: (continued) Optical and X-ray properties of the new SDSS DAs.

SDSS J	1RXS J	HR1	HR2	DL	Identification	Comments
093122.86+362209.4	093119.2+362223	$-1.00 \pm 0.49$	$1.00 \pm 2.80$	7	Eisenstein et al. (2006)	DB
153225.49+472700.9	153221.7+472648	$-1.00 \pm 0.48$	$1.00 \pm 3.55$	8	Eisenstein et al. (2006)	DB
114635.23+001233.5	114634.6+001238	$-0.94 \pm 0.07$	$1.00 \pm 3.37$	33	WD 1144+004	PG 1159
114312.57+000926.6	114313.8+000955	$0.37 \pm 0.40$	$0.64 \pm 0.36$	7	WD 1140+004	DA/M; suspect $i$
134100.03+602610.4	134101.0+602556	$-1.00 \pm 0.09$	$0.00 \pm 0.00$	18	WD 1339+606	DA/M
223051.15+125706.8	223051.6+125713	$1.00 \pm 0.92$	$1.00 \pm 1.25$	9	Silvestri et al. (2006)	DA/M

part<sup>3</sup>. Finally, for SDSS J162814.59+363008.3 a very faint ( $g = 21.45 \pm 0.04$ ) UV-excess object (with  $(u-g) = 0.18 \pm 0.13$ ) is positionally coincident with a FIRST radio source. In all three cases the RASS sources are not super-soft ( $\text{HR1} = -0.77 \pm 0.17$ ,  $0.11 \pm 0.31$ , and  $-0.37 \pm 0.35$ , respectively), and it seems likely that the UV-excess objects are quasars and X-ray sources. Follow-up spectroscopy is required to confirm whether this is in fact the case, but we consider these DAs to be unlikely RASS-source counterparts.

Of the 17 remaining possible X-ray-emitting DAs, there are five cases in which inspection of the RASS field, combined with the RASS source hardness ratio, suggests that the WD is probably not the X-ray source—but does not provide a strong alternate X-ray counterpart candidate. In these fields, spectroscopy of multiple objects or high spatial resolution X-ray observations are needed to identify the X-ray source. And then there is the interesting case of SDSS J232658.89–002339.9 and J232659.23–002348.0, both of which are within  $1'$  of 1RXS J232701.2–002337, for which  $\text{HR1} = 0.31 \pm 0.51$ . While it seems unlikely that either WD is therefore the X-ray source, a high spatial resolution X-ray observation of the field is required in order to reveal the X-ray emitter.

We list the 10 confident new SDSS DA WD/RASS source associations in Table 4.2 and add these last seven possible associations. As in Table 4.1, we present key X-ray and optical data for these objects. Since these are SDSS discoveries, we list the SDSS WD paper in which the spectroscopic identification was made. For the seven possible identifications we suggest, where possible, an alternate counterpart to the X-ray source.

#### 4.2.3 Other SDSS X-ray-emitting WDs

Among the matches obtained when correlating the Eisenstein et al. (2006) WDs with the RASS catalogs were a handful of non-DA WDs. Four are actually binary pairs where a DA WD has an M star companion. Four are DB WDs; these are WDs with

---

<sup>3</sup>Interestingly, there is a radio source in this field cataloged by both the NRAO Very Large Array (VLA) Sky Survey (NVSS; Condon et al., 1998) and the VLA Faint Images of the Radio Sky at Twenty-Centimeters (FIRST; Becker et al., 1995) survey that does not have an SDSS counterpart.

helium-rich atmospheres. In addition, there is one DC WD (a WD lacking absorption lines in its spectrum) and one PG 1159 star (a pre-WD star showing strong oxygen and carbon lines). Once again we eliminate those WDs in fields with cataloged quasars; there are three such fields here, all with RASS sources that are not soft ( $HR1 = 0.52 \pm 0.46$ ,  $-0.15 \pm 0.15$ , and  $0.09 \pm 0.18$ ). This removes two of the DB WDs and the DC WD from our list of potential X-ray sources.

For two other RASS sources the SDSS data suggest other counterparts. SDSS J123337.71+570335.4 is a  $z = 0.351$  redshift quasar nearer to the RASS source ( $HR1 = 0.20 \pm 0.42$ ) than SDSS J123345.52+570343.9, another one of the DB WDs. The UV-excess object SDSS J155209.12+433821.8 ( $(u - g) = 0.45 \pm 0.04$ ) is also closer to the RASS source ( $HR1 = -0.18 \pm 0.37$ ) than SDSS J155205.59+433825.8, one of the DA/M star binaries. While spectroscopic confirmation is needed in the latter case, we conclude that both of these RASS sources are in fact quasars.

The remaining six objects are listed in Table 4.3; the columns are as in Table 4.2. The first two are DB white dwarfs newly identified by Eisenstein et al. (2006); both are at relatively large offsets from the corresponding RASS source, which has a low detection likelihood. Higher resolution X-ray observations are needed to confirm that these DBs are in fact X-ray sources, particularly since they are both cooler than one would expect for non-DA X-ray emitters (e.g., discussion in O'Dwyer et al., 2003). The next four objects are all poorly fit by the automated model-fitting routine used to obtain temperature and surface gravity estimates from the SDSS spectra, and the values in Table 4.3 should therefore not be trusted. The first of these four objects is the previously known PG 1159 star SDSS J114635.23+001233.5; the other three are DA/M star systems, of which one is an SDSS discovery, SDSS J223051.15+125706.8 (Silvestri et al., 2006).

#### 4.2.4 SDSS X-ray-emitting WDs identified since DR4

In the time since the production of the Eisenstein et al. (2006) SDSS WD catalog, new WDs have been identified through inspection of the more recent survey spectroscopy.

In addition, we have collected a few objects whose spectra were taken earlier in the survey but that were not included in the Kleinman et al. (2004) or Eisenstein et al. (2006) samples; we refer to all of these objects as post-DR4. They are not confirmed WDs, and have not been fit to obtain their physical parameters, so our analysis is preliminary.

Among the 42 RASS sources with new candidate WDs within  $1'$ , we selected the super-soft sources by requiring that  $\text{HR1} \leq -0.8$ . Nine sources met this criterion. Two are the known DA WDs WD 1325+512 and WD 1415+132 cataloged by McCook & Sion (1999) and confirmed as X-ray emitters<sup>4</sup>. Interestingly, the SDSS spectra suggest that both have possible M-star companions.

Inspection of the SDSS data for the seven uncataloged sources (all of which have DA-like spectra) suggests that in five cases the association of RASS source and SDSS WD is very strong. In the two other cases, spectroscopic follow-up is required to confirm that the SDSS WD is indeed the RASS source. For SDSS J114142.84+143356.5, a  $g = 15.76 \pm 0.01$  star is nearer to the RASS position. This star, were it to be the X-ray source counterpart, would have  $\log(f_X/f_g) = -1.04$ , which is high for a main sequence stellar X-ray emitter. On the other hand, this is the least soft of the RASS sources ( $\text{HR1} = -0.88 \pm 0.20$ ). For SDSS J155109.55+454252.2, a UV-excess object ( $g = 17.55 \pm 0.02$ ,  $(u - g) = -0.39 \pm 0.03$ ) is virtually coincident with the RASS position. Since the RASS source is super-soft, a WD counterpart is very likely. But the UV-excess object cannot be ruled out as the X-ray emitter: it may also be a WD, or a cataclysmic variable; the latter are also frequently super-soft emitters (see Chapter 3).

All nine matches are listed in Table 4.4. We provide their SDSS name and  $g$  magnitude. The corresponding RASS source names, offsets ( $\sigma$ ) between the SDSS objects and RASS positions, count rates, hardness ratios, and detection likelihood are also included. The last column is the  $\log(f_X/f_g)$  calculated as above using the Maccacaro et al. (1988) formula. In Table 4.5 we list 27 of the 33 other candidate WDs.

---

<sup>4</sup>WD 1415+132 is included in Fleming et al. (1996); WD 1325+512 is listed in SIMBAD as a known X-ray source, but is not included in Fleming et al. (1996) or Zickgraf et al. (2003). It is unclear how it was identified as a RASS source.

Table 4.4: Optical and X-ray properties of the post-DR4 SDSS WD/RASS associations. The last two are the known DAs WD 1325+512 and WD 1415+132 (McCook & Sion, 1999).

SDSS J	PSF $g$	1RXS J	$\sigma$	counts s <sup>-1</sup>	HR1	HR2	DL	$\log(f_X/f_g)$
100543.92+304744.9	16.35 ± 0.02	100543.7+304809	1.3	0.046 ± 0.016	-1.00 ± 0.22	0.00 ± 0.00	11	-0.42
114142.84+143356.5	16.34 ± 0.01	114145.3+143349	1.7	0.020 ± 0.009	-0.88 ± 0.20	-1.00 ± 0.00	7	-0.80
125338.50+051542.1	18.37 ± 0.02	125338.5+051630	1.9	0.054 ± 0.021	-1.00 ± 0.39	-1.00 ± 9.99	9	0.45
133024.24-001636.8	16.84 ± 0.01	133025.0-001607	1.3	0.023 ± 0.011	-1.00 ± 0.39	0.00 ± 0.00	8	-0.53
143736.67+362213.4	17.35 ± 0.03	143738.0+362237	1.3	0.029 ± 0.009	-1.00 ± 0.14	0.00 ± 0.00	15	-0.23
155109.55+454252.2	16.01 ± 0.02	155108.6+454312	1.0	0.036 ± 0.011	-1.00 ± 0.14	0.00 ± 0.00	15	-0.67
161614.02+080905.8	16.46 ± 0.01	161616.2+080913	1.6	0.015 ± 0.007	-1.00 ± 0.81	-1.00 ± 0.59	7	-0.88
132725.72+505711.2	17.50 ± 0.03	132725.7+505713	0.1	0.047 ± 0.012	-1.00 ± 0.00	0.00 ± 0.00	18	0.04
141740.23+130148.7	15.04 ± 0.02	141741.2+130206	1.1	0.032 ± 0.012	-1.00 ± 0.18	0.00 ± 0.00	10	-1.11



Table 4.5: Optical and X-ray properties of the less likely post-DR4 SDSS WD/RASS associations.

SDSS J	PSF $g$	1RXS J	$\sigma$	counts s <sup>-1</sup>	HR1	HR2	DL	$\log(f_X/f_g)$
072841.76+412723.0	20.89 ± 18.40	072839.4+412728	1.4	0.035 ± 0.011	-0.11 ± 0.31	1.00 ± 1.23	18	1.27
075052.63+223228.0	20.06 ± 0.02	075052.2+223232	0.3	0.054 ± 0.014	0.09 ± 0.30	-0.09 ± 0.36	18	1.12
075343.70+240235.5	17.17 ± 0.02	075343.2+240301	2.0	0.017 ± 0.008	0.83 ± 0.69	0.29 ± 1.98	10	-0.54
075937.85+174346.2	16.22 ± 0.01	075941.6+174345	1.5	0.050 ± 0.022	0.88 ± 0.32	-0.52 ± 0.47	8	-0.44
083244.09+083831.6	18.12 ± 0.01	083243.1+083826	1.1	0.038 ± 0.014	-0.11 ± 0.41	-1.00 ± 1.14	13	0.20
101704.61+064822.7	16.39 ± 0.03	101707.8+064847	4.1	0.021 ± 0.009	-0.69 ± 0.27	0.00 ± 0.00	11	-0.76
103015.36+341349.1	18.37 ± 0.03	103012.2+341319	1.9	0.014 ± 0.007	0.41 ± 0.44	-0.64 ± 1.02	7	-0.13
110014.52+514013.4	17.53 ± 0.02	110019.3+514010	2.0	0.022 ± 0.009	-0.63 ± 0.25	-1.00 ± 1.70	7	-0.28
115205.64+333505.6	15.12 ± 0.03	115205.7+333512	0.5	0.036 ± 0.011	-0.05 ± 0.29	0.44 ± 0.37	16	-1.03
115210.99+554808.3	16.69 ± 0.04	115205.1+554816	3.1	0.021 ± 0.009	-0.38 ± 0.34	0.01 ± 0.63	10	-0.63
121616.77+565144.3	20.13 ± 0.03	121616.7+565137	0.3	0.022 ± 0.010	-0.58 ± 0.40	-0.13 ± 1.23	7	0.77
124858.63+154729.0	17.38 ± 0.03	124856.0+154720	2.0	0.030 ± 0.012	-0.02 ± 0.35	1.00 ± 1.32	9	-0.20
130916.90+452342.7	18.84 ± 0.02	130918.0+452436	4.6	0.042 ± 0.011	0.12 ± 0.26	-0.13 ± 0.31	25	0.53
141336.96-012430.2	17.22 ± 0.02	141334.9-012505	3.6	0.016 ± 0.008	0.75 ± 0.28	-0.74 ± 1.77	11	-0.54

Table 4.5: (continued) Optical and X-ray properties of the less likely post-DR4 SDSS WD/RASS associations.

SDSS J	PSF $g$	1RXS J	$\sigma$	counts s <sup>-1</sup>	HR1	HR2	DL	log ( $f_X/f_g$ )
144735.76+034011.3	18.67 ± 0.02	144733.7+034016	1.8	0.019 ± 0.010	0.34 ± 0.46	-1.00 ± 0.62	8	0.12
150625.32-015824.2	18.66 ± 0.02	150626.0-015754	1.8	0.017 ± 0.009	1.00 ± 0.85	-0.06 ± 0.50	8	0.05
153611.09+580206.4	22.78 ± 0.11	153611.1+580150	0.9	0.007 ± 0.003	1.00 ± 0.57	0.50 ± 0.36	11	1.35
160226.21+430355.4	19.76 ± 0.03	160224.2+430413	0.6	0.037 ± 0.015	0.12 ± 0.38	-0.36 ± 0.36	10	0.85
161327.53+222352.1	18.40 ± 0.03	161325.5+222417	1.1	0.011 ± 0.005	0.56 ± 0.45	1.00 ± 0.33	7	-0.22
162340.42+454519.4	20.58 ± 0.03	162338.0+454452	2.7	0.019 ± 0.009	1.00 ± 0.59	-0.38 ± 0.33	8	0.88
162949.85+304317.8	16.75 ± 0.02	162948.3+304301	1.5	0.023 ± 0.008	-0.42 ± 0.30	0.06 ± 0.63	11	-0.57
163535.01+290829.8	19.67 ± 0.02	163533.6+290921	6.0	0.062 ± 0.013	-0.06 ± 0.20	-0.21 ± 0.27	53	1.03
165738.74+341031.4	19.34 ± 0.02	165739.3+341125	4.5	0.025 ± 0.007	-0.52 ± 0.19	0.38 ± 0.45	20	0.50
170119.18+185350.3	18.44 ± 0.01	170119.7+185448	3.1	0.014 ± 0.006	0.39 ± 0.52	1.00 ± 0.65	7	-0.11
170226.91+330827.2	17.27 ± 0.01	170228.5+330843	1.1	0.017 ± 0.006	0.09 ± 0.36	0.58 ± 0.54	9	-0.49
171952.56+645735.6	16.80 ± 0.02	171952.7+645748	1.4	0.007 ± 0.002	0.73 ± 0.25	0.56 ± 0.19	28	-1.04
210455.59-073834.1	16.90 ± 0.02	210456.3-073825	0.6	0.017 ± 0.007	1.00 ± 0.25	0.69 ± 0.26	9	-0.65

Four of the candidates not listed are SIMBAD-cataloged A stars. In the two other fields, the X-ray source is known, and is not the WD (one is an M star and the other is a quasar). The columns are as in Table 4.4. We note that in three of the RASS fields there is a known quasar in addition to the new candidate WD (1RXS J101707.8+064847, J141334.9-012505, and J165739.3+341125); another field, 1RXS J075343.2+240301, has a nearby cataloged radio source. Finally, the spectrum of SDSS J153611.09+580206.4 suggests it is a possible WD/M star binary.

#### 4.2.5 $\log(f_X/f_g)$ and temperature distributions

In Figure 4.1 we plot the  $\log(f_X/f_g)$  distributions for the subset of 36 Fleming et al. (1996) X-ray-emitting DA WDs that fall within the SDSS footprint. The median  $\log(f_X/f_g)$  for these WDs is  $-0.23$ , with the  $2\sigma$  range being from  $-1.72$  to  $1.26$ —a range that comfortably includes the  $\log(f_X/f_g)$  values for the 17 WDs not cataloged in Fleming et al. (1996) that we have confidently identified as X-ray emitters (7 are from Table 4.1 and 10 from Table 4.2). Although we have not included them in this Figure, we note that the 10 additional less certain X-ray-emitting DA WDs listed in Table 4.1 and Table 4.2, and the nine post-DR4 X-ray emitters in Table 4.4 (which are statistically most likely to be DAs) also have  $\log(f_X/f_g)$  values within these  $2\sigma$  limits.

In Figure 4.2 we compare the temperature distribution for our sample of X-ray-emitting DAs to that of the 76 Fleming et al. (1996) DAs for which Marsh et al. (1997a) obtained temperatures. We include only the 15 previously known and 10 new DAs for which the association with a RASS source is most secure in this plot. While eight of the Fleming et al. (1996) DAs are among our WDs, only three have Marsh et al. (1997a) temperatures and are plotted twice: WD 1026+453, 1429+373, and 1725+5863. For these DAs, the difference between the Eisenstein et al. (2006) and Marsh et al. (1997a) temperatures are rather large (2700, 1900, and 8900 K, respectively), with the Eisenstein et al. (2006) temperature being greater in each case. Discrepancies such as these have been noticed in comparisons between SDSS temperatures and those in the literature for previously cataloged WDs, and are particularly noticeable for the hotter

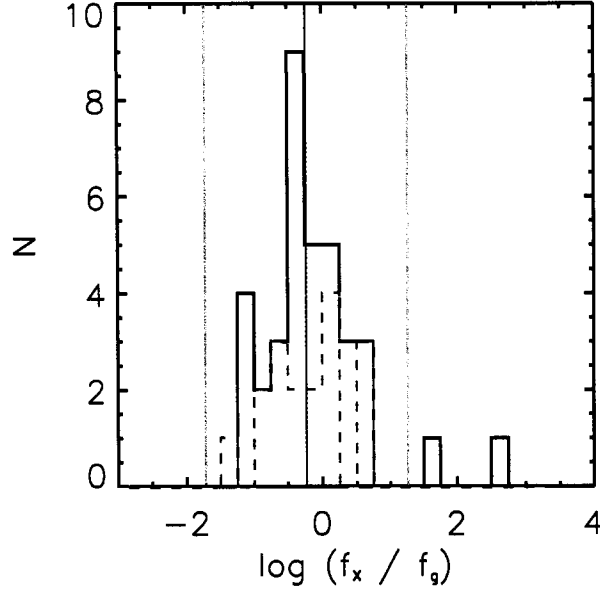


Figure 4.1:  $\log(f_X/f_g)$  distributions for X-ray-emitting DA WDs. The black histogram is for the 36 Fleming et al. (1996) DAs in the SDSS footprint; the dashed blue one is for the sample identified here (eight recovered Fleming et al. (1996) DAs are not included in the latter histogram). The red vertical line is the mean flux ratio, and the green vertical lines bracket the  $2\sigma$  ranges, for the Fleming et al. (1996) sample.

objects, with the differences reaching about 10% at 50,000 K (D. Eisenstein 2006, private communication). Nevertheless, the temperature distributions for our sample of X-ray-emitting DAs and that of Fleming et al. (1996) are very similar, as expected.

For comparison, we also plot the temperature distribution for 7578 Eisenstein et al. (2006) DAs, normalized to the maximum of the Fleming et al. (1996) distribution. The separation between X-ray emitters and “ordinary” WDs is clear, with the Fleming et al. (1996) DAs having a median temperature of  $\sim 39,000$  K, compared to 14,000 K for the Eisenstein et al. (2006) DAs. Interestingly, 1251 of the Eisenstein et al. (2006) DAs are hotter than 22,153 K, the temperature of the coolest Fleming et al. (1996) DA. Even if, as suggested by Fleming et al. (1996), 90% of DAs—including hot ones—are opaque to X rays, we would expect  $\sim 125$  of these to be X-ray sources. If we include the uncertain WD/RASS associations, we have to date found roughly half that number. One possible explanation for this discrepancy is that the use of the Fleming et al. (1996) definition

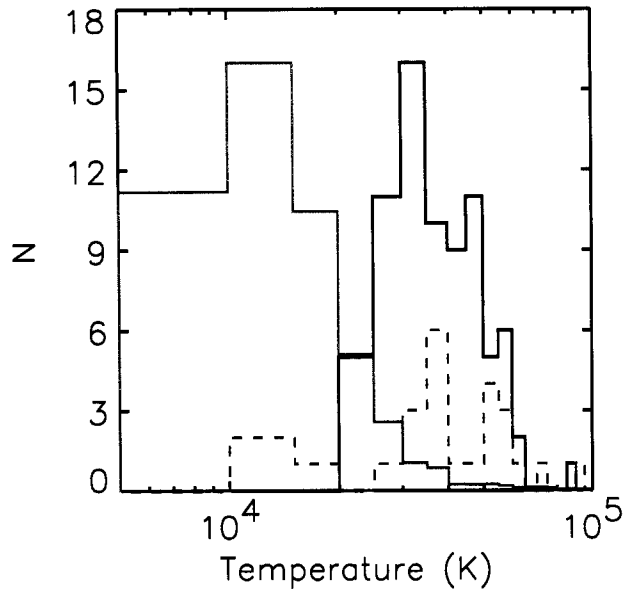


Figure 4.2: Temperature distributions for X-ray-emitting and “ordinary” DA WDs. The black histogram is the Fleming et al. (1996) sample of X-ray emitters; the blue dashed one is the sample identified here. The green histogram is the normalized distribution for 7578 Eisenstein et al. (2006) DAs.

for super-softness is too restrictive at fainter X-ray fluxes, where the hardness ratios have larger errors. We plan to explore this possibility at a later time.

We note that three of the new X-ray-emitting DAs are cooler than the coolest Fleming et al. (1996) DA and therefore below 23,000 K, which is thought to be the minimum temperature needed for X-ray emission from a DA (e.g., Jordan et al., 1994). The three DAs, SDSS J101339.56+061529.5 (14,400 K), J120432.67+581936.9 (15,700 K), and J163418.25+365827.1 (10,100 K) are optically faint ( $g > 19$  mag), and the quoted temperatures should therefore be considered with caution<sup>5</sup>; the SDSS spectra are presented in Figure 4.3. In addition, the three corresponding RASS sources have low X-ray detection likelihoods. Follow-up optical and especially X-ray observations are therefore called for, and we plan to use these observations to investigate these objects<sup>6</sup>.

<sup>5</sup>However, model fits to lower temperature SDSS spectra are typically very reliable because of the strength of the Balmer absorption lines (D. Eisenstein 2006, private communication; see also Figure 4.4).

<sup>6</sup>Interestingly, nearly all of the less certain DA/RASS associations we list in Table 4.1 and Table 4.2

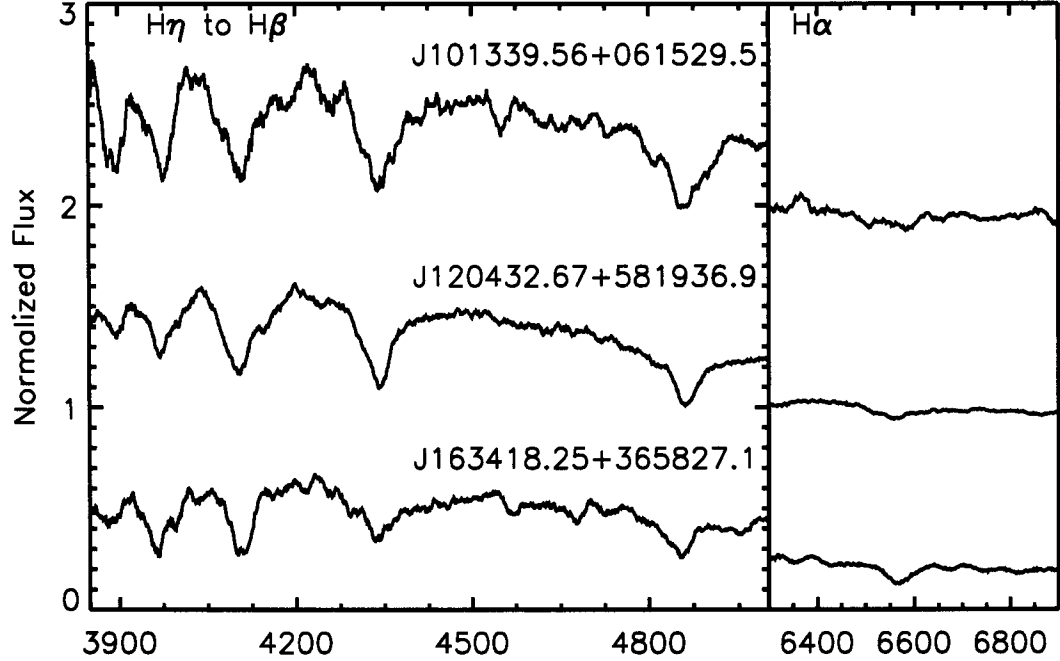


Figure 4.3: SDSS spectra for our candidate cool DA X-ray emitters. The x axis is wavelength in Å; the fluxes have been smoothed and normalized and are offset for plotting purposes. The  $g$  band signal-to-noise ratio for these spectra range from  $\sim 3$  for SDSS J1013+0615 to  $\sim 6$  for SDSS J1204+5819 (Eisenstein et al., 2006).

### 4.3 Composite DA White Dwarf Spectra

We wished to use the high quality and uniformity of the SDSS spectroscopy, and the large number of WDs cataloged by the survey, to examine whether temperature-dependent composite spectra of WDs might reveal anything new about their composition. In particular, we hoped to investigate whether there are compositional differences between X-ray-emitting and non-emitting WDs that may not be detectable in individual spectra, but might be visible in stacked spectra with high signal-to-noise ratios. Creating composite spectra would have the additional benefit of allowing us to

---

are also cooler than 23,000 K. We may have an excellent sample with which to test the minimum temperature paradigm.

divide individual spectra by the corresponding composite to highlight possible hidden features such as weak magnetic lines.

We began by applying a model transformation to the observed SDSS  $(u - i)$  color to obtain effective temperatures for the Kleinman et al. (2004) DAs (the model was produced by P. Bergeron and provided by S. Kleinman 2004, private communication). We then adapted the code developed by D. Vanden Berk to produce composite SDSS quasars (Vanden Berk et al., 2001) in order to create our stacked spectra. The SDSS spectra are flux normalized and re-binned in wavelength before being co-added.

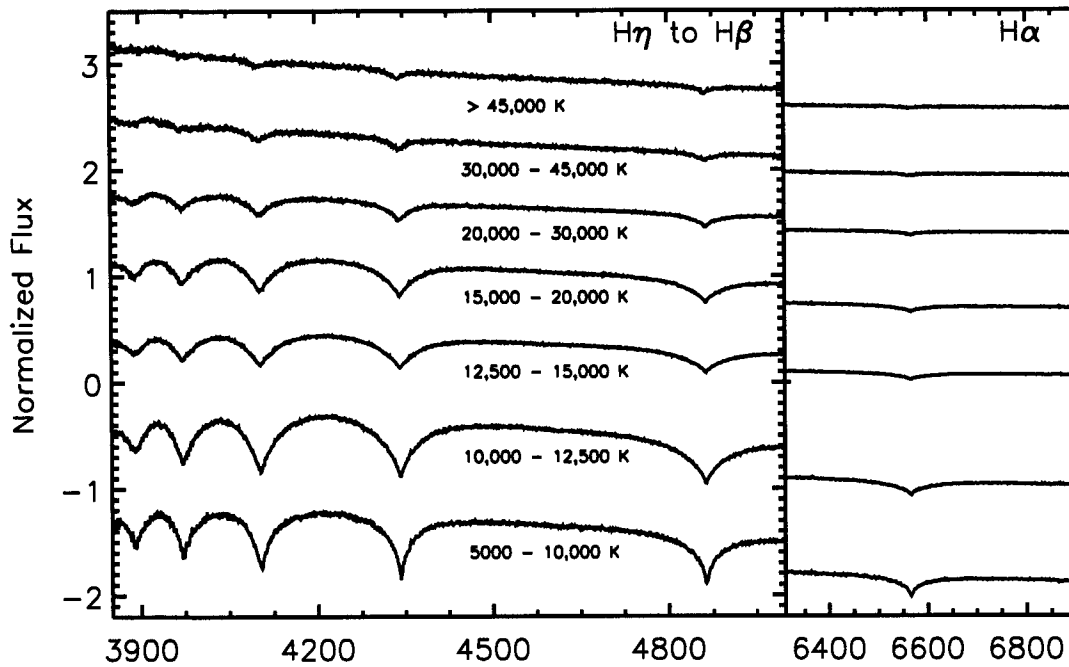


Figure 4.4: Composite DA WD spectra. The x axis is wavelength in Å; the fluxes have been normalized and offset for plotting purposes. About 1100 DR1 WDs were used to make these composites.

The seven spectra presented in Figure 4.4 are composites from a sample of Kleinman et al. (2004) 1129 DAs for which  $|(u - i)_{obs} - (u - i)_{model}| \leq 0.02$ , where the model temperature versus  $(u - i)$  relation is for  $\log g = 8$  DA WDs (the mean  $\log g$  for the

Table 4.6: Number of DAs used to create the composite spectra in Figure 4.4.

Temperature range	DAs
5000 – 10,000 K	278
10,000 – 12,500 K	299
12,500 – 15,000 K	253
15,000 – 20,000 K	211
20,000 – 30,000 K	52
30,000 – 45,000 K	28
> 45,000 K	8

DR1 DAs is 8.06; Kleinman et al., 2004). The temperature binning was done in 2500 or 5000 K increments at the cool end (5000 to 25,000 K), with larger bin sizes at the hotter end (30,000 to 40,000 K and 45,000 K and above) where the Kleinman et al. (2004) DAs are rarer. The number of DAs in each bin is given in Table 4.6.

As discussed above, the sample of X-ray-emitting DAs with SDSS spectra is both small and hot relative to the overall number of confirmed SDSS DAs. 21 of the 25 confident SDSS DA/RASS identifications listed in Table 4.1 and Table 4.2 have temperatures above 30,000 K, where our sample of “ordinary,” non-X-ray-emitting DAs is sparsest. As a result, the work presented below should be considered no more than a preview of a possible application of the technique.

We bin the 10 X-ray-emitting DAs with temperatures between 30,000 and 45,000 K and the 11 with temperatures > 45,000 K (a number greater than used to make the corresponding composite in Figure 4.4) to create the composites shown in Figure 4.5. We also plot the corresponding “ordinary” composites for reference. Only one of the X-ray-emitting DAs presented here was included in our original Kleinman et al. (2004) sample, and we removed it to produce the “ordinary” 30,000 – 45,000 K DA composite.

The composite spectrum for X-ray-emitting DAs between 30,000 and 45,000 K shows structure in its  $H\gamma$  and  $H\delta$  lines that appear to be due to noise in the indi-



vidual spectra. A larger sample would allow us to verify whether these features are in fact real.

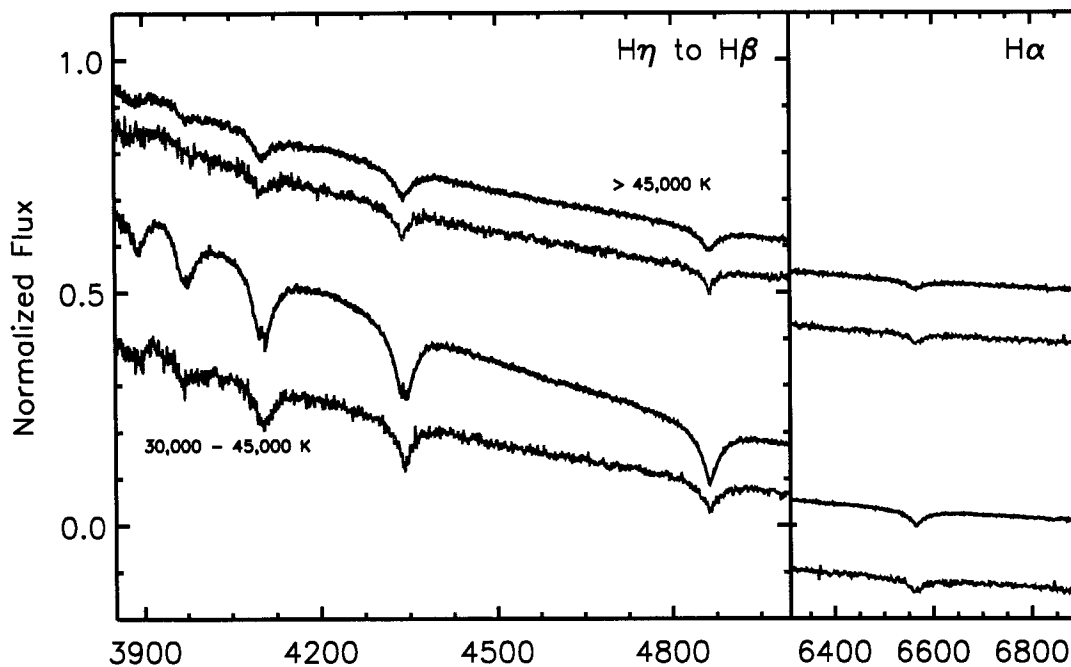


Figure 4.5: Composite spectra for both the X-ray and the “ordinary” (in green) DA WDs. The spectra are plotted as in Figure 4.4.

### ***Acknowledgments***

Much of the research described here was undertaken during two stays at the Space Telescope Science Institute that were made possible by NASA Jenkins Predoctoral Fellowship Program Summer Research Grants. We thank Bruce Margon and Ron Downes for their guidance and assistance before, during, and after those visits to Baltimore, and James Winter for his hospitality there. We are grateful to Dan Vanden Berk for making his composite-spectra code available and helping us adapt it to our purposes.

## Chapter 5

**CANDIDATE ISOLATED NEUTRON STARS  
AND OTHER OPTICALLY BLANK X-RAY FIELDS IDENTIFIED  
FROM THE *ROSAT* ALL-SKY AND SLOAN DIGITAL SKY SURVEYS**

*This chapter originally appeared in the Astronomical Journal (Agüeros et al., 2006, © the American Astronomical Society). Its content is reproduced by permission of the American Astronomical Society. It has been edited to conform to University of Washington's requirements for doctoral theses.*

### 5.1 Introduction

Neutron stars (NSs) were empirically confirmed first as radio pulsars (Hewish et al., 1968), and these objects continue to dominate neutron star statistics. Currently there are over 1500 pulsars cataloged, and the number grows steadily<sup>1</sup>. If one includes the number of observed X-ray binary systems (e.g., Liu et al., 2000, 2001), most of which are thought to contain a neutron star,  $\sim 2000$  NSs are known. Yet a neutron star is born in the Milky Way every 30 to 100 years, suggesting that the total population is  $10^8 - 10^9$  objects (or roughly 1% of the stars), depending on the Galaxy's star formation history (Neuhäuser & Trümper, 1999). Of these neutron stars, only the youngest will be detected as radio pulsars, provided they are aligned favorably; after a few million years, the pulsar will have radiated away its rotational and internal energy, and the pulses will cease (Treves et al., 2000). As a result, the total number of pulsars in the Milky Way is only a few times  $10^5$ ; for every active pulsar there are  $\sim 1000$  radio-quiet neutron stars (Kulkarni & van Kerkwijk, 1998).

Ostriker et al. (1970) proposed that some of these defunct pulsars could reheat by accreting matter from the surrounding interstellar medium (ISM) through Bondi-

---

<sup>1</sup>For an up-to-date catalog of known pulsars, see the Australia Telescope National Facility's database: <http://www.atnf.csiro.au/research/pulsar/psrcat/>.

Hoyle accretion. The ISM would need to be relatively dense, the NS velocity relatively low, and the NS magnetic field somewhat decayed to allow accreting matter to reach the star's surface (see also Treves & Colpi, 1991). If these conditions are met, the neutron star might emit approximately as a blackbody with a peak in the extreme ultraviolet/soft X-ray energy band (Treves et al., 2000). For nearby NSs, this thermal emission is observable, and it was thought that *ROSAT* would detect  $10^2$  to  $10^3$  reheated isolated neutron stars (INSs), thereby potentially providing strong constraints on the neutron star equation of state (EOS) (see, e.g., Treves & Colpi, 1991; Blaes & Madau, 1993).

Yet today the list of *ROSAT*-detected radio-quiet isolated neutron stars contains just seven entries (for a recent review of the so-called Magnificent Seven, see Haberl, 2004). Recent work has suggested at least one plausible explanation for this discrepancy between the predicted and observed numbers of INSs: Bondi-Hoyle accretion may not be an adequate mechanism for reheating large numbers of INSs, in part because the conditions described above are unrealistic (particularly if one considers the observed pulsar velocity distribution; e.g., Perna et al., 2003). Indeed, Popov et al. (2000) have suggested instead that at the bright end of the X-ray log N-log S distribution, where most INS searches have taken place, the current number of known INSs is compatible with population models for young, cooling neutron stars. This is consistent with observations of the Magnificent Seven suggesting they may have magnetic fields and velocities too large for Bondi-Hoyle accretion.

While the X-ray characteristics of the Magnificent Seven are broadly consistent with thermal emission, the current sample has managed to be both too small and too diverse in detail to definitively address the neutron star EOS. For example, while at least five of the Magnificent Seven are X-ray pulsars (Zane et al., 2005), the upper limit for the amplitude of X-ray pulsations in RX J1856.5-3754, the brightest known INS, is  $\leq 1.3\%$  (Burwitz et al., 2003). In addition, rather than bland blackbody spectra, X-ray spectroscopy of four of the Seven has revealed unexpected broad absorption features (Trümper, 2005). The nature and significance of each of these differences are also topics of current debate (e.g., Burwitz et al., 2003; Trümper, 2005; Zane et al.,

2005), although some have argued that all the observational evidence is consistent with blackbody emission altered by the presence of a hydrogen atmosphere and magnetic fields of differing intensities (van Kerkwijk et al., 2004). Clearly, if we are to find unifying patterns by which to disentangle the various possible roles of magnetic fields, geometry, and atmospheres, obtaining a larger sample of INSs is required, especially to make eventual progress toward understanding the fundamental questions of the neutron star EOS.

In the past, a major obstacle to finding isolated neutron stars was the absence of a large-area optical survey of equivalent sensitivity with which to identify the  $> 124,000$  X-ray sources cataloged in the *ROSAT* All-Sky Survey (RASS; Voges et al., 1999). The availability of a suitable companion optical survey would allow the removal of “contaminants” to INS searches (i.e., the bulk of more common X-ray-emitting subclasses: quasars, bright stars, clusters of galaxies, etc.), thereby narrowing the list of RASS error circles in which to search for new INSs. Rutledge et al. (2003) attempted to identify candidate INSs from among the 19,000 RASS sources in the Bright Source Catalog (BSC; Voges et al., 1999) by eliminating matches to the United States Naval Observatory (USNO) A2.0 optical catalog, but in the interim the Sloan Digital Sky Survey (SDSS; York et al., 2000) has emerged as a more powerful companion optical survey to RASS, especially for extending the search for new INSs to the RASS Faint Source Catalog (FSC; Voges et al., 2000).

Here we describe a program to identify the best candidate isolated neutron stars from correlations of the RASS Bright and Faint Source Catalogs and an early version of the SDSS Data Release 4 (DR4; Adelman-McCarthy et al., 2006). In §5.2 we outline the properties of the two surveys. Section 5.3 describes the method used to select our candidate fields, and in §5.4 we describe the properties of the individual candidate fields identified by this program. Section 5.5 is a discussion of our results and includes a comparison of our method with that of Rutledge et al. (2003), an earlier search for INSs that also used the RASS.<sup>2</sup> We conclude in §5.6.

---

<sup>2</sup>Chierigato et al. (2005) have recently published four *ROSAT*-detected X-ray sources without optical counterparts to the Guide Star Catalog faint limit of 19 – 23 mag (depending on the optical band and

## 5.2 RASS and SDSS: A Match Made in the Heavens

The *ROSAT* All-Sky Survey (RASS) was the first of its kind in soft X rays ( $\sim 0.1 - 2.4$  keV). Using the Position Sensitive Proportional Counter, *ROSAT* imaged the sky with exposures of lengths ranging from  $\sim 400$  to  $\sim 40,000$  s at the ecliptic equator and poles, respectively, with 99.7% of the sky observed in exposures at least 50 s long (Voges et al., 1999). The typical limiting sensitivity of the resulting RASS catalog is a few times  $10^{-13}$  ergs  $\text{cm}^{-2} \text{s}^{-1}$ , and more than 124,000 sources are included when one merges the RASS Bright and Faint Source Catalogs (Voges et al., 1999, 2000).

The Sloan Digital Sky Survey provides a uniform optical photometric and spectroscopic dataset with which to correlate the RASS catalog. SDSS is currently mapping the sky at optical wavelengths using a dedicated 2.5-m telescope at Apache Point Observatory (APO), NM, and producing homogeneous five color  $u, g, r, i, z$  CCD images to a depth of  $r \sim 22.5$  (Fukugita et al., 1996; Gunn et al., 1998; Hogg et al., 2001; Smith et al., 2002; Gunn et al., 2006), with associated photometry accurate to 0.02 magnitudes (Ivezić et al., 2004). Astrometric accuracy is better than  $0.1''$  per coordinate (rms) for sources with  $r < 20.5$  (Pier et al., 2003); morphological information drawn from SDSS images allows for reliable star/galaxy separation to  $r \sim 21.5$  (Lupton et al., 2002). The survey's coverage of  $\sim 10^4 \text{ deg}^2$  around the north Galactic cap and of  $\sim 200 \text{ deg}^2$  in the southern Galactic hemisphere will result in photometric measurements for over  $10^8$  stars and a similar number of galaxies. SDSS will also obtain spectra for  $10^6$  galaxies and  $10^5$  quasars. DR4 includes photometric data for  $6670 \text{ deg}^2$  of sky, and catalogs  $1.8 \times 10^8$  objects (Adelman-McCarthy et al., 2006).

Largely by coincidence, the RASS and SDSS are extremely well-matched, making SDSS an ideal tool for identifying large numbers of *ROSAT* sources (e.g., Anderson et al., 2003). In particular, if one considers the known range of  $f_X/f_{\text{opt}}$  for common X-ray emitters, even the faintest optical counterparts to typical RASS sources are bright enough to be detected in the SDSS photometric survey and targeted for SDSS

---

the source position on the sky). These are High Resolution Imager observations, and the area of sky covered and the X-ray error circles are both much smaller than for the RASS.

spectroscopy. For the typical classes of X-ray emitters, including normal stars, normal galaxies, quasars, and BL Lac objects, the highest X-ray-to-optical flux ratios have  $\log (f_X/f_{opt})$  values of about  $-1$ ,  $0$ ,  $+1$ , and  $+1.5$ , respectively (e.g., Stocke et al., 1991; Zickgraf et al., 2003). Given the RASS flux limit quoted above, this implies that a faint optical counterpart in each of these categories of typical X-ray counterparts will have  $m \leq 15, 17, 20$ , and  $21$ , respectively, and therefore that SDSS will obtain accurate photometry for the vast majority of RASS counterparts within its footprint. (We use the Maccacaro et al. (1988) formula for calculations of  $\log (f_X/f_{opt})$ , and substitute  $g$  magnitudes for  $V$ <sup>3</sup>.) Furthermore, at these magnitudes the SDSS spectroscopic survey will frequently obtain spectra with good signal-to-noise ratios for targeted suspected counterparts, allowing for confident identifications.

### 5.3 Using SDSS to Identify Optically Blank RASS Fields

Isolated neutron stars, however, are not among the typical classes of X-ray emitters, and have anomalously large  $\log (f_X/f_{opt})$  values compared to other X-ray sources due to their optical faintness. Of the Magnificent Seven, four have suggested optical counterparts with  $V$  between  $25.8$  and  $28.7$  and associated  $\log (f_X/f_V)$  values between  $4.4$  and  $5.0$  (Kaplan et al., 2003). Clearly, an optical counterpart to an INS is unlikely to be found using SDSS. Rather, we use SDSS to search for RASS fields devoid of plausible optical counterparts to the SDSS  $m \sim 22$  limit. Such error circles host X-ray sources with such extreme  $f_X/f_{opt}$  ratios that an INS becomes a plausible identification.

We select the RASS BSC and FSC objects within the SDSS DR4 footprint by querying the DR4 database for a complete list of SDSS field positions. SDSS fields are  $2048 \times 1489$  pixels and consist of the frames in the five SDSS filters for the same part of the sky. An SDSS field is in some sense the survey's smallest imaging unit in that all elements of a given field are processed by the photometric pipeline at one time. Matching the RASS positions with those of the  $\sim 250,000$  DR4 fields obtained, we find that  $\sim 22,700$  RASS sources are within the area defined by the DR4 fields, which covers

---

<sup>3</sup>While  $g$  and  $V$  are not equal, the color-dependent difference between the two is relatively small:  $g = V + 0.05$  for a typical low-redshift quasar with  $(B - V) = 0.3$  (Fukugita et al., 1996).

6670 deg<sup>2</sup>. Since there are roughly three RASS sources per deg<sup>2</sup>, this number of X-ray sources in the DR4 footprint is consistent with the number of RASS sources expected from a simple surface density argument. Unlike other INS candidate searches (e.g., Rutledge et al., 2003), we do not apply a cut based on the measured X-ray hardness ratios (HR1 and HR2; see Voges et al., 1999). The Magnificent Seven have HR1 ratios that range from  $-1$  to  $0$ , not a strong constraint when the possible range is  $-1$  to  $1$ . While the HR2 ratio may provide a better tool with which to identify soft X-ray emitters, the uncertainties associated with the count rates for RASS faint X-ray sources make this ratio practically undetermined for many of the sources we consider here.

To find the best isolated neutron star candidate fields, we search the 22,700 RASS sources for those with small X-ray positional uncertainties and select the  $\sim 9500$  with quoted positional errors ( $1\sigma$ ) smaller than  $15''$  (the median RASS positional error for this sample is  $13''$ ). In identifying counterparts to these sources in SDSS and other catalogs (and thereby eliminating them), we generally restrict our search to objects within a disk centered on the RASS position and having a radius of either  $1'$  or 4 times the quoted X-ray positional error. Voges et al. (1999) provide one empirical distribution of the positional offsets of optical counterparts relative to the quoted BSC positional errors (see their Figure 8, compiled from correlations with the Tycho catalog Hog et al., 1998). An examination of their most reliable matches indicates that this distribution is not adequately described overall by a two-dimensional Gaussian, and that a one-dimensional Gaussian may be a better fit at larger multiples of the quoted positional error. We therefore estimate that among the 9500 sources we consider further, fewer than 1 is expected to have a counterpart with a positional offset larger than 4 times the *ROSAT* X-ray positional error. For simplicity, we describe this search radius in the rest of the text as equal to 4 *p.e.* (for positional error), and the associated error circle as the 4 *p.e.* error circle.

Previous work suggests that roughly one-third of the  $\sim 9500$  sources with small positional errors are quasars and that another third are bright stars (e.g., Zickgraf et al., 2003). We therefore match the 9500 sources with small positional errors to the most recent SDSS catalog of  $> 4000$  spectroscopically identified RASS quasars (e.g., Anderson

et al., 2003). We take  $1'$  as our matching radius, meaning that any X-ray source with a spectroscopically confirmed quasar within an error circle of radius  $\geq 4$  *p.e.* is eliminated from further consideration. Similarly, we use the SDSS DR4 photometric catalog to eliminate RASS fields with a  $g < 15$  mag object<sup>4</sup> within  $1'$ . When querying the DR4 database, we request “primary” photometry, which requires that objects have a single entry in the database, that they not be deblended, and that they fall within the survey boundaries (for details, see Stoughton et al., 2002). The median count rate for our sample of RASS sources with small positional errors is  $0.034$  counts  $\text{s}^{-1}$ , so that  $g < 15$  objects have  $\log(f_X/f_g) \leq -1.1$  and are most probably the X-ray source counterparts (see Table 1 in Stocke et al., 1991). Both of these cuts are extremely conservative, as they are applied without specific  $f_X/f_{opt}$  restrictions and extend to a large positional offset for each source. Still, a confirmed quasar, or a bright star or galaxy, even with an atypical  $f_X/f_{opt}$  and at a large positional offset, might be a more plausible identification than an INS. Roughly half of the 9500 originally selected sources with small positional errors remain at the end of this stage of our algorithm.

To reduce the number further, we use the DR4 database to eliminate X-ray error circles with any UV-excess objects. These are objects satisfying  $(u - g) < 0.6$  and  $u \leq 22.0$ , the SDSS 95% completeness limit (Stoughton et al., 2002); for the most part, these are candidate (photometric) quasars (e.g., Richards et al., 2002), but this cut also identifies and removes white dwarfs and cataclysmic variables/X-ray binaries. Here we calculate the separation between each such object and the RASS source and eliminate those fields in which a UV-excess object falls within the 4 *p.e.* error circle of the associated X-ray source. Finally, because the occasional pathologically bland quasar (a few percent of all cases; Vanden Berk et al., 2001) or a quasar in a selected redshift range can have colors consistent with those of normal stars and cannot easily be identified using SDSS-color cuts, we remove fields with objects that have quasar-like X-ray-to-optical flux ratios (defined as  $\log(f_X/f_g) \leq 1.2$ , the typical upper limit

---

<sup>4</sup>In querying the database for photometry, we request both PSF and model magnitudes, and make our cuts based on both. Typically, PSF fitting provides better estimates of isolated star magnitudes, while model fitting is best for galaxies (see Stoughton et al., 2002).



for AGN given by Stocke et al., 1991) *regardless of their optical colors*. We eliminate all fields in which such an object with  $g \leq 22.2$  (the 95% completeness limit in that band) is cataloged within 4 *p.e.* of the X-ray position. This removes about four-fifths of the remaining sources, leaving us with 410 X-ray sources, about 4% of our initial sample of RASS sources with small positional errors<sup>5</sup>.

We then require, when matching these sources to the SDSS catalog, that SDSS primary photometry within the 4 *p.e.* error circle be available, thereby eliminating false positives—fields that would otherwise be defined as optically blank at this stage of the algorithm only because there is no reliable SDSS photometry for them. Over 80% of the 410 fields lack SDSS photometry; this is frequently because of the presence of a saturating star or because the RASS source falls on the edge of the DR4 footprint. The remaining 74 RASS sources are then fed to SIMBAD and the NASA/IPAC Extragalactic Database (NED), with which we eliminate 19. Roughly half of these sources are cataloged clusters within 1', while the rest include known BL Lac objects or bright Two Micron All Sky Survey galaxies within the 4 *p.e.* error circle. We also eliminate the 22 X-ray error circles with a cataloged NRAO Very Large Array (VLA) Sky Survey (NVSS; Condon et al., 1998) or VLA Faint Images of the Radio Sky at Twenty-Centimeters (FIRST; Becker et al., 1995) source within 4 *p.e.* of the associated X-ray position; this is intended especially to eliminate uncataloged BL Lac candidates. These steps reduce the list of candidates to 33 RASS X-ray error circles.

Visual inspection of the SDSS images of these remaining 33 fields finds three cases with an obvious candidate optical counterpart to the X-ray source that has somehow evaded our algorithm. In two cases the most likely explanation is the absence of primary SDSS photometry for a bright star present in the center of one field and for a galaxy in the center of the other. In the third case, SDSS spectroscopy of a  $g = 20.44$  object reveals it to be an emission line galaxy and therefore a conceivable (though unusual) X-ray source. We eliminate these fields and are left with a list of 30 X-ray error

---

<sup>5</sup>This cut is sufficiently stringent that it may render some of the previous steps unnecessary. However, it would not alone eliminate spectroscopically confirmed SDSS BL Lac objects, for example, a significant fraction of which do have  $\log(f_X/f_g) > 1.2$  (Anderson et al., 2003).

circles that are optically blank (devoid of plausible optical counterparts) at the SDSS catalog level as defined by our algorithm.

Table 5.1: X-ray and optical data for the 11 candidate isolated neutron star fields. Note that 1RXS J003413.7–010134 and 013630.4+004226 are outside of the optical cluster catalog footprint; 1RXS J130547.2+641252 was rejected as an INS (Rutledge et al., 2003); and 1RXS J160518.8+324907 is a known INS.

RASS					SDSS	
Source name		Count rate	Detection	Exp.	$g$	Min.
1RXS J	$1\sigma$	$10^{-2}$ cps	likelihood	s	mag	$\log (f_X/f_g)$
003413.7−010134	14''	$1.3 \pm 0.6$	10	630	23.22	1.8
013630.4+004226	13''	$2.5 \pm 1.0$	16	283	21.82	1.5
092310.1+275448	14''	$2.5 \pm 1.0$	14	407	21.74	1.5
103415.1+435402	14''	$1.7 \pm 0.8$	9	502	21.66	1.3
110219.6+022836	15''	$1.8 \pm 0.8$	11	423	21.80	1.3
122344.6+373015	15''	$2.8 \pm 1.1$	11	490	21.97	1.6
130547.2+641252	9''	$16.7 \pm 2.1$	122	544	22.05	2.4
131400.1+072312	15''	$1.8 \pm 1.0$	8	333	21.69	1.3
141428.5+601707	14''	$1.4 \pm 0.7$	9	630	21.99	1.3
151855.1+355543	9''	$3.3 \pm 0.9$	32	518	21.04	1.3
160518.8+324907	7''	$87.5 \pm 4.1$	1140	566	22.80	3.4

Visual inspection of the *ROSAT* hard- and soft-band images of these 30 fields allows us to eliminate nine RASS sources from further consideration. These eliminated sources include possible artifacts and extended or very uncertain X-ray detections. Among the RASS sources eliminated at this stage is 1RXS J115309.7+545636, one of the sources observed with the *Chandra X-Ray Observatory* as a candidate INS by Rutledge et al. (2003). Their observations confirmed that 1RXS J115309.7+545636 is in fact not an INS (see §5.5.1).

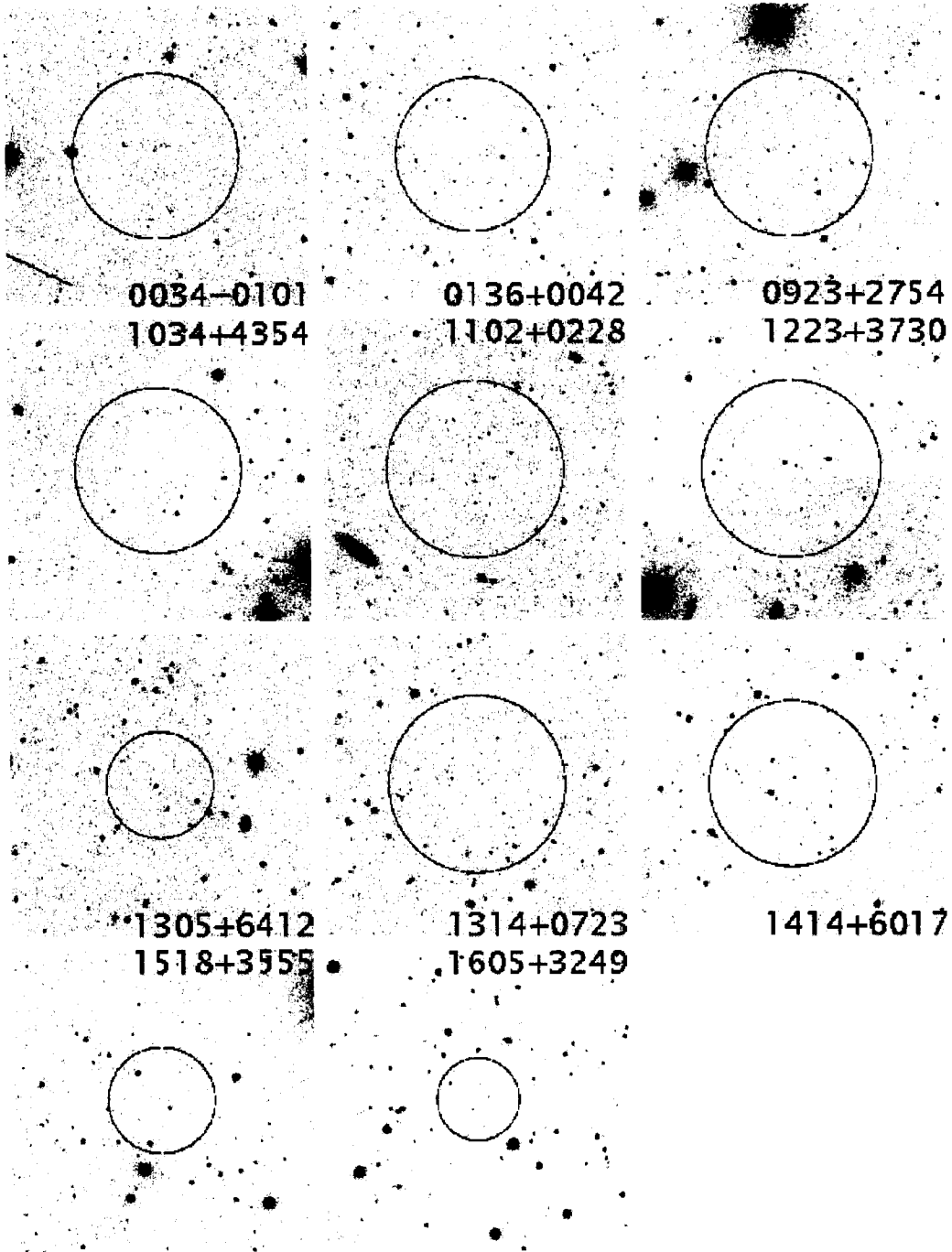


Figure 5.1: SDSS composite  $g, r, i$  images of our best INS candidate fields, with the stretch being the same for all. North is up and east is to the left; the images are roughly  $3.5'$  on a side. The 4  $p.e.$  RASS error circle is shown in each image. The brightest SDSS object within any of the error circles is  $g = 21.04$  mag. Rutledge et al. (2003) rejected 1RXS J130547.2+641252 as an INS; 1RXS J160518.8+324907 is a known INS.

Three additional RASS sources were set aside at this stage. Their quoted positional error of  $6''$  appears to be an underestimate if one considers the count rates and exposure lengths for these sources (see §5.7 for further discussion).

Some fraction of the remaining X-ray sources are likely to be associated with optically faint clusters of galaxies. We therefore correlate our remaining X-ray positions with a catalog of optically selected SDSS clusters (J. Annis 2005, private communication). Two of our X-ray sources fall outside of the cluster catalog’s footprint, and were therefore not subject to this cluster analysis; see Table 5.1. The optical clusters are described in part by their  $n_{gal}$  value, the number of red sequence galaxies brighter than  $0.5L_*$  within a 1 Mpc radius volume, with SDSS colors providing a photometric estimate of the redshifts. If there is a candidate cluster with  $n_{gal} \geq 3$  with an offset  $\leq 1'$  from the X-ray position, we eliminate the X-ray source as a candidate INS. This removes two RASS sources from consideration and is consistent with our elimination, earlier in our algorithm, of cases with a cataloged NED/SIMBAD cluster within  $1'$ .

In identifying clusters at larger angular separations as likely RASS X-ray sources, we take  $5'$  as our maximum separation for considering matches. There is a drop off in the surface density of candidate SDSS optical clusters at that separation. We choose  $n_{gal} \geq 6$  as our richness criterion for considering a cluster to be a likely X-ray source, in these high positional offset cases, and thereby eliminate another five RASS error circles as candidate clusters (see §5.7 for further discussion of these candidate clusters).

These steps winnowed the original list of 9500 RASS sources in the SDSS DR4 footprint to 11 X-ray sources that are bereft of plausible counterparts and are therefore candidate blank-field X-ray sources. It is highly reassuring that among these surviving blank-field X-ray sources is the field containing RX J1605.3+3249, the only previously known isolated neutron star in the SDSS DR4 footprint. We argue in §5.5.1 that our selection using SDSS is an order of magnitude more stringent than the Rutledge et al. (2003) hallmark blank-field search for INSs.

## 5.4 Properties of the Candidate Isolated Neutron Star Fields

The 11 fields discussed in this section are those that survived our winnowing algorithm and are most likely to harbor either isolated neutron stars or some other rare and exotic X-ray emitter such as radio-quiet BL Lac objects, obscured AGN, and dark clusters. They include one previously rejected candidate INS field Rutledge et al. (2003), as well as the field of RX J1605.3+3249, the only known INS falling within the SDSS DR4 footprint. Figure 5.1 is a mosaic of the SDSS composite  $g, r, i$  images of all 11 of the candidate fields with the RASS 4 *p.e.* error circles superimposed. Table 5.1 includes the *ROSAT* parameters for all of these RASS sources (counts  $\text{s}^{-1}$ , detection likelihood, and exposure time; see Voges et al., 1999), as well as the  $g$  magnitude of the *brightest* SDSS object within the 4 *p.e.* RASS error circle and the corresponding *minimum*  $\log (f_X/f_g)$  for the optical counterpart to the X-ray source.

Below we provide additional information about several of these X-ray sources: those that might have viable optical counterparts at unexpectedly large positional offsets, and those previously identified in the literature as INS candidates.

### 5.4.1 New candidate INS fields with other possible counterparts at large offsets

There are two candidate INS fields in which a known quasar or a bright star lies just outside the 4 *p.e.* RASS error circle. Although we expect  $< 1$  case of an optical counterpart being found at such large positional offsets from our entire starting set of 9500 RASS X-ray sources, in this section we call special cautionary attention to these cases. Good angular resolution X-ray images would quickly resolve such issues definitively. These two cases are:

- **1RXS J003413.7–010134** The 4 *p.e.* error circle just barely excludes a  $g = 16.75$  star for which we obtained a spectrum with the APO 3.5-m telescope. This spectrum is of a G star with no emission; the star's  $\log (f_X/f_g)$  of  $-0.8$  is unlikely for G stars, whose (log) flux ratios are typically between  $-4.3$  and  $-2.4$  (see Table 1 of Stocke et al., 1991), suggesting that it is probably not the X-ray source.

In addition, we note the presence of a spectroscopically confirmed quasar, SDSS J003413.04–010026.8,  $1.13'$  (4.8 times the quoted RASS positional error) from this source. This  $g = 17.20$  quasar has a  $\log(f_X/f_g) = -0.63$ , within the range for AGN given by Stocke et al. (1991) of  $-1$  to  $1.2$ .

- **1RXS J141428.5+601707** SDSS J141431.67+601807.2, a spectroscopically confirmed quasar, lies  $1.09'$  (4.7 times the quoted RASS positional error) from this source. This quasar has  $g = 17.82$  mag, so that its  $\log(f_X/f_g) = -0.36$ , within the range for AGN given by Stocke et al. (1991).

#### 5.4.2 *Previously known candidate INS fields*

There are two previously suggested candidate isolated neutron stars that are also included among our 11 candidates. One is a confirmed INS, while the other was later refuted as an INS:

- **1RXS J130547.2+641252** This source was proposed and rejected as a candidate INS by Rutledge et al. (2003) because of its X-ray variability (see §5.5.1 for further discussion).
- **1RXS J160518.8+324907** This is the only previously known INS in the SDSS DR4 footprint. It is very reassuring that this confirmed case is recovered by our algorithm.

### 5.5 *Discussion*

#### 5.5.1 *Comparison with Previous Work*

An important effort involving RASS/optical selection of candidate isolated neutron stars was that of Rutledge et al. (2003). Rutledge et al. identified candidate INS fields by correlating the RASS BSC with NVSS, the *Infrared Astronomical Satellite* Point Source Catalog, and the USNO A2.0 optical catalog. They obtained a list of 32 candidate blank-field RASS sources (including two known INSs), from which they selected

eight for *Chandra* observations. None of these eight sources was found to be an INS (Rutledge et al., 2003).

The current availability of both SDSS spectroscopy and much deeper SDSS photometric data—two or three magnitudes fainter than USNO A2.0—permits us to invoke a much more stringent set of selection criteria. To compare our method with that of Rutledge et al., we discuss the properties of the 11 candidate fields from their original list of 32 that fall within the SDSS DR4 footprint, as well as those of the six of their eight *Chandra* targets that do not fall within the SDSS footprint but for which Rutledge et al. provide Digitized Sky Survey (DSS) data. Finally, we speculate on how the remaining 15 Rutledge et al. blank-field candidates would fare at the hands of our algorithm *if* they were in the SDSS DR4 footprint.

#### *Rutledge et al. (2003) sources within SDSS DR4*

Of the initial 32 Rutledge et al. candidate sources, 11 fall within the DR4 footprint, including the previously known INS, RX J1605.3+3249. All 11 candidates were processed by our winnowing algorithm in a double-blind, end-to-end fashion. Reassuringly, RX J1605.3+3249 survives our algorithmic selection, and is among our 11 INS candidates.

Six of the remaining 10 Rutledge et al. sources, for which they identified “ordinary” optical counterparts, were eliminated early on by our algorithm. The source 1RXS J091010.2+481317 disappears from our list of candidate sources when matched against spectroscopically confirmed SDSS quasars. Three other Rutledge et al. sources (1RXS J104710.3+633522, J130402.8+353316, and J130753.6+535137) are eliminated because of the presence of candidate photometric SDSS quasars<sup>6</sup>. Finally, the sources 1RXS J123319.0+090110 and J130034.2+054111 fail our test for sources with no objects brighter than  $g = 15$  within  $1'$ .

A seventh source, 1RXS J094432.8+573544, is eliminated when our X-ray sources are matched to the radio catalogs; it also has an SDSS spectrum, which suggests that it is a BL Lac object. Two of the three other sources survive to the last stages of our

---

<sup>6</sup>This eliminates 1RXS J104710.3+633522 and J130753.6+535137, fields with known cataclysmic variables, as these also have  $(u - g) \leq 0.6$ .

algorithm before being eliminated. Visual inspection of the RASS images of 1RXS 115309.7+545636 reveals it to be an extended source, and it is therefore eliminated as a candidate INS by our algorithm. 1RXS J145234.9+323536 is identified as a candidate optical cluster and is also removed from our list of INS candidates (see §5.7). Rutledge et al. obtained *Chandra* observations of both of these sources and did not detect an X-ray source in either case (Rutledge et al., 2003).

Only one of the remaining 10 Rutledge et al. sources, 1RXS J130547.2+641252, survives to make our list of the best candidate isolated neutron stars. Rutledge et al. rejected this source as a candidate based on its X-ray variability, measured by comparing its RASS data to observations of the same source with the High Resolution Imager on *ROSAT* (Rutledge et al., 2003). We queried the *Chandra* and *XMM-Newton* lists of observed targets, as well as the various *ROSAT* catalogs, and found that none of our other INS candidates has the complementary X-ray observations required for the detection of such variable or transient sources. We therefore cannot discount the possible contamination of our candidate list by such sources.

In summary, of the 11 Rutledge et al. candidate isolated neutron star fields that fall within the DR4 footprint, only two survive our winnowing process. One is a likely transient or variable source, previously discounted as an INS via *Chandra* observations by Rutledge et al. (2003). The other is a successful recovery of the one previously confirmed INS in the SDSS DR4 imaging area, RX J1605.3+3249. Our algorithm is therefore significantly more efficient at removing contaminants from our candidate list while simultaneously recovering the only previously confirmed INS in the SDSS DR4 footprint.

#### *Sources for which Rutledge et al. provide DSS data*

Rutledge et al. also obtained *Chandra* observations for six sources that do not fall within the SDSS DR4 footprint. However, Rutledge et al. do discuss the DSS photometric properties of these six sources: for three they find fairly bright likely optical counterparts, and for three they find counterparts near the DSS faint limit, all offset



from the RASS source by less than three times the quoted positional error (Rutledge et al., 2003). While these six sources are not in the DR4 footprint, it is almost certain that if they had been, none would have made our list of candidate isolated neutron stars.

In three of the X-ray error circles (1RXS J024528.9+262039, J132833.1–365425, and J163910.7+565637), Rutledge et al. identify the likely optical counterparts as two  $B \sim 15$  late-type stars and a  $B = 17.8$ ,  $z = 1.65$  quasar, respectively (Rutledge et al., 2003). With SDSS data, the magnitudes of the late-type stars and/or their  $f_X/f_{opt}$  ratios (approximately  $-0.5$  and  $-0.9$ , respectively, within the range for M stars in Stocke et al., 1991) would very likely have caused our algorithm to eliminate these error circles, and perhaps even suggested the proper identifications. The low redshift quasar’s colors might have been unusual, causing our algorithm to remove it from our candidate list early on; if not, its  $f_X/f_{opt}$  ratio ( $\sim 0.2$ ) likely would also have caused it to be eliminated by our algorithm (an SDSS spectrum might also have been available).

In the cases of 1RXS J020317.5–243832, 145010.6+655944, and 122940.6+181645, the three other sources, SDSS photometry would be available, as the SDSS faintness limit is  $\sim 2$ – $3$  magnitudes deeper than the DSS limit, depending on the band. Rutledge et al. suggest a faint cataclysmic variable (CV) and two faint AGNs as the optical counterparts to these X-ray sources (Rutledge et al., 2003). The colors of the objects, again along with their  $f_X/f_{opt}$  ratios, would probably have disqualified these fields from further consideration.

Our algorithm therefore would probably have eliminated all six of these additional sources observed with *Chandra* by Rutledge et al. (2003), none of which were confirmed as an INS.

#### *Other Rutledge et al. sources*

There remain 15 sources that Rutledge et al. initially considered as candidate isolated neutron stars, but ultimately rejected in post-algorithmic screening. The optical content of these RASS error circles as described by Rutledge et al., or as directly de-

terminated from DSS images by us, is such as to virtually guarantee that 14 would be rejected by our algorithm *if* they fell within the SDSS footprint. These fields include 12 with bright stars, a CV in the globular cluster M3, and a known Seyfert 1 galaxy. The 15<sup>th</sup> source is another known INS, RX J1308.6+2127.

In summary, these comparisons verify that our algorithm, relying especially on the greater optical photometric depth of SDSS, successfully recovers the only previously known INS in our survey area, and also rejects an order of magnitude more contaminating RASS error circles than the Rutledge et al. search for isolated neutron stars.

### 5.5.2 Comparison With Galactic INS Population Models

The current dearth of candidate isolated neutron stars beyond the Magnificent Seven has led to several efforts to rethink the expected population of INSs within the Galaxy. In particular, Popov et al. (2000) compared the space density of accreting (i.e., reheated and old) isolated neutron stars to that of cooling (i.e., young) neutron stars, using a number of assumptions about, for example, the Galactic neutron star birth rate, the large-scale distribution of gas in the interstellar medium, the cooling time for a newborn neutron star.

Popov et al. (2000) find that at the bright end (*ROSAT* count rates  $\geq 0.1$  counts s<sup>-1</sup>,  $L_X \sim 10^{29} - 10^{30}$  ergs s<sup>-1</sup>), the predicted population of INSs is essentially just the small number of young neutron stars seen at an early enough evolutionary stage—the first 10<sup>6</sup> years of their lives—to still be quite hot. They also find that these coolers are typically three orders of magnitude brighter than accreting, older isolated neutron stars. However, the total number of predicted accretors is about two orders of magnitude larger than that of coolers, so that at lower count rates/X-ray fluxes, the number of accretors is comparable to that of coolers. Indeed, Popov et al. predict that at fluxes below  $\sim 10^{-13}$  ergs cm<sup>-2</sup> s<sup>-1</sup> the number of accretors exceeds the number of coolers. The overall Popov et al. prediction for the Galactic INS population is consistent with current observations, if one assumes that the Magnificent Seven are indeed all young, bright coolers. Interestingly, it also suggests that at the fainter flux limits of the RASS

Faint Source Catalog, there are a significant number of as yet undetected isolated neutron stars.

Of the  $\sim 9500$  RASS X-ray sources with small positional errors from which we selected our candidate INSs, 80% have count rates  $\geq 0.017$  counts  $\text{s}^{-1}$ , and we adopt this value as a rough lower limit to our search sensitivity. This corresponds to the peak in the cumulative distribution of count rates for our sample, and is also consistent with the value of the flux for which Shen et al. (2006) quote a 50% completeness level for RASS detections in the SDSS Data Release 1 area. Popov et al. (2000) predict that the total number of isolated neutron stars with count rates greater than this limit should be  $3 - 10$  steradian $^{-1}$ , or  $40 - 125$  over the entire sky. Based on their models, a naive prediction is that the SDSS DR4 area contains  $5 - 20$  isolated neutron stars, a range consistent with the number of new candidates we identify here. We note, however, that our list is not complete: it is very likely that good INS candidates were lost because of their chance proximity to unrelated SDSS objects, which caused our algorithm to eliminate those RASS error circles from consideration.

## 5.6 Conclusion

In an effort to expand the sample of known isolated neutron stars, we have developed a selection algorithm based on a cross-correlation of the RASS and SDSS data to identify X-ray error circles devoid of plausible optical counterparts. We use SDSS spectroscopy and, especially, deep SDSS DR4 photometric data to quantitatively characterize the 11 RASS fields that survive our winnowing algorithm as optically blank to the SDSS  $g \sim 22$  mag faint limit. Our search is an order of magnitude more selective than similar previous searches for optically blank RASS error circles; in selecting our INS candidates, we have excluded 99.9% of the RASS error circles in our initial sample.

The 11 RASS fields we identify as potentially hosting an INS include the only confirmed INS in the DR4 footprint, RX J1605.3+3249, along with a source previously considered as an INS candidate and rejected on the basis of *Chandra* observations, 1RXS J130547.2+641252 Rutledge et al. (2003). The remaining nine new candidates

may host INSs or other similarly exotic X-ray sources, such as unusual X-ray binaries, high-redshift quasars, dark clusters of galaxies, type 2 quasars, or extreme BL Lac objects (e.g., Chierigato et al., 2005).

We note that the number of candidates we find is consistent with the predictions from recent INS population models for the number expected in the SDSS DR4 footprint. Planned *Chandra* follow-up observations of these candidate fields will help confirm whether they contain isolated neutron stars or some alternate exotic X-ray emitters. At the minimum, our sample may help increase the diversity of neutron stars available for study.

### 5.7 Appendix: Additional Interesting Fields

In addition to the candidate fields listed in Table 5.1 and discussed in §5.4, we present a number of interesting X-ray fields identified in the process of developing the algorithm described above. These fields can be divided into two groups. The first seven are candidate faint optical clusters that failed the last step in our algorithm (see Figure 5.2). The other group is of six fields that barely fail the final version of the algorithm (all but one were correlated with the cluster catalog without being eliminated, however; see Figure 5.3). While this is not a complete list of either potential new RASS/SDSS clusters, or of interesting fields not quite good enough to make our final list, it does provide a sense of the properties of X-ray fields considered borderline optically blank by our algorithm.

Table 5.2 includes the main *ROSAT* parameters for these RASS sources, and the  $g$  magnitude of the *brightest* SDSS object within the 4 *p.e.* RASS error circle and the corresponding *minimum*  $\log(f_X/f_g)$  for the optical counterpart. Below we give additional information about a number of these fields.

#### 5.7.1 Candidate clusters with other possible optical counterparts

In this section we list candidate clusters identified by our program in which another plausible optical counterpart to the X-ray source is also present (see §5.3 for a discus-

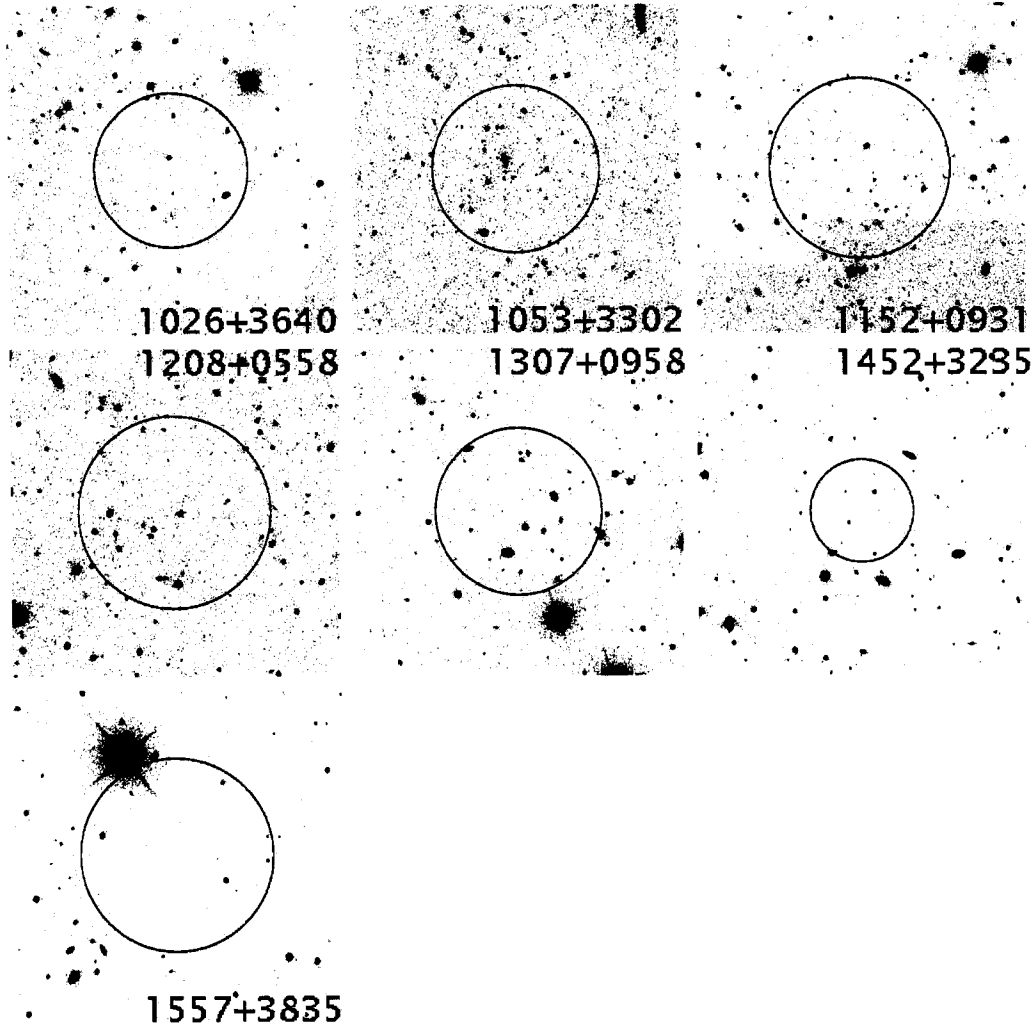


Figure 5.2: SDSS composite  $g, r, i$  images of candidate fields that did not survive the cluster-detecting stage of our algorithm. The orientation and scale are the same as in Fig. 5.1. The brightest object in any of the 4  $p.e.$  error circles is  $g = 19.35$  mag; for most fields the brightest object is  $g > 21.0$ . Rutledge et al. (2003) identified 1RXS J145234.9+323536 as a candidate INS, but no X-ray source was detected by their follow-up *Chandra* observations.

sion of the cluster identification stage of our algorithm).

- **1RXS J102659.6+364039** Two potential optical counterparts to this X-ray source are cataloged by Zickgraf et al. (2003). However, both are too faint ( $B > 20$ ) to be unambiguously identified by Zickgraf et al. as the X-ray source. To our knowl-

edge no spectrum of either of these potential counterparts has been taken.

- **1RXS J130723.7+095801** Three optical objects within  $1'$  of this X-ray source are cataloged by Zickgraf et al. (2003). Again, however, these are too faint ( $B > 19$ ) to be unambiguously identified by Zickgraf et al. as the X-ray source; no spectra of these potential counterparts exist to our knowledge.
- **1RXS J155705.0+383509** This is a source with a bright ( $g = 15.10$ ) star near the edge of its  $4\text{ p.e.}$  error circle. We obtained a spectrum for this star with the APO 3.5-m telescope; it appears to be a late G/early K star with no emission. G/K stars typically have  $(\log)$  flux ratios between  $-4.3$  and  $-1.5$  (Stocke et al., 1991), while this star has  $\log(f_X/f_g) = -1.11$ , and is therefore unlikely to be the X-ray source.

### 5.7.2 Other interesting fields

Three of these six fields meet all of our selection criteria (1RXS J105648.6+413833, 1RXS 162526.9+455750, and 1RXS J205334.0–063617). However, the RASS images of these fields, along with their count rates and exposure times, suggest that their cataloged positional error of  $6''$  is an underestimate. They cannot therefore be considered among our best INS candidates. The other three fields were identified in preliminary work as possibly hosting interesting X-ray sources. Below we provide additional information about one of the  $6''$  fields, and we describe why the three “early” fields were eliminated but remain interesting.

- **1RXS J105648.6+413833** A known  $g = 19.86$  quasar, QORG J105651.3+413809, is  $39''$  (6.4 times the quoted RASS positional error) from the X-ray position (Flesch & Hardcastle, 2004); it is also the radio source FIRST J105651.2+413809. While this quasar has  $\log(f_X/f_g) = 0.53$ , within the range for AGN (Stocke et al., 1991), such a large positional offset relative to the quoted positional error means that

this quasar is unlikely to be a RASS source, unless the quoted X-ray positional error is underestimated.

A *Galaxy Evolution Explorer* (Martin et al., 2005; Morrissey et al., 2005) source with a near-ultraviolet magnitude of  $21.85 \pm 0.29$  is positionally coincident ( $1''$ ) with a  $g = 22.67$  SDSS source within the 4 *p.e.* error circle. The nature of this object, SDSS J105649.58+413837, is difficult to determine from its SDSS pho-

Table 5.2: X-ray and optical data for seven cluster candidates. Six other interesting fields are listed below the horizontal line. 1RXS J145234.9+323536 was previously identified as a candidate INS, but no source was detected by *Chandra* (Rutledge et al., 2003); 1RXS J162526.9+455750, 162526.9+455750, and 205334.0–063617 have cataloged X-ray positional errors that appear to be underestimated; and 1RXS J205334.0–063617 is outside of the optical cluster catalog footprint.

Source name 1RXS J	RASS				SDSS	
	Count rate $1\sigma$	Detection $10^{-2}$ cps	Exp. likelihood	Exp. s	$g$ mag	Min. $\log(f_X/f_g)$
102659.6+364039	$12''$	$6.1 \pm 1.6$	26	371	20.43	1.3
105352.5+330255	$13''$	$3.0 \pm 1.1$	15	384	21.05	1.3
115247.0+093118	$14''$	$2.8 \pm 1.1$	13	433	21.51	1.4
120844.3+055839	$15''$	$2.9 \pm 1.2$	11	410	21.50	1.4
130723.7+095801	$13''$	$14.2 \pm 2.6$	47	303	19.35	1.3
145234.9+323536	$8''$	$8.0 \pm 1.3$	74	614	21.52	1.9
155705.0+383509	$15''$	$3.0 \pm 1.4$	9	272	21.12	1.3
105648.6+413833	$6''$	$1.6 \pm 0.7$	7	413	22.40	1.5
140654.5+525316	$12''$	$1.3 \pm 0.6$	10	617	22.50	1.5
141944.5+113222	$6''$	$2.2 \pm 1.1$	7	288	24.70	2.6
142423.3–020201	$6''$	$2.6 \pm 1.1$	8	322	22.08	1.6
162526.9+455750	$6''$	$1.4 \pm 0.6$	7	572	22.26	1.4
205334.0–063617	$6''$	$2.1 \pm 0.8$	9	434	23.16	1.9

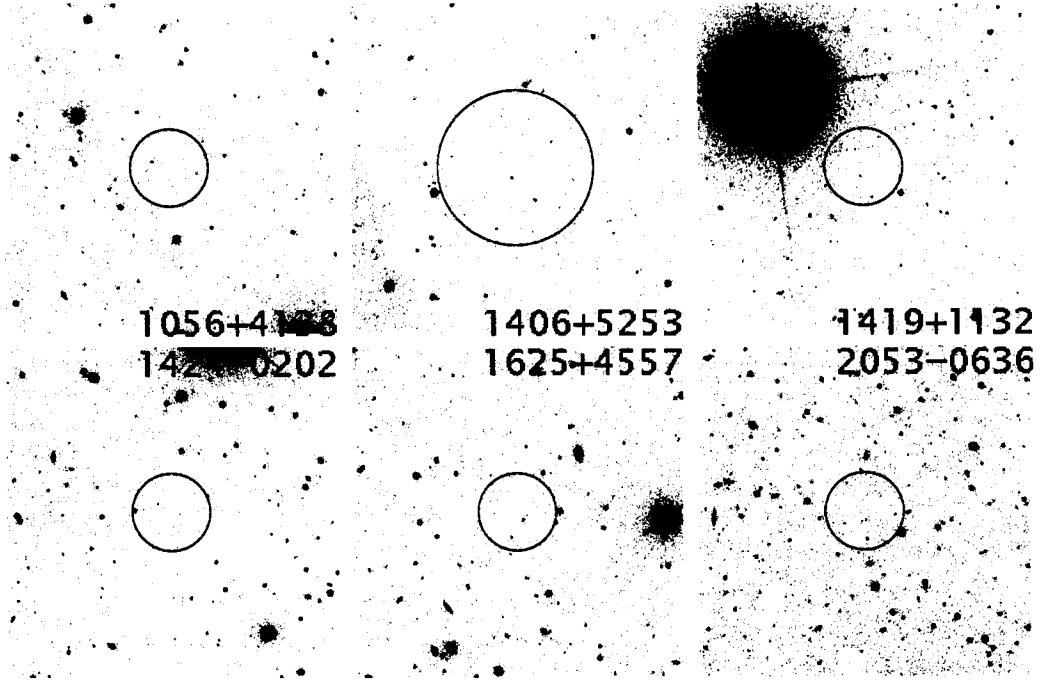


Figure 5.3: SDSS composite  $g, r, i$  images of six fields that did not survive our final version of the algorithm but may host interesting X-ray emitters. The orientation and scale are the same as in the previous figures. The brightest object in any of the 4  $p.e.$  error circles is  $g = 22.08$  mag.

tometry because of its faintness ( $u = 23.9$ ,  $g = 22.7$ ) and resulting uncertainties in its optical colors.

- **1RXS J140654.5+525316** This field was eliminated because of a  $g = 21.70$ ,  $\log(f_X/f_g) = 1.16$  object offset from the RASS source by between three and four times the quoted positional error. However, this object's photometry is suspect and its colors are inconsistent ( $(u - g) = 3.5 \pm 2.5$ ) with that of a typical AGN.
- **1RXS J141944.5+113222** This field was eliminated when the X-ray images of our fields were examined: it cannot be completely ruled out that this X-ray source and its neighbor, the bright star 1RXS J141949.0+113619, are actually the same source. While it meets all of our algorithm's other criteria, we therefore include it in this list rather than among our INS candidates.



- **1RXS J142423.3–020201** This field was eliminated by our algorithm because of the presence of a  $g = 20.65$  object with  $\log(f_X/f_g) = 1.05$  about 4 *p.e.* from the RASS position. We obtained several spectra of this object with the APO 3.5-m telescope. These spectra indicate that the object is most likely an ordinary G star with no signs of emission, and that it is therefore unlikely to be the X-ray source. The next brightest SDSS object within the 4 *p.e.* error circle is  $g = 22.08$ , so the counterpart to the X-ray source would then have  $\log(f_X/f_g) \geq 1.6$ .

### **Acknowledgments**

We thank Kevin Covey, Anil Seth, and the observing specialists at the telescope for their assistance with the APO observations. We thank the referee, Marten van Kerkwijk, for suggestions that improved the manuscript.

Funding for the creation and distribution of the SDSS Archive has been provided by the Alfred P. Sloan Foundation, the Participating Institutions, the National Aeronautics and Space Administration, the National Science Foundation, the U.S. Department of Energy, the Japanese Monbukagakusho, and the Max Planck Society. The SDSS Web site is at <http://www.sdss.org/>.

The SDSS is managed by the Astrophysical Research Consortium for the Participating Institutions. The Participating Institutions are the University of Chicago, Fermilab, the Institute for Advanced Study, the Japan Participation Group, The Johns Hopkins University, the Korean Scientist Group, Los Alamos National Laboratory, the Max-Planck-Institute for Astronomy, the Max-Planck-Institute for Astrophysics, New Mexico State University, the University of Pittsburgh, University of Portsmouth, Princeton University, the United States Naval Observatory, and the University of Washington.

This research has made use of the SIMBAD database, operated at CDS, Strasbourg, France, and of NED, which is operated by the Jet Propulsion Laboratory, California Institute of Technology, under contract with the National Aeronautics and Space Administration. We have also made use of PyRAF and TABLES, which are products of

the Space Telescope Science Institute, which is operated by AURA for NASA.

The DSS was produced at the Space Telescope Science Institute under U.S. Government grant NAG W-2166. The images of these surveys are based on photographic data obtained using the Oschin Schmidt Telescope on Palomar Mountain and the UK Schmidt Telescope. The plates were processed into the present compressed digital form with the permission of these institutions.

## Chapter 6

### CONCLUSION

The work presented in this thesis is part of a program to produce a complete sample of *ROSAT* All-Sky Survey (RASS; Voges et al., 1999) X-ray source identifications from correlations with the Sloan Digital Sky Survey (SDSS; York et al., 2000). Until 2000, our ability to identify the roughly 124,000 sources in the Bright and Faint Source Catalogs (BSC and FSC; Voges et al., 1999, 2000) was significantly limited by the absence of large-scale optical photometric and especially spectroscopic surveys with which to correlate the RASS data. As a result, the nature of fewer than 10% of RASS sources is known (Mickaelian et al., 2006). With SDSS, however, we now have such a survey: the upcoming Data Release Five contains photometric data for over  $2 \times 10^8$  objects, with over  $10^6$  having been targeted for spectroscopy, and covers an area of  $8000 \text{ deg}^2$  (Adelman-McCarthy et al., 2006, in preparation). SDSS is therefore an excellent tool for identifying large numbers of *ROSAT* sources (e.g., X-ray-emitting active galactic nuclei; Anderson et al., 2003). In this Chapter I review the main results from my work using SDSS to identify Galactic stellar X-ray emitters, and also discuss a few possible future research directions based on these results.

#### *Normal stars*

About a third of the RASS counterparts should be Galactic stars (e.g., Bade et al., 1998; Gioia et al., 2003; Zickgraf et al., 2003), most of which are coronally emitting X-ray sources brighter in the optical than the  $m \approx 15$  mag SDSS spectroscopic limit. While these objects do have SDSS photometric data, the survey cannot directly identify them as X-ray source counterparts, as this requires knowledge of the stars' spectral type. In Chapter 2, I described a method based on correlations of the RASS BSC and FSC, the SDSS Data Release 1 (DR1; Abazajian et al., 2003), the Two Micron All Sky

Survey (2MASS; Skrutskie et al., 2006), and public databases (particularly SIMBAD), which produced a sample of roughly 2000 candidate stellar X-ray emitters. One-fifth of these stars had previously cataloged spectral types, and I used these to determine empirical  $\log(f_X/f_{opt})$  ranges for each spectral class.

Using the Dual Imaging Spectrograph on the 3.5-m telescope at the Apache Point Observatory, NM, I then obtained spectra for objects in roughly 900 of the remaining RASS fields. The vast majority of these are fields in which the separation between the bright SDSS star and the RASS source was  $\leq 30''$ , increasing the likelihood that the star is the X-ray emitter. Flux ratios were then calculated and compared to the empirical ranges for the appropriate spectral class.

In total, this program yielded 834 stellar identifications, of which 492 were previously uncataloged stars (i.e., lacking a spectral type). Of those, 167 are F stars (35 are new), 236 are G stars (146), 214 are K stars (140), and 187 are M stars (171). In addition, I recovered six known X-ray-emitting white dwarfs, and four known X-ray-emitting cataclysmic variables.

Overall, I was able to identify the spectroscopic target as the RASS X-ray source roughly 66% of the time. For a significant number of RASS fields, the X-ray counterpart is therefore still unknown. With the SDSS spectroscopic survey having grown significantly since I produced my list of targets<sup>1</sup>, a reanalysis of these fields may well allow me to make the identifications (e.g., if there is a previously unknown quasar in the field). Once I have completed the DR1 analysis, I hope to use the assembled sample to calibrate an algorithm, based only on available SDSS photometric and spectroscopic data, with which to identify likely RASS counterparts in the entire SDSS footprint. The SDSS area has grown by a factor of four since DR1, and a program to obtain individual spectra for all of the candidate stellar counterparts is probably unrealistic.

The X-ray-emitting M star sample will be studied in some detail in a forthcoming paper (Hilton et al., 2006, in preparation). Some of these stars were observed while flaring, and comparisons between the merely active and the flaring M stars will al-

---

<sup>1</sup>DR1 objects with interesting photometric characteristics (e.g., UV excess) may not have been targeted for spectroscopy until later in the survey.

low us to explore the properties of the latter. I also plan to obtain high-resolution spectroscopy of the possible exotic binary system I identified.

### *Cataclysmic variables*

While most of the stellar X-ray sources are coronally emitting F to M stars, a small fraction are more exotic. Some are cataclysmic variables (CVs), white dwarf/late-type star binaries for which the typical optical magnitude is within the SDSS spectroscopic target range. The survey data alone are therefore sufficient for identifying X-ray-emitting CVs, and in Chapter 3, I compiled the published data for 40 spectroscopically identified CVs in the SDSS footprint that are RASS sources (Szkody et al., 2002, 2003, 2004a, 2005, 2006). I also discussed eight other emission-line systems not currently published in the SDSS CV catalog that are probable RASS sources. Two of these are previously known CVs, and three others are SDSS discoveries.

I used the Patterson & Raymond (1985a) relationship between  $\log(f_X/f_{opt})$  and the equivalent width of the  $H\beta$  emission line to examine the likelihood that several of the currently uncategorized CVs are magnetic systems. Follow-up observations will be required to test my predictions, and the continuing spectroscopic identification of new SDSS CVs will expand the sample for which these predictions can be made and tested.

### *White dwarfs*

White dwarfs (WDs) are another exotic stellar source of X-ray emission for which SDSS spectroscopy is frequently available. In Chapter 4, I presented the results of correlations of the most recent SDSS WD catalog, that of Eisenstein et al. (2006), and of the RASS. The total number of X-ray-emitting WDs identified in this manner is small: 25 DA WDs, of which 10 are SDSS discoveries (another 4, although known DAs, were not previously known to be X-ray sources), with another 10 being less certain associations.

A handful of non-DAs were also identified as RASS sources: three DA/M star bina-

ries, one PG 1159 star (a pre-WD), and most interestingly, two DB WDs, which have helium-rich (rather than hydrogen-rich) atmospheres, and are relatively cool.

These two DBs, along with three of the DAs, form a small sample of cooler-than-expected X-ray-emitting WDs. X-ray emission is thought to be visible only from DAs hotter than 23,000 K (e.g., Jordan et al., 1994) and only in even hotter non-DAs (e.g., Motch et al., 1993; Marsh et al., 1997b). Further work, including possibly pointed X-ray observations, is clearly required to confirm my findings.

New candidate WDs have been identified in the SDSS spectroscopy in the time since the production of the Eisenstein et al. (2006) catalog, and I identified nine X-ray emitters among these. Two were previously known X-ray-emitting DAs, while the seven others are SDSS discoveries. These new WDs appear to be DAs, but confirming their nature requires fitting the SDSS spectra; I will then be able to compare their properties to those of the other SDSS X-ray-emitting DAs.

### *Isolated neutron stars*

Finally, I used RASS/SDSS correlations to search for new candidate isolated neutron stars (INSs)—probably the most elusive stellar X-ray sources in the RASS; only seven INSs are currently known. In Chapter 5, I describe the algorithm I developed to identify blank fields RASS sources, where the absence of a likely optical counterpart to the SDSS  $m \approx 22$  mag limit implies that the source is a good candidate INS (INSs typically have  $m \geq 25$ ).

I currently have a *Chandra X-ray Observatory* program to obtain short exposures of 13 of the candidate INS fields found in this manner. These data should provide pinpoint positions for the X-ray sources cataloged in the RASS. I will then verify that the source is not in fact positionally coincident with any SDSS object. If the small *Chandra* error circle is optically blank, I will follow up with deep optical observations to find the counterpart and with X-ray spectroscopy to characterize the INS.

If instead the source is coincident with an SDSS object, optical spectroscopy will be used to determine the nature of the source—which is likely to be exotic, since these

fields do not include any potential X-ray counterparts with typical  $f_X/f_{opt}$  ratios (for example, the source might be an unusual X-ray binary or a high-redshift quasar; Chierigato et al., 2005).

## BIBLIOGRAPHY

- Abazajian, K., et al. 2003, *AJ*, 126, 2081
- Adelman–McCarthy, J. K., et al. 2006, *ApJS*, 162, 38
- Agüeros, M. A., et al. 2006, *AJ*, 131, 1740
- Allred, J. C., et al. 2005, *ApJ*, 630, 573
- . 2006, *ApJ*, 644, 484
- Anderson, S. F., et al. 2003, *AJ*, 126, 2209
- Antiochos, S. K., et al. 1986, *ApJL*, 307, L55
- Aschwanden, M. J., et al. 2000, *ApJ*, 541, 1059
- Ayres, T. R., et al. 1981, *ApJ*, 250, 293
- . 2003, *ApJ*, 598, 610
- . 2005, *ApJL*, 627, L53
- Bade, N., et al. 1998, *A&AS*, 127, 145
- Bailer–Jones, C. A. L. 2004, *A&A*, 419, 703
- Barstow, M. A. 1989, *LNP Vol. 328: IAU Colloq. 114: White Dwarfs*, 328, 156
- Barstow, M. A. et al. 1993, *MNRAS*, 264, 16
- Bauer, F. E., et al. 2000, *ApJS*, 129, 547
- Becker, R. H., et al. 1995, *ApJ*, 450, 559
- Bercik, D. J., et al. 2005, *ApJ*, 631, 529
- Blaes, O., & Madau, P. 1993, *ApJ*, 403, 690
- Burwitz, V., et al. 2003, *A&A*, 399, 1109
- Cassinelli, J. P., & Swank, J. H. 1983, *ApJ*, 271, 681
- Catura, R. C., et al. 1975, *ApJL*, 196, L47
- Chieregato, M., et al. 2005, *A&A*, 444, 69
- Chu, Y.-H., et al. 2004, *AJ*, 127, 477
- Condon, J. J., et al. 1998, *AJ*, 115, 1693



- Cox, A. N. 2000, *Allen's astrophysical quantities* (Allen's astrophysical quantities, 4th ed. Publisher: New York: AIP Press; Springer, 2000. Edited by Arthur N. Cox. ISBN: 0387987460)
- Craig, I. J. D., et al. 1978, *A&A*, 70, 1
- Daniel, K. J., et al. 2002, *ApJ*, 578, 486
- de Martino, D., et al. 2006, *A&A*, 454, 287
- Dennis, B. R., & Schwartz, R. A. 1989, *Sol. Phys.*, 121, 75
- Dennis, B. R., & Zarro, D. M. 1993, *Sol. Phys.*, 146, 177
- Dietrich, J. P. et al. 2006, *A&A*, 449, 837
- Dobler, W., et al. 2006, *ApJ*, 638, 336
- Downes, R. A., et al. 2001, *PASP*, 113, 764
- . 2004, *AJ*, 127, 2838
- Durney, B. R., et al. 1993, *Sol. Phys.*, 145, 207
- Edlén, B. 1943, *Zeitschrift fur Astrophysik*, 22, 30
- Eisenstein, D. J., et al. 2006, accepted, to appear in *AJ*
- Favata, F., & Micela, G. 2003, *Space Science Reviews*, 108, 577
- Feigelson, E. D., et al. 2004, *ApJ*, 611, 1107
- Finlator, K., et al. 2000, *AJ*, 120, 2615
- Fleming, T. A., et al. 1996, *A&A*, 316, 147
- Flesch, E., & Hardcastle, M. J. 2004, *A&A*, 427, 387
- Freyberg, M. J., et al. 2005, *astro-ph/0512157*
- Friedman, H., et al. 1951, *Physical Review*, 83, 1025
- Fukugita, M., et al. 1996, *AJ*, 111, 1748
- Gioia, I. M., et al. 1984, *ApJ*, 283, 495
- . 1990, *ApJS*, 72, 567
- . 2003, *ApJS*, 149, 29
- Green, P. J. et al. 2004, *ApJS*, 150, 43
- Grindlay, J. E. et al. 2005, *ApJ*, 635, 920
- Güdel, M. 2004, *A&A Rev.*, 12, 71
- Gunn, J. E., et al. 1998, *AJ*, 116, 3040

- . 2006, *AJ*, 131, 2332
- Haberl, F. 2004, *Advances in Space Research*, 33, 638
- Haberl, F., et al. 1997, *A&A*, 326, 662
- Hagen, H.-J., et al. 1995, *A&AS*, 111, 195
- Haisch, B., & Schmitt, J. H. M. M. 1996, *PASP*, 108, 113
- Haisch, B., et al. 1991, *ApJL*, 383, L15
- Hands, A. D. P., et al. 2004, *MNRAS*, 351, 31
- Harnden, F. R., et al. 1979, *ApJL*, 234, L51
- Hawley, S. L., & Pettersen, B. R. 1991, *ApJ*, 378, 725
- Hawley, S. L., et al. 1995, *ApJ*, 453, 464
- . 1996, *AJ*, 112, 2799
- Henry, J. P., et al. 2006, *ApJS*, 162, 304
- Hewish, A., et al. 1968, *Nature*, 217, 709
- Hog, E., et al. 1998, *A&A*, 335, L65
- Hogg, D. W., et al. 2001, *AJ*, 122, 2129
- Ishibashi, K., et al. 2006, *ApJL*, 644, L117
- Ivezić, Ž., et al. 2004, *Astronomische Nachrichten*, 325, 583
- Jordan, S., et al. 1994, *A&A*, 290, 834
- Kahn, S. M., et al. 1984, *ApJ*, 278, 255
- Kaplan, D. L., et al. 2003, *ApJL*, 588, L33
- Kim, D.-W. et al. 2004, *ApJ*, 600, 59
- Kleinman, S. J., et al. 2004, *ApJ*, 607, 426
- Koester, D., Schulz, H., & Weidemann, V. 1979, *A&A*, 76, 262
- Krautter, J., et al. 1999, *A&A*, 350, 743
- Kulkarni, S. R., & van Kerkwijk, M. H. 1998, *ApJL*, 507, L49
- Kuulkers, E., et al. 2003, *astro-ph/0302351*
- Laycock, S., et al. 2005, *ApJL*, 634, L53
- Linsky, J. L., & Haisch, B. M. 1979, *ApJL*, 229, L27
- Linsky, J. L., et al. 1998, *ApJ*, 492, 767

- Liu, Q. Z., et al. 2000, *A&AS*, 147, 25
- . 2001, *A&A*, 368, 1021
- Lupton, R. H., et al. 2002, in *Survey and Other Telescope Technologies and Discoveries*. Edited by Tyson, J. Anthony; Wolff, Sidney. *Proceedings of the SPIE*, Vol. 4836, 350–356
- Maccacaro, T., et al. 1988, *ApJ*, 326, 680
- Maddox, S. J., et al. 1990, *MNRAS*, 243, 692
- Madej, J., et al. 2004, *A&A*, 419, L5
- Marsh, M. C., et al. 1997a, *MNRAS*, 286, 369
- . 1997b, *MNRAS*, 287, 705
- Martin, D. C., et al. 2005, *ApJL*, 619, L1
- McCook, G. P., & Sion, E. M. 1999, *ApJS*, 121, 1
- Mickaelian, A. M., et al. 2006, *A&A*, 449, 425
- Morrissey, P., et al. 2005, *ApJL*, 619, L7
- Motch, C., et al. 1993, *A&A*, 268, 561
- . 1998, *A&AS*, 132, 341
- . 2003, *Astronomische Nachrichten*, 324, 61
- Muno, M. P., et al. 2005, *ApJL*, 622, L113
- Neuhäuser, R., & Trümper, J. E. 1999, *A&A*, 343, 151
- Neupert, W. M. 1968, *ApJL*, 153, L59+
- Nieto-Santisteban, M. A., et al. 2004, in *ASP Conf. Ser. 314: Astronomical Data Analysis Software and Systems (ADASS) XIII*, ed. F. Ochsenbein, M. G. Allen, & D. Egret, 666–+
- O'Dwyer, I. J., et al. 2003, *AJ*, 125, 2239
- Osten, R. A., et al. 2005, *ApJ*, 621, 398
- Ostriker, J. P., et al. 1970, *Astrophys. Lett.*, 6, 179
- Paerels, F. B. S., & Heise, J. 1989, *ApJ*, 339, 1000
- Pallavicini, R., et al. 1981, *ApJ*, 248, 279
- Patterson, J., & Raymond, J. C. 1985a, *ApJ*, 292, 535
- . 1985b, *ApJ*, 292, 550

- Perna, R., et al. 2003, *ApJ*, 594, 936
- Pevtsov, A. A., et al. 2003, *ApJ*, 598, 1387
- Pier, J. R., et al. 2003, *AJ*, 125, 1559
- Pizzolato, N., et al. 2003, *A&A*, 397, 147
- Poletto, G., et al. 1975, *Sol. Phys.*, 44, 83
- Popov, S. B., et al. 2000, *ApJL*, 544, L53
- Ramsay, G., et al. 2004, *MNRAS*, 350, 1373
- Rappaport, S., et al. 1974, *ApJL*, 187, L5+
- Reid, I. N., & Hawley, S. L. 2005, *New Light on Dark Stars: Red Dwarfs, Low-Mass Stars, Brown Dwarfs (New Light on Dark Stars: Red Dwarfs, Low-Mass Stars, Brown Dwarfs, by I.N. Reid and S.L. Hawley. Springer-Praxis books in astrophysics and astronomy. Praxis Publishing Ltd, 2005. ISBN 3-540-25124-3)*
- Reid, I. N., et al. 2000, *AJ*, 119, 369
- Richards, G. T., et al. 2002, *AJ*, 123, 2945
- Richman, H. R. 1996, *ApJ*, 462, 404
- Robrade, J., & Schmitt, J. H. M. M. 2005, *A&A*, 435, 1073
- Rogel, A. B., et al. 2006, *ApJS*, 163, 160
- Rosner, R., et al. 1978, *ApJ*, 220, 643
- Rutledge, R. E., et al. 2000, *ApJS*, 131, 335
- . 2003, *ApJ*, 598, 458
- Schmidt, G. D., et al. 2005a, *ApJ*, 630, 1037
- . 2005b, *ApJ*, 620, 422
- Schmitt, J. H. M. M., et al. 1995, *ApJ*, 450, 392
- Schrijver, C. J. 1987, *A&A*, 172, 111
- Schrijver, C. J., et al. 1984, *A&A*, 138, 258
- Schwope, A. D., et al. 2002, in *ASP Conf. Ser. 261: The Physics of Cataclysmic Variables and Related Objects*, ed. B. T. Gänsicke, K. Beuermann, & K. Reinsch, 102—
- Sciortino, S., et al. 1990, *ApJ*, 361, 621
- Shen, S., et al. 2006, *MNRAS*, 582
- Shipman, H. L. 1976, *ApJL*, 206, L67

- Silvestri, N. M., et al. 2006, *AJ*, 131, 1674
- Skrutskie, M. F. et al. 2006, *AJ*, 131, 1163
- Skumanich, A. 1972, *ApJ*, 171, 565
- Smith, J. A., et al. 2002, *AJ*, 123, 2121
- Smith, K., et al. 2005, *A&A*, 436, 241
- Sokoloski, J. L. 2003, *Journal of the American Association of Variable Star Observers (JAAVSO)*, 31, 89
- Space Telescope Science Institute, & Osservatorio Astronomico di Torino. 2001, *VizieR Online Data Catalog*, 1271, 0
- Staude, A., et al. 2003, *A&A*, 406, 253
- Stoeck, J. T., et al. 1983, *ApJ*, 273, 458
- . 1991, *ApJS*, 76, 813
- Stoughton, C., et al. 2002, *AJ*, 123, 485
- Szkody, P., et al. 2002, *AJ*, 123, 430
- . 2003, *AJ*, 126, 1499
- . 2004a, *AJ*, 128, 1882
- . 2004b, *AJ*, 128, 2443
- . 2005, *AJ*, 129, 2386
- . 2006, *AJ*, 131, 973
- Trümper, J. E. 2005, *astro-ph/0502457*
- Treves, A., & Colpi, M. 1991, *A&A*, 241, 107
- Treves, A., et al. 2000, *PASP*, 112, 297
- van Kerkwijk, M. H., et al. 2004, *ApJ*, 608, 432
- Vanden Berk, D. E., et al. 2001, *AJ*, 122, 549
- Verbunt, F., et al. 1997, *A&A*, 327, 602
- Voges, W., et al. 1999, *A&A*, 349, 389
- . 2000, *VizieR Online Data Catalog*, 9029, 0
- Walter, F. M., et al. 1996, *Nature*, 379, 233
- Warner, B. 1972, *MNRAS*, 158, 425

- . 1995, *Cataclysmic Variable Stars* (Cambridge Astrophysics Series, Cambridge, New York: Cambridge University Press, —c1995)
- Watson, M. G. et al. 2001, *A&A*, 365, L51
- West, A. A., et al. 2004, *AJ*, 128, 426
- Wickramasinghe, D. T., & Ferrario, L. 2000, *PASP*, 112, 873
- York, D. G., et al. 2000, *AJ*, 120, 1579
- Zane, S., et al. 2005, *ApJ*, 627, 397
- Zickgraf, F.-J., et al. 1997, *A&AS*, 123, 103
- . 2003, *A&A*, 406, 535

## VITA

Marcel Agüeros's journey from the Manhattan tenements of his youth to the upper echelons of the astrophysical community would not provide a truer embodiment of the American Dream were it penned by Horatio Alger himself. To see Marcel lost in thought, the brass buttons on his official (and tax-exempt) work uniform glittering as he rocks rhythmically to Prince Paul's masterful beats, is to see to see an astronomer at the peak of his career, decoding the secrets of the universe. Indeed, Marcel shows no signs of the self-doubt or crises of confidence that afflict so many other middle-aged intellectuals.

Marcel's keen mind is the cornerstone of his academic career, finding its purest expression in his professional dedication to unraveling the mysteries of the neutron star equation of state. His curiosity was evident at the earliest ages; in an attempt to feed an insatiable literary appetite, young Marcel surreptitiously obtained subscriptions to the leading literary journals of the day, a decision only revealed to his mother months later, when the invoices came due! Marcel's promise as a scholar was clearly visible by the time he reached high school, where his teachers often remarked that he seemed to be nearly a full year ahead of many of his classmates. All the more impressive, Marcel maintained this laudable academic standing while remaining engaged in an impressive array of extra-curricular activities, most notably serving as an active member of the Parisian Reggae Appreciation Club, the Brussels Late Night Power Walkers and the all-volunteer Parking Meter Removal Team.

These academic achievements, however, have not come at the cost of a rich and textured life. Marcel's astronomical career was even briefly put on hold when, lured by the promise of brisk morning runs, invigorating chin-up competitions, and complimentary blue velvet track suits, Marcel succumbed to the siren call of a tour in the French military. This penchant for physical exertion underlies Marcel's passion for sport; Marcel

channels his athletic energies onto the basketball court and has been described as possessing the grace of Shaquille O'Neal, Bruce Bowen's sense of fair play, and the looks of Sam Cassell. (It should be noted this last point is a matter of some dispute, as others claim Marcel and Rick Fox were likely separated at birth.). Marcel is also a dedicated athletic supporter; not only is he a devoted fan of his hometown New York Yankees and New York Knickerbockers, but even takes the time to provide encouragement and support to schoolchildren in the local kickball leagues.

Aside from sport, Marcel's other passion is travel; particularly fond memories include a charming trek and bus ride to Kathmandu, a refreshing stroll up Fuji-san and losing track of time on the beaches of the Philippines. Marcel's journeys have, however, given him firsthand experience of the inability of the rest of the world to measure up to the standards of his native New York, where he will be moving this fall to begin his postdoctoral work. Marcel hopes to continue his long-standing charitable support of the New York Philharmonic, and resume his impromptu tours of the Columbia campus and its environs; one of his Columbia classmates remembers fondly how Marcel secured her a chauffeured ride cross-town after personally escorting her to a local produce vendor.

But the joy that will be provided by the Prodigal Astronomer's return to New York will be the opportunities to create warm new memories with friends and family. Separated from her beloved dog Winnie, Marcel's beautiful and charming partner Melissa will undoubtedly enjoy the scads of dog walkers that frequent Central Park, where Marcel's earliest experience of the warmth and joy of canine companions took place. Marcel will also be able to spend more time with his father and sister, who both still live in New York; once again Marcel will be able to bring the family together around the warmth of a fire in the living room.

*(As told to Kervin R. Covei.)*